The role of platelets in hepatic ischemia reperfusion injury in mice

Die Rolle von Thrombozyten im hepatischen ischämischen Reperfusionsschaden in Mäusen

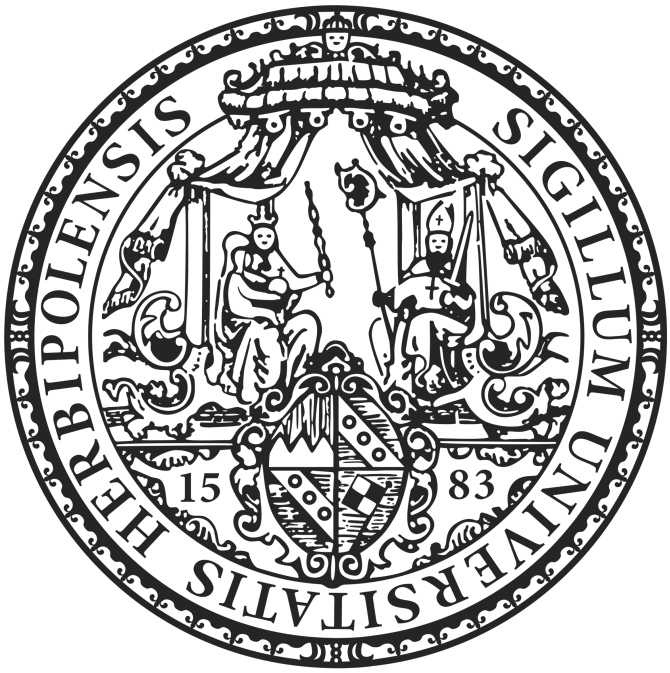

Doctoral thesis for a doctoral degree
at the Graduate School of Life Sciences,
Julius-Maximilians-Universität Würzburg
Section Biomedicine

submitted by

Carina Gross
from Gronau/Westf.

Würzburg, 2020

Submitted on: ……

Office Stamp

Members of the *Promotionskomitee*:

Chairperson: Prof. Dr. Manfred Gessler

Primary Supervisor: Dr. David Stegner

Supervisor (Second): Prof. Dr. Katrin Heinze

Supervisor (Third): Prof. Dr. Valbona Mirakaj

Date of Public Defense: ……

Date of Receipt of Certificates: ……

Summary

Platelets are the second most abundant blood cells and their main function is maintenance of vascular integrity. In addition, platelets are increasingly recognized as cells with immune functions, as they participate in the recruitment of immune cells and modulate the progression and severity of an immune response. So-called lipid mediators, which are – besides other cells – released by activated platelets, influence the immune response. LTB_4 is one of these potent lipid mediators and is able to activate neutrophils and induce their infiltration into injured tissue.

In order to investigate the involvement of platelets in inflammatory processes, a murine model of hepatic ischemia reperfusion injury as well as confocal intravital microscopy of the liver were established. Both methods were used to analyze the influence of platelets on the inflammation that follows sterile liver inflammation. We found platelet function to be unaltered after three hours of reperfusion and platelet aggregation to be irrelevant for the outcome of hepatic ischemia reperfusion injury. However, a strong impact of the GPIb-vWF axis could be observed, as antibody mediated blockade of GPIb as well as vWF-deficiency significantly reduced liver damage markers and decreased neutrophil infiltration. GPIb-IL-4R mice were used to exclude the possibility that the protective effects of the anti-GPIbα antibody treatment (p0p/B) results from something else than blocking GPIbα. Furthermore, the slope of neutrophil infiltration was decreased in p0p/B-treated mice, leading to overall decreased neutrophil numbers in the liver after three hours of reperfusion. Blockade of the integrin αIIbβ3, however, showed no reduction in neutrophil infiltration into the post-ischemic liver, in line with unaltered liver damage.

To study the role of leukotriene B_4, conditional and constitutive knockout mice for the LTA_4 hydrolase, which catalyzes the last step in LTB_4 synthesis, were generated. Lta4h deficiency did not affect general platelet functionality in hemostasis and thrombosis. Interestingly, *Lta4h*$^{-/-}$ mice were not protected from cellular damage following hepatic ischemia, despite lower neutrophil numbers in the post-ischemic liver.

Intravital microscopy of the pancreas was established and revealed increased $CD4^+$ T cell numbers in GPVI-deficient animals compared to WT controls in line with the pre-diabetic phenotype of *Gp6*$^{-/-}$ mice that was revealed in Grzegorz Sumara's group. Furthermore, platelet 'behavior' in pancreatic islets was observed following glucose injection. We found a high number of platelets adherent to islet sinusoids under basal conditions and no rolling/decelerating of platelets following glucose injection. This was accompanied by temporary sinusoidal constriction and stop of the blood flow. This phenomenon was not observed in control settings (injection of PBS, insulin or L-glucose).

In a side project, which was carried out jointly with Tobias Heib, a side by side comparison of the classical syringe-based flushing and the centrifugation-based spinning method to isolate murine bone marrow was conducted. Flow cytometry revealed no differences in the distribution of hematopoietic stem cells and immune cells and functional analysis with primary and cultured megakaryocytes (MKs) showed comparable results in all conducted assays. Thus, our data demonstrated that the faster and more efficient spinning method can be used for the isolation of bone marrow cells.

Zusammenfassung

Thrombozyten gehören zu den am stärksten im Blut vertretenen Zellen, deren Hauptaufgabe der Erhalt der vaskulären Integrität darstellt. Des Weiteren werden Thrombozyten immer mehr als „Immunzellen“ betrachtet, da sie andere Zellen rekrutieren, sowie zum Verlauf und der Schwere der Immunantwort beitragen. So genannte Lipidmediatoren, die neben anderen Zellen auch von Thrombozyten freigesetzt werden, sind in der Lage die Immunantwort zu beeinflussen. Leukotrien B_4 (LTB_4) ist ein solcher hochwirksamer Lipidmediator, der dafür bekannt ist, Neutrophile zu aktivieren und deren Infiltration in verletztes/entzündetes Gewebe zu begünstigen.

Um einen besseren Einblick in den Beitrag von Thrombozyten in entzündlichen Prozessen zu bekommen, wurden ein Mausmodell des hepatischen Ischämie/Reperfusionsschadens sowie konfokale Intravitalmikroskopie etabliert. Beide Methoden wurden benutzt, um den Einfluss von Thrombozyten auf eine sterile Entzündungsreaktion zu untersuchen. Wir konnten zeigen, dass die Thrombozytenaktivität nach 3-stündiger Reperfusion unverändert blieb. Des Weiteren scheint Thrombozytenaggregation für den Ausgang im hepatischen Ischämie- und Reperfusionsmodell vernachlässigbar zu sein, während ein deutlicher Einfluss der GPIb-vWF Achse beobachtet wurde. Antikörper vermittelte GPIb-Blockade sowie vWF Defizienz zeigten reduzierte Werte des Leberschadens sowie geringere Neutrophilzahlen im Lebergewebe. Um auszuschließen, dass die schützenden Effekte der anti-GPIbα Applikation (p0p/B) durch etwas anderes als die Blockade von GPIbα verursacht werden, wurden GPIb-IL-4R Tiere verwendet. Hinzu kommt ein flacherer Anstieg der Neutrophilzahlen in p0p/B behandelten Tieren, was letztlich auch zur geringeren Gesamtzahl nach 3-stündiger Reperfusion führt. Die Blockade des Integrins αIIbβ3 zeigte im Vergleich zu Kontrolltieren unveränderte Einwanderung von neutrophilen Granulozyten in der post-ischämischen Leber, was in Einklang mit dem unveränderten Leberschaden nach Ischämie/Reperfusion steht.

Um den Einfluss von Leukotrienen zu untersuchen, wurden konstitutive und konditionelle Knockout Tiere für die LTA_4 Hydrolase generiert, die den letzten Schritt der LTB_4-Synthese katalysiert. LTA_4H-Defizienz hatte keinen Einfluss auf normale Thrombozytenfunktion in Thrombose und Hämostase. Interessanterweise zeigten diese Tiere jedoch keinen Leber-spezifischen Schutz nach Ischämie, obwohl die Zahl der einwandernden neutrophilen Granulozyten signifikant verringert war.

Intravitalmikroskopie des Pankreas wurde erfolgreich etabliert und zeigte erhöhte $CD4^+$ T-Zellzahlen in GPVI-defizienten Tieren im Vergleich zu WT Kontrolltieren. Diese Ergebnisse sind im Einklang mit dem von Grzegorz Sumaras Gruppe gefundenen prä-diabetischen Phänotyp in *Gp6*$^{-/-}$ Mäusen. Des Weiteren wurde das „Verhalten“ von Thrombozyten in Langerhans-Inseln nach Glukoseinjektion untersucht. Wir fanden bereits unter

Grundbedingungen eine hohe Anzahl von adhärenten Thrombozyten im Gefäßsystem, jedoch kein Verlangsamen/Rollen von Thrombozyten nach Glukose Injektion. Dieser Effekt wurde von einer temporären Verengung des Gefäßsystems und einem Stoppen des Blutflusses begleitet und konnte nicht in Kontrollbedingungen (Injektion von PBS, Insulin oder L-Glukose) beobachtet werden.

In einem Nebenprojekt, das gemeinsam mit Tobias Heib durchgeführt wurde, wurden die klassische nadel-basierte Flush- sowie die Zentrifugations-basierte Spin-Methode zur Isolation von murinem Knochenmark verglichen. Durchflusszytometrie zeigte, dass die Verteilung von Stamm- und Immunzellpopulationen unverändert war. Des Weiteren zeigten funktionale Analysen von primären und kultivierten Megakaryozyten (MKs) vergleichbare Ergebnisse in allen durchgeführten Tests. Somit haben unsere Daten gezeigt, dass die schnellere und effizientere Spin-Methode zur Isolierung von Knochenmarkszellen verwendet werden kann.

„Be brave. Take risks. Nothing can substitute experience. “

- Paulo Coelho -

1. Introduction

1.1 Hematopoiesis

Hematopoiesis is the continuous, tightly regulated process of renewal, proliferation, differentiation and maturation of all blood cells originating from hematopoietic stem cells (HSCs). This process leads to the formation of differentiated blood cells that are released from the bone marrow into the circulation. Since mature blood cells have a limited lifespan, cell populations need to be replenished to maintain homeostasis.

1.1.1 Hematopoietic stem cells

Hematopoietic stem cells (HSCs) are defined by their characteristic of pluripotency and self-renewal. Pluripotency describes the capacity of a single HSC to generate any of the mature blood cell types, whereas self-renewal is a cell division specific for HSCs, which allows them to maintain their undifferentiated state [1, 2]. The differentiation and fate of HSCs is tightly regulated by transcription factors, signaling pathways, adhesion molecules, cytokines and chemokines.

Analyses revealed a hierarchical structure of the development of hematopoietic cells, where the multipotency is progressively restricted and finally completely lost. Studies showed stem cell populations termed LSKs, which are negative for specific *lineage markers* (Lin-), while expressing CD117 (c-Kit) and *stem cell antigen* (Sca-1). This population accounts for 0.05% of all *bone marrow* (BM) cells [3]. Identification of HSCs within the LSK population is characterized by expression of CD34, CD48 and CD150 [4]. The HSC population accounts for 0.01% of the BM and depending on the extraction method only about ~5000 cells can be isolated from one mouse [5, 6].

Based on the tree-like hierarchy model (Fig. 1), expression of CD34 allows the differentiation of *long-term* (LT-HSCs) and *short-term* HSCs (ST-HSCs). LT-HSCs are omnipotent cells and mostly present in a quiescent state or reversible growth arrest [1]. MEK/*extracellular signal-regulated kinase* (ERK) as well as *phosphoinositide-3-kinase* (PI3K)/ AKT (serine/threonine kinase1 or protein kinase B) /*mechanistic target of rapamycin* (mTOR) pathways regulate transition towards a propagating, ST-HSC, cell type. These cells then develop further into *multipotent progenitors* (MPPs), which already lost the capacity for self-renewal, however, keep their full lineage differentiation potential [7]. MPPs develop into oligopotent progenitors – the *common lymphoid progenitors* (CLPs) and the *common myeloid progenitors* (CMPs), which ultimately give rise to the lineage-committed effector cells of the hematopoietic system. CLPs for example differentiate and give rise to all lymphoid cell populations, including T cells, B cells

and NK cells. The CMPs give rise to *megakaryocyte/erythrocyte progenitors* (MEPs) and *granulocyte/macrophage progenitors* (GMPs), differentiating into the cell types already indicated by their names [8] (Fig. 1).

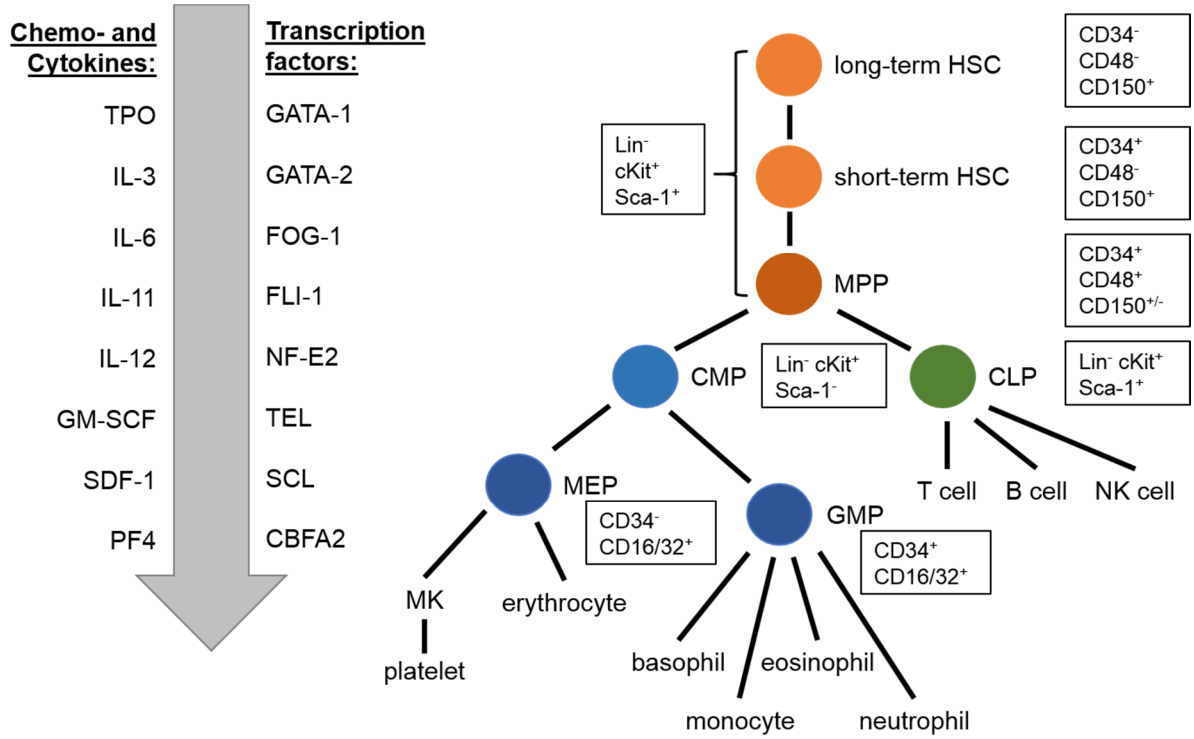

Figure 1: Simplified overview of stem cell differentiation. Long-term HSCs develop into short-term HSCs, which in turn differentiate into multipotent progenitors (MPPs). Depending on the cytokine/chemokine environment, MPPs give rise to common lymphoid progenitors (CLPs) or common myeloid progenitors (CMPs). The latter further differentiate into megakaryocyte/erythrocyte progenitors (MEPs) and granulocyte/monocyte progenitors (GMPs). Boxes display surface marker used for flow cytometric analysis.

1.1.2 Megakaryopoiesis

Megakaryocytes (MKs) are large lobulated cells (50-100 µm) which reside in the bone marrow. Their main function is the production of platelets, a strikingly organized process to guarantee proplatelet production and platelet maturation in the vasculature to maintain constant platelet counts [9]. Under normal physiological conditions MKs account for only 0.1% of BM cells. This number, however, may increase drastically under inflammatory or diseased conditions up to 10-fold [10-12]. In addition to the BM, MKs can also be found in the yolk sack, fetal liver and spleen during early development of mice [13].

In 1994, the *myeloproliferative leukemia protein* (c-Mpl) was discovered to be one of the driving receptors that promote MK development [14-18]. Together with its ligand *thrombopoietin* (TPO), c-Mpl is the most important mediator of megakaryopoiesis [15]. TPO is constantly expressed and released into the bloodstream, where it binds to c-Mpl on the platelet surface. Binding leads to dimerization of the receptor, resulting in subsequent activation of *janus kinase*

2 (JAK2). The kinase phosphorylates the receptor itself and further activates *signal transducers and activators of transcription* (STAT) 3 and 5 (Fig. 2). TPO binding also mediates *protein kinase* (PK) C activation, *phosphoinositide-3-kinase* (PI3K) and *mitogen-activated protein kinase* (MAPK) activation as well as *extracellular signal-regulated kinase* (ERK) 1 and 2. These pathways are involved in the induction of genes important for MK maturation [19, 20]. Plasma TPO levels are inversely correlated to the platelet count via an autoregulatory feedback mechanism of platelet c-Mpl binding to TPO, reducing the amount of TPO in the plasma and *vice versa* [15, 16].

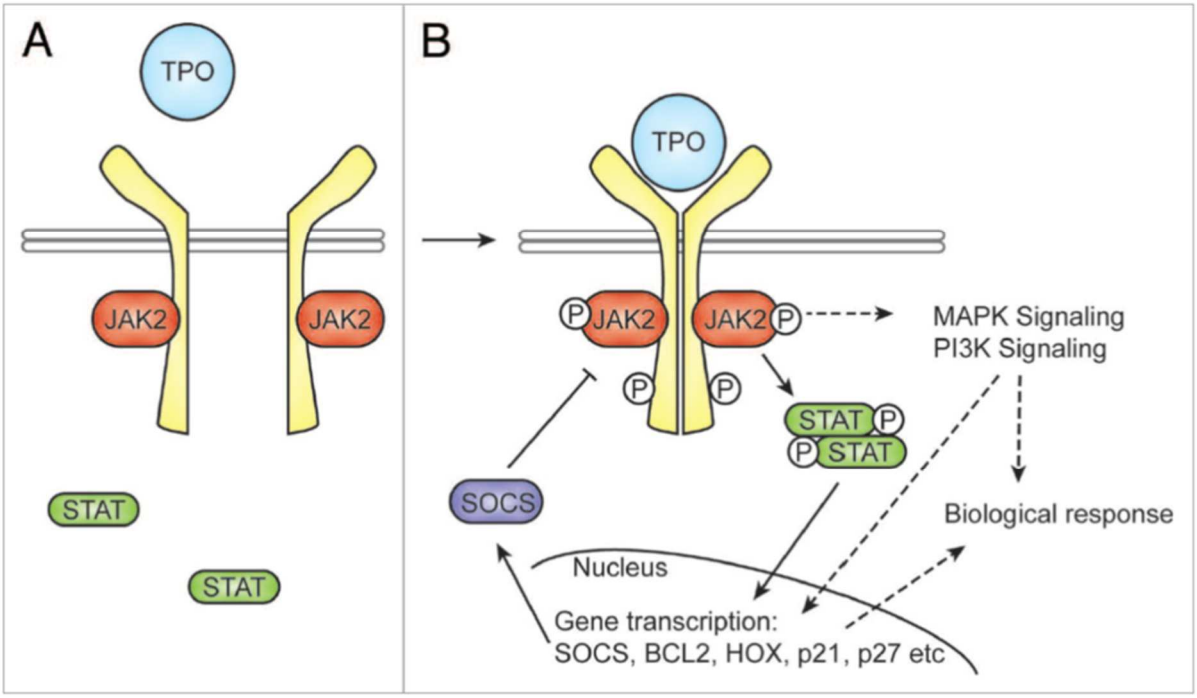

Figure 2: TPO signaling pathway. (A) Unstimulated cells. Mpl (yellow) exists as a monomer and signaling molecules are inactive. **(B)** Upon activation, Mpl dimerizes, resulting in phosphorylation of JAK2 and Mpl, respectively. Ultimately, downstream signaling pathways, including STATs, the MAPK pathway and the PI3K pathway are activated. JAK2 can phosphorylate STAT3 and STAT5 in response to TPO signaling, which results in dimerization and translocation to the nucleus. Taken from de Graaf *et al*. [21].

During their maturation, MKs undergo several rounds of endomitosis, a process characterized by repeated, incomplete cell cycles with failure of both karyokinesis and cytokinesis [22]. This process leads to polyploid and multi-lobed nuclei with a range from 2 N – 128 N and a mean ploidy of 16 N in humans and mice, respectively. This process is accompanied by the synthesis of organelles, granules and cytoskeletal proteins. A characteristic of mature MKs is the development of the *demarcation membrane system* (DMS), a highly invaginated membrane system, which has continuity with the plasma membrane and serves as a membrane reservoir for future platelets [23]. At the end of this maturation process MKs are equipped with the components needed for platelet production.

In vivo, mature MKs release up to 5000 platelets into the circulation. Therefore, they form transendothelial pseudopods that elongate into 100 to 500 µm long proplatelet shafts. Microtubules polymerize throughout the proplatelet shaft and form ring-like structures at the tip. This structure resembles the microtubule coil in resting platelets and is important for later platelet function. The branched proplatelets undergo shear force dependent abscissions to finally shed off circulating platelets [24] (Fig. 3).

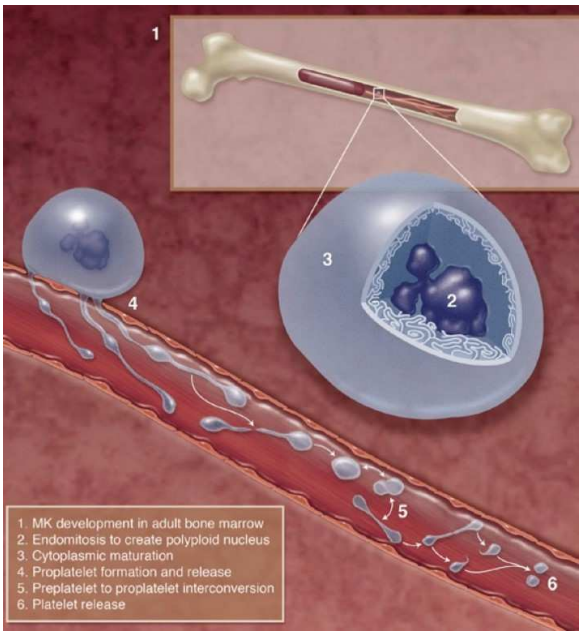

Figure 3: Scheme of *in vivo* platelet formation. TPO levels determine bone marrow HSC differentiation into MKs (1). During maturation, MKs undergo endomitosis resulting in polyploid cells, with a DNA content up to 128 N (2). Further, MKs develop the so-called demarcation membrane system, providing membranes for future platelets (3). In the last step, MKs extend protrusions into the vessel lumen (4), where the formed proplatelets (5) undergo multiple abscissions to form platelets (6). Adapted from Machluls and Italiano [23].

1.2 Platelets

Platelets are small, anucleate, discoid-shaped cell fragments with a size of 3-4 µm in humans and approximately 2 µm in mice [25]. With numbers of 150-450 x10^3/µL in humans and approximately 1000 x10^3/µl in mice, they are the second most abundant cell type in blood and are constantly released from MKs [9]. Human platelets have a lifespan of 7-10 days, whereas mouse platelets have a shorter lifespan of ~5 days [26]. Aged, pre-activated or dysfunctional platelets are constantly removed from the bloodstream by macrophages in the liver or spleen by the reticulo-endothelial system and replenished by constant platelet production of BM MKs (see 1.1.2) [27, 28].

The main function of platelets is described as maintenance of hemostasis. In the last decades, however, studies found platelets to be involved in processes including immune surveillance and inflammation [29-33]. Platelets can rapidly respond to damage of the vessel wall forming plaques to prevent massive blood loss. Thereby, platelets interact with exposed proteins of the *extracellular matrix* (ECM) such as laminins or collagens and initiate platelet adhesion and

activation [34, 35]. In addition, soluble agonists are released by activated cells that, together with locally produced thrombin, amplify platelet activation, thus increasing thrombus formation at the site of injury. Under pathological conditions, such as thrombosis or rupture of an atherosclerotic plaque, uncontrolled and sustained platelet activation can lead to occlusive thrombus formation leading to vessel occlusion and infarction of vital organs, such as ischemic stroke or myocardial infarction [36, 37]. Therefore, platelet activation has to be tightly regulated. On the one hand, proper platelet function ensures efficient plaque formation minimizing blood loss, while on the other hand, uncontrolled platelet adhesion and activation has to be prevented. This requires tight regulation of multiple activatory and inhibitory platelet receptors and a complex network of signaling events.

1.2.1 Platelet activation and thrombus formation

Platelet activation and subsequent thrombus formation is a multi-step process which can be divided into three major steps: 1) initial platelet tethering, 2) platelet activation and granule release and 3) firm adhesion and thrombus growth (Fig. 4).

Under intermediate or high shear conditions (1,000-10,000 s^{-1}) *glycoprotein* (GP) Ibα, which is part of the GPIb-V-IX complex, weakly binds to collagen-associated *von Willebrand factor* (vWF). This interaction only takes place at shear forces >1000 s^{-1} and its importance is increasing with the shear rate. GPIbα binding to vWF leads to deceleration and rolling of platelets along the vessel wall and enables further interactions with proteins from the ECM such as fibronectin, collagen or laminin [38].

After deceleration, platelets can directly bind to the collagen on the ECM via GPVI. This interaction induces platelet activation via intracellular signaling through *immunoreceptor tyrosine-based activation motifs* (ITAM) in the associated *FC receptor* (FcR) γ-chain, ultimately leading to platelet activation. During this process, levels of intracellular calcium (Ca^{2+}) increase, negatively charged *phosphatidylserine* (PS) is exposed on the platelet surface. Furthermore, cytoskeletal rearrangements take place as well as mobilization of dense and α-granules, thus releasing second wave mediators *adenosine triphosphate* (ATP), *adenosine diphosphate* (ADP), *thromboxane A2* (TxA2), calcium and serotonin [29]. In combination with exposed *tissue factor* (TF), thrombin generation is induced, leading to strong platelet activation via *G-Protein coupled receptor* (GPCR) stimulation.

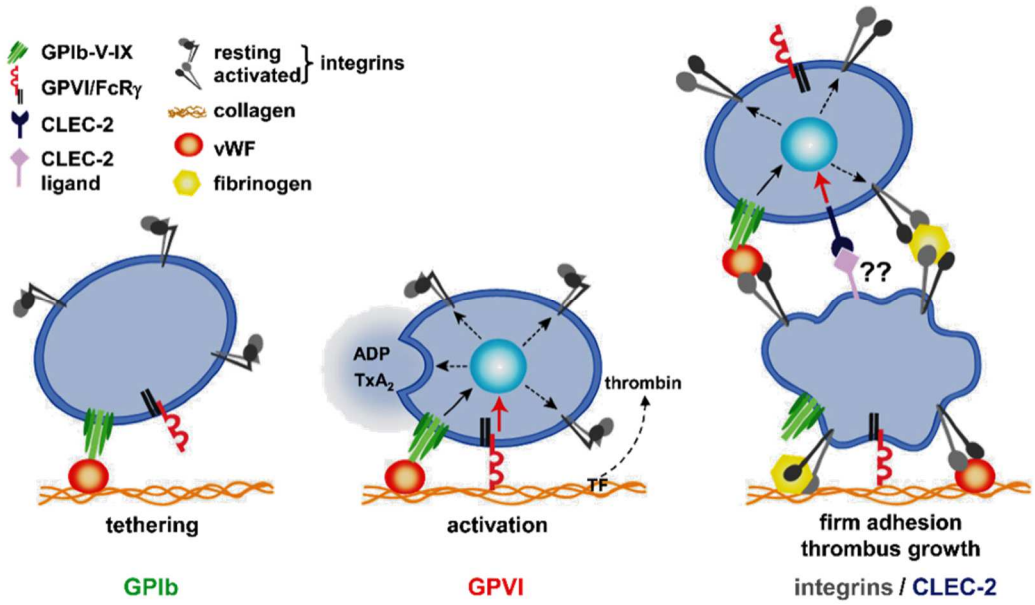

Figure 4: Schematic overview of platelet activation and thrombus formation. Cellular damage exposes components of the extracellular matrix (ECM) and enables platelets to tether via interaction of GPIb with collagen bound vWF. Tethering then enables interaction of GPVI to collagen, inducing a cascade of signaling events that lead to the release of second wave mediators, such as ADP or thromboxane A2. Exposure of tissue factor triggers thrombin generation, which contributes to platelet activation and PS exposure. These events lead to integrin activation, converting them to a high affinity state, where they mediate firm platelet adhesion and result in thrombus growth. Taken from Nieswandt *et al.*, 2011 [29].

Finally, firm adhesion and thrombus growth is mediated by integrin activation. Here, the integrin receptors undergo a conformational change from a low affinity state (inactive) to a high-affinity stage (active) through extra- and intracellular signaling events (inside-out signaling) [34, 35]. Activated α2β1 integrins can then bind to collagen and laminin, α5β1 integrin to fibronectin, α6β1 integrin to laminin, whereas αvβ3 integrin binds to vitronectin and the αIIβ3 integrin to collagen via vWF (outside-in signaling) [39, 40]. The binding of αIIbβ3 to fibrinogen, mediates platelet-platelet interactions and incorporation into the growing thrombus [29].

1.2.2 Platelet functions beyond thrombosis and hemostasis

In addition to thrombosis and hemostasis, platelets play important roles in (patho)physiological processes, such as embryonal angiogenesis [41], cancer metastasis [42] and inflammation [43-45]. There, platelets are involved in recruitment of immune cells and maintenance of vascular integrity after immune cell extravasation or clearance. Further, during the last decade, platelets were gradually recognized as immune modulators and cells with immune functions [32, 44, 46]. Their ability to interact with potentially all other immune cells enables them to influence both the innate and adaptive immune response, respectively [31, 47, 48].

The general mechanisms are similar to platelet activation: initial attachment is mediated by GPIbα interactions towards P-selectin and vWF, whereas firm adhesion is mediated by the

integrin αIIbβ3 binding to fibrinogen and *intercellular adhesion molecule* 1 (ICAM1) [49, 50]. However, other receptors can account for platelet-immune cell interactions and are currently under investigation.

Blockade of functional GPIbα using p0p/B Fab fragments [51], preventing GPIbα-vWF interactions, as well as lack of the extracellular domain of GPIbα (using transgenic GPIb-hIL-4R mice) [52] significantly reduce infarct volumes and neurological scores without increasing the risk for intracerebral hemorrhage in a model of ischemic stroke. Likewise, pharmacological inhibition of GPIbα using anfibatide, a snake venom derived antagonist, leads to comparable results [47]. Blockade of GPIbα reduced microvascular occlusions, improving blood flow, vessel patency and tissue perfusion [37, 53].

Blockade of the main activatory collagen receptor GPVI in ischemic stroke and *acute myocardial infarction* (AMI) results in reduced infarct size and improved neurological outcome [37, 54, 55], whereas enhanced GPVI signaling leads to opposite results with increased infarction volumes and severe neurological defects [56]. In line, GPVI stimulation results in the production of proinflammatory IL-1α/β-rich platelet-derived microparticles, which further promote inflammation in experimental rheumatoid arthritis [57, 58]. Furthermore, GPVI depletion leads to reduced neutrophil infiltration in AMI [59] resulting in better outcomes. Although blockade or depletion of GPVI might be a promising tool for the treatment of myocardial infarction or other ischemic settings, the mechanism of how GPVI depletion protects against ischemia reperfusion injury is not fully clear.

The integrin αIIbβ3 is the most abundant integrin on the platelet surface [60] and plays an important role in promoting platelet interactions towards the endothelium [29]. In addition, it is critically required to form stable platelet aggregates [61] and therefore represents an attractive target to reduce platelet aggregates in a variety of clinical scenarios. At the moment, there are three GPIIb/IIIa (αIIbβ3) inhibitors approved for clinical use: abciximab, eptifibatide and tirofiban [62-64]. These inhibitors have been studied in the no-reflow phenomenon, which is defined through inadequate perfusion in the absence of mechanical vessel obstructions (ref). After GPIIb/IIIa antagonist administration the no-reflow phenomenon was found to be increased, indicating a positive role for GPIIb/IIIa in this process [65, 66]. Furthermore, a rat model of myocardial infarction showed a dose dependent beneficial effect of GPIIb/IIIa blockade, which correlated with decreased cardiomyocyte apoptosis and reduced neutrophil infiltration [67]. Similar results were obtained in humans, where integrin blockade resulted in improved microvascular perfusion, vessel patency as well as diminished platelet-leukocyte interaction [68]. In other settings of ischemia, the situation differs dramatically. In experimental models of ischemic stroke, a complete blockade of GPIIb/IIIa led to significantly increase in intracranial bleeding [37]. Furthermore, mice which do not die from intracranial bleedings

following GPIIb/IIIa antagonist administration, exhibit infarct volumes comparable to control animals. Translation into clinical studies confirmed a poorer outcome following GPIIb/IIIa blockade thus dampening enthusiasm for this approach [69].

Another mechanism for platelets to act as cells with immune function is the expression of *CD40 ligand* (CD40L = CD154). CD40L is a transmembrane molecule involved in cell signaling of innate and adaptive immunity [70, 71]. It is expressed in a variety of cells with activated T cells and platelets being the most abundant ones. The main receptor is CD40 and can be found on antigen-presenting cells such as B cells, macrophages or dendritic cells [70-73]. CD40L however, can also be shed from the surface leading to a soluble form of CD40L (sCD40L). The soluble form acts as a potent chemotactic agent and is able to activate integrins on neutrophils and upregulation of endothelial platelet ICAM-1, *vascular cell adhesion molecule 1* (VCAM-1) and E-selectin. Furthermore, interaction of platelets and sCD40L lead to increased P-selectin exposure, platelet aggregation as well as increased binding to leukocytes [74-76]. CD40 is highly expressed in inflamed tissue and inhibition of sCD40L generation attenuates (platelet-derived) *reactive oxygen species* (ROS) production [77], dampening the inflammatory response.

An association of platelets/thrombosis and cancer has been recognized as early as 1865 by Amrand Trousseau and has been studied since [78]. Especially in the last decades new findings were made. The high risk of cancer patients to develop thrombosis accounts for the capacity of cancer cells to activate platelets via different routes. This can be achieved by direct release of platelet-activating mediators such as ADP [79], thrombin [79, 80] or thromboxane A_2 [79, 81] or the expression of platelet ligands such as podoplanin [82, 83], the ligand for CLEC-2, from cancer cells. Furthermore, cancer cells can bind to FcγRIIa and induce dense granule secretion, including mediators such as ADP and serotonin [84].

In the tumor vasculature, platelets contribute to homeostasis by maintaining vascular integrity thus preventing hemorrhage [85]. Antibody-induced thrombocytopenia results in profound bleeding within the tumor, without affecting non-tumor vasculature [86, 87]. Interestingly, platelet depletion leads to the accumulation of chemotherapeutic agents in the tumor vasculature, slowing down tumor progression [88]. Due to massive side effects on hemostasis, platelet depletion is no valid treatment option. Therefore, platelet receptors such as GPVI are under investigation to identify molecular mechanisms on how platelets maintain vascular integrity in tumors without affecting classical hemostasis. Our group was able to show that the inhibition of GPVI induces massive intra-tumor hemorrhage [89], without increasing the overall risks of bleeding complications. Furthermore, GPVI administration leads to enhanced delivery of chemotherapeutic agents into the tumor, diminishing tumor growth.

1.2.3 Platelet – neutrophil interactions

Upon inflammation, neutrophils are rapidly recruited from the blood stream to the site of inflammation, where they release proinflammatory chemokines and cytokines to attract other inflammatory cells [90]. In addition to their well-known functions in hemostasis and thrombosis, platelets are essential regulators of leukocyte recruitment and effector function in a wide range of inflammatory conditions. Platelet depletion or blockade of their interaction with neutrophils or endothelial cells significantly reduces neutrophil recruitment in settings of pulmonary inflammation, atherosclerosis, peritonitis and others, suggesting that platelets are required for their recruitment [91-93].

Neutrophil recruitment follows a distinct pattern starting with loose tethering to the vessel wall, followed by rolling along the endothelium, integrin mediated arrest and firm adhesion with subsequent activation and release of pro-inflammatory mediators into the surrounding tissue, intravascular crawling and transmigration [94-96]. There is evidence, that these interactions can take place with and without platelets, however platelets seem to amplify the interaction [49, 97].

As described in 1.2.1, platelets are able to adhere to immobilized vWF at high shear rates. This deceleration enables platelet activation via various receptors, ultimately leading to GPIIb/IIIa integrin activation. Subsequent binding to fibrinogen and other ligands mediates firm adhesion to the vessel wall. Neutrophil rolling on immobilized platelets is mediated by platelet P-selectin and neutrophil *P-selectin glycoprotein ligand-1* (PSGL-1) binding. Blockade of this interaction using P-selectin deficient animals or antibody-mediated PSGL-1 blockade, results in diminished neutrophil rolling or abolished interaction with each other or with the endothelium [91, 98-102]. Binding of this receptor-ligand pair induces inside-out signaling that causes neutrophil β2 integrins to adopt an open confirmation [103-105].

Firm adhesion of platelets and neutrophils is achieved by interactions of platelet ICAM-2 and neutrophil integrin *leukocyte function antigen*-1 (LFA-1, αLβ2) as well as platelet GPIbα and neutrophil integrin *macrophage-1 antigen* (Mac-1, αMβ2) [106]. Furthermore, platelets and neutrophils can bind via platelet CD40L and neutrophil CD40 (Fig. 5A and B). Without platelets, the interaction of neutrophils with the endothelium is mediated by interactions between neutrophil integrins VLA-4 (α4β1), Mac-1 and LFA-1 and receptors on the endothelial surface such as ICAM-1, ICAM-2, VCAM-1 or the *receptor for advanced glycation endproducts* (RAGE) [107].

Activated platelets release a wide range of chemokines that are able to activate neutrophils. These chemokines include *platelet factor 4* (PF4, CXCL4), *RANTES* (CCL5), *neutrophil activating peptide-2* (NAP-2, CXCL7) and are involved in neutrophil chemotaxis and neutrophil

transmigration. Neutrophil transmigration can take place at the site of tight junctions between adjacent cells (paracellular) or through an endothelial cell (transcellular) [50, 108-111].

Activated endothelium enhances expression of adhesion molecules such as ICAM-1 and VCAM-1 which form pro-adhesive sites termed *endothelial adhesive platforms* (EAPs) [95, 112]. Intracellular signaling induced by neutrophil binding leads to changes in endothelial contractility or junctional integrity by regulation of tight junction proteins such as V-cadherin [113, 114]. There is experimental evidence, that paracellular neutrophil transmigration is actively facilitated by *platelet endothelial cell adhesion molecule 1* (PECAM-1), ICAM-1 and *junctional adhesion molecule A* (JAM-A) [111]. However, the underlying mechanisms are still under investigation. The following, simplified sequence of events shows distinct and sequential roles of the aforementioned receptors. First, a haptotactic gradient to guide neutrophils to the endothelial junctions is provided by ICAM-1 molecules on the luminal surface of the endothelial cell. Once, neutrophils are within the junctions, homophilic interactions between endothelial and neutrophil PECAM-1 stimulate neutrophils to express the laminin receptor, integrin a6β1, facilitating the passage through the endothelial layer. The completion of this transition is mediated by endothelial JAM-1 binding, possibly towards LFA-1 [115, 116].

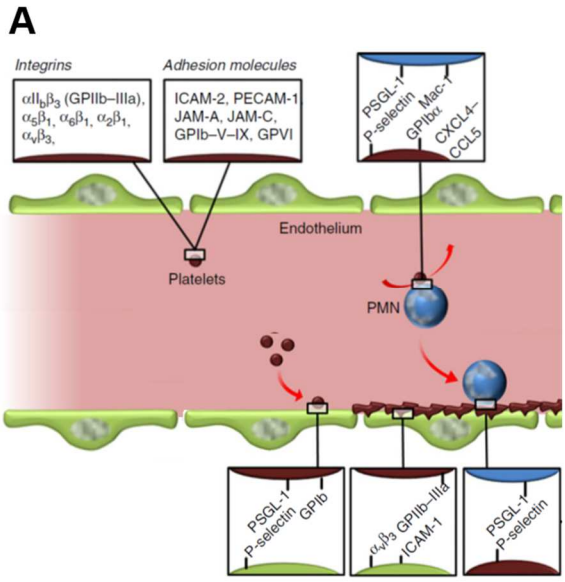

B

Endothelial cells		Platelet		Neutrophil
CD40	↔	CD40L	↔	CD40
Fibrinogen, fibronectin	↔	GPIIb/IIIa	↔	Mac-1
P-selectin, vWF	↔	GPIbα	↔	Mac-1, ICAM-1
		ICAM-2	↔	LFA-1
Possibly GPIbα	↔	P-selectin	↔	PSGL-1, L-selectin

Figure 5: Model of platelet-neutrophil interactions (A) Mechanisms of platelet-neutrophil and platelet-endothelial cell interactions. Receptors and corresponding ligand pairs are shown in boxes. Initial platelet- endothelial interactions are mediated by P-selectin and PSGL1, whereas firm adhesion is mediated by GPIIb/IIIa and ICAM1. Platelet-neutrophil interactions take place via P-selectin – PSGL-1 and GPIbα – Mac-1 binding. Secondary capture to the endothelial-bound platelets is mediated via P-selectin and PSGL-1. (Modified from Herter *et al.* [44]). **(B)** Receptor-ligand pairs of endothelial cells, platelets and neutrophils. (Modified from Zarbock [117]).

Initiation of transcellular neutrophil migration (Fig. 6) is similar to paracellular migration. After firm adhesion to the endothelium, neutrophils migrate over the endothelial cell, searching for arears to build transcellular pores [118]. Neutrophils form *invadosome-like protrusions* (ILPs),

which cause small endothelial cell surface invaginations [119, 120]. At sites of sufficiently low endothelial resistance ILPs breach the endothelium intracellularly. As in paracellular transmigration, ICAM-1 and PECAM-1 seem to be involved in the transmigratory process [50, 111, 121].

Platelets or platelet-derived microparticles can also be found in inflamed tissue [122], although the underlying mechanism of how platelets “extravasate” is unclear. Three possible scenarios are suggested: indirect transport by piggy-backing on neutrophils, indirect flushing through damaged and leaky endothelium or active migration mediated by chemotaxis [123-126]. As there is evidence for all possibilities, further studies need to be performed, to determine whether all possibilities happen in equal measure or whether it is time-, organ- and/or inflammation-dependent.

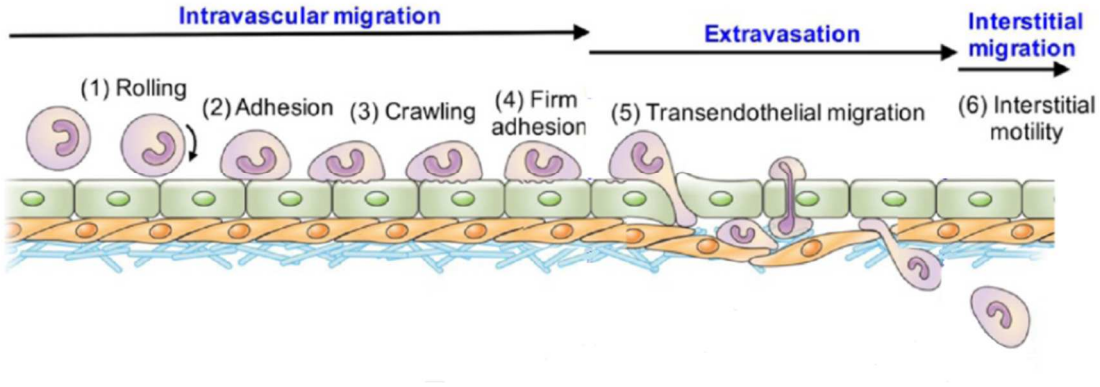

Figure 6: Scheme of the neutrophil transmigration cascade. During the process of intravascular migration, neutrophils interact with endothelial cells via (1) rolling, (2) adhesion and (3) crawling. Thereafter firm adhesion (4), the neutrophil approaches a proper site for extravasation, (5) where they transmigrate through the endothelial cells, pericyte and basement membrane (modified from Park *et al*. [127]).

1.3 The liver

In vertebrae, the liver is the largest glandular organ and plays key roles in metabolism. It is a regulatory center for the production of proteins such as coagulation factors, utilization of nutritional components, production of bile and concomitant breakdown of metabolic products, toxins and medications [128].

1.3.1 Structure and cellular organization of the liver

In humans, the liver locates in the right upper quadrant of the abdomen, to the right of the stomach, directly below the diaphragm. It can have a width of ~15 cm and weigh up to 1.5 kg [129]. The murine liver weighs up to 3 g accounting for 3-5% of the body weight and spans the

whole subdiaphragmatic space [130]. In contrast to humans, the murine liver is relatively smooth and uninterrupted by large and thick surface ligaments [131]. The human liver can be separated into four distinct lobes: the large right lobe and the small left one on the anterior of the organ as well as upper caudate and the lower quadrate lobe on the visceral surface. Peritoneal ligaments not only secure the liver position in the upper abdominal cavity, but also serve as landmarks [129]. Most prominent are the *falciforum* ligament, which separates right and left lobe as well as the coronary ligament, that attaches the liver to the diaphragm. Caudate and quadrate lobe are separated by the liver *hilus*, where portal vein and hepatic artery enter the liver and the hepatic bile duct is present (Fig. 7A).

Abdominal ligaments traversing and distinctly delineating liver lobes are not evident in mice (Fig. 7B). However, the murine liver can be divided into right, median, left and caudate lobe as well. Although lobe patterns differ, functions are highly conserved in both species.

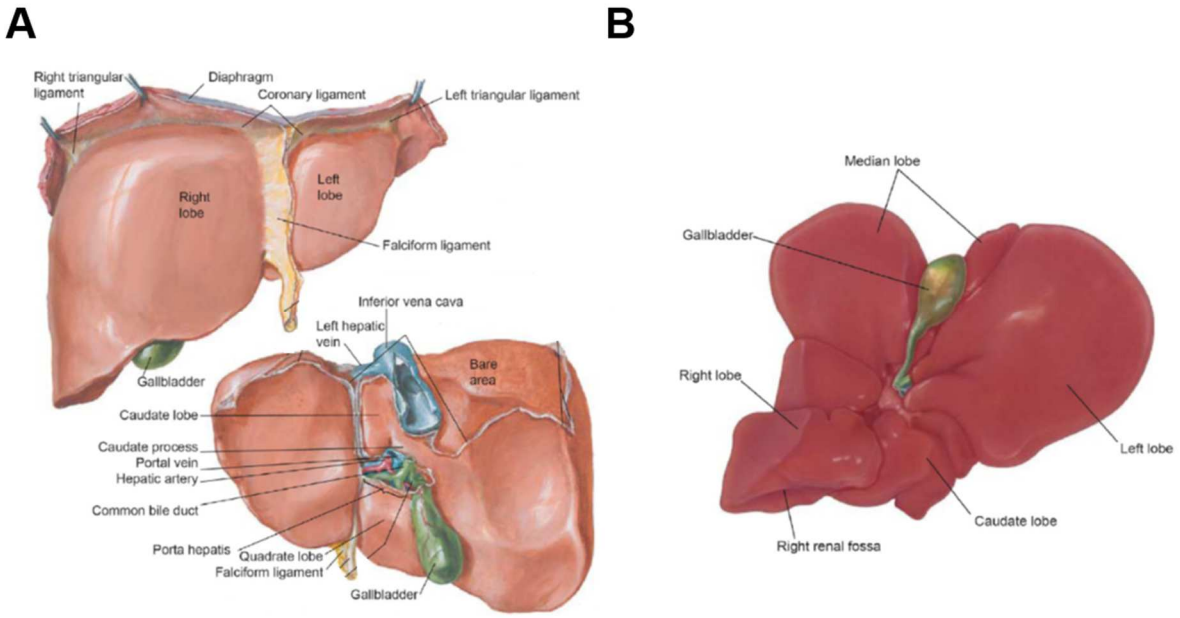

Figure 7: Regional and gross anatomy of the human and murine liver. (A) The human liver is marked by numerous prominent surface ligaments and composes of four lobes: left, right, caudate and quadrate lobe. **(B)** The mouse liver lacks obvious surface ligaments and composes of the left, right, median and caudate lobe. (Adapted from [130]).

Microscopically, human and mouse liver are very similar to each other. They are built up of lobules, the hexagonal, functional units of the liver (Fig. 8), which are comprised of parenchymal cells (hepatocytes) and organized in chord like structures through non-parenchymal cells such as (biliary) epithelial cells, *Kupffer cells* (KCs) or *hepatic stellate cells* (HepSC) [132]. Each lobule has a central vein and is surrounded by so called portal triads at the corners of the lobule. The term portal triad is misleading, since the portal triad is built of five structures, but was established before all of its components were discovered [133]. The

portal triad consists of a hepatic artery, which supplies the tissue with oxygen, a venule branch of the hepatic vein, which carries blood high in nutrients but low in oxygen as well as a bile duct, lymphatic vessels and a branch of the *vagus* nerve [134].

The liver sinusoids, capillary like veins, extend from portal veins and meet in the central vein. Approximately 15-30 hepatocytes arrange alongside the sinusoids and fulfill quite heterogeneous functions, such as glycolysis (pericentral area) or urea synthesis (periportal side), depending on their location [135]. The sinusoid walls are built from *liver sinusoidal endothelial cells* (LSECs), endothelial cells lacking a basement membrane and displaying clusters of fenestrations (50-150 nm; sieve plates), making them the most permeable endothelial cells in the body [136]. LSECs clear waste products, immune complexes or lipoproteins (<0.5 µm) through endocytic receptors and create a barrier for bi-directional transport of small molecules between blood and the space of Disse, the area between LSECs and hepatocytes [137], where HepSCs reside. Large particles are cleared by liver resident macrophages (KCs), the cleaned blood finally collects in central veins.

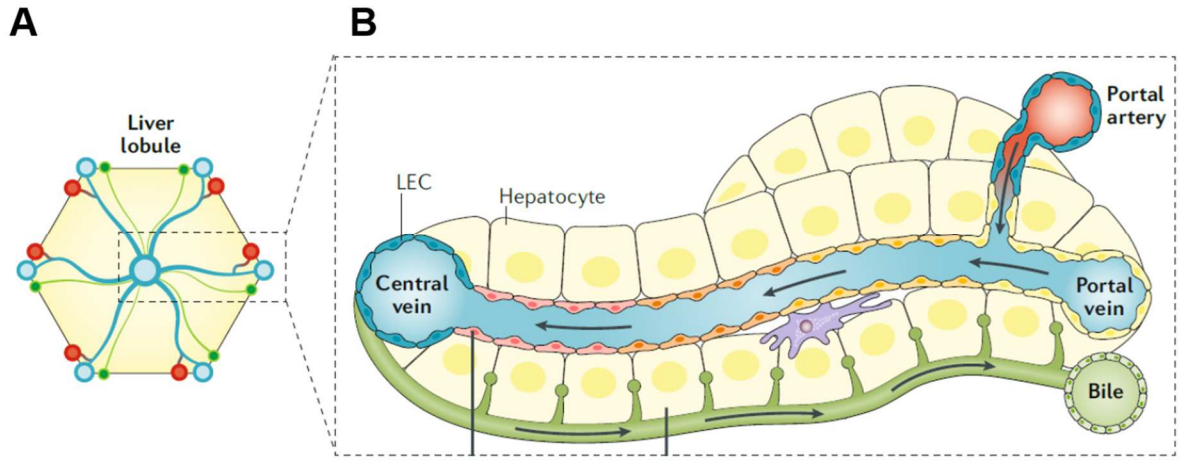

Figure 8: Microscopic structure of the liver. (A) Classical architecture of a liver lobule. The hexagonal structure is centered by a draining vein, with portal triads, consisting of portal vein, hepatic artery, bile duct at each of the corners. **(B)** Architecture of a liver acinus. Blood flows from the portal triad towards the central vein. LEC: liver sinusoid endothelial cell; purple: Kupffer cell. (adapted from Ben-Moshe [138]).

1.3.2 Hepatic ischemia reperfusion injury (h I/RI)

Ischemia reperfusion injury (I/RI) is a phenomenon, where the tissue damage in a hypoxic organ exacerbates following restoration of blood supply [139, 140]. Unfortunately, it is so far an unavoidable surgical complication of organ transplantation or partial liver resection and can lead to early graft dysfunction [141].

Hepatic ischemia reperfusion injury has been extensively studied in mice and rats [142] with 20-100% liver occlusion for different ischemic periods. Hepatic ischemia can either be “warm” (normothermic) or “cold” (hypothermic) [143]. Warm ischemia indicates, that the procedure

takes place at body temperature, whereas cold ischemia usually takes place during transplantation, where the donor organ is kept on ice to reduce metabolic activities and cellular damage [144, 145].

Most studies are conducted animal models with 60 minutes of 70% warm ischemia, by occlusion of the left and median lobe, and 3-6 hours or 24-48 hours of reperfusion. Nonetheless, the duration of the ischemic phase is decisive for the severity of injury. Ischemic periods of 70% liver occlusion show that up to 60 minutes result in reversible cell damage, whereas periods of 90-180 minutes result in irreversible cell damage associated with high mortality rates [146, 147].

Already after one hour of reperfusion, liver associated damage markers such as AST, ALT and LDH increased and peaked after 3-4 hours [148]. H&E stainings reveled first structural changes after 30 min ischemia and 3 hours of reperfusion [149].
Prolongation of the ischemic period to 60 minutes results in even higher serum transaminase levels as compared to 30 minutes ischemia [150]. Damage and inflammation markers peak at around 6 hours and decline afterwards [151, 152]. 60 minutes ischemia leads to hepatocyte swelling and a significantly increased amount of necrotic and apoptotic cell death as well as substantial neutrophil infiltration after three hours of reperfusion [152, 153]. However, 60 minutes of ischemia are not considered to be lethal [151, 154].
The point of no return seems to take place, when the duration of 60-90 minutes of 70%, warm ischemia is exceeded [155]. 90 minutes ischemia are accompanied by low survival and massive cellular damage, including hepatocellular necrosis [156, 157], swelling [157] as well as mixed dilation and congestion in the sinusoids [146, 157, 158]. Neutrophil infiltration throughout the sinusoidal spaces and necrotic areas could be observed as well [156, 158].

The I/RI cascade can be divided into three phases: ischemia, early reperfusion and late reperfusion, which ideally results in complete resolution of the inflammation. Figure 9 gives an overview of the course of inflammation and cell types involved in reperfusion injury.

Recanalization initiates the early phase of reperfusion. Hepatocytes are metabolic highly active cells, so oxygen exhaustion results in immediate ATP depletion and an imbalance in ion homeostasis, leading to swelling and subsequent activation of LSECs and KCs.

Nitric oxide (NO), a vasodilator, relaxes the inner muscles of blood vessels leading to widening of the vessel. Endothelins, are peptides which regulate constriction of the blood vessel (vasoconstrictors). Under steady state, NO and endothelin maintain constant blood flow and pressure [159]. Following ischemia, NO synthesis is decreased which leads to narrowing of the sinusoidal lumen causing microcirculatory dysfunction [160-162]. At the same time, the

narrowing induces KC activation which leads to additional release of ROS and pro-inflammatory cytokines, including *tumor necrosis factor alpha* (TNF-α), *interleukin-1* (IL-1) and *Leukotriene* (LT) B_4 [148, 163, 164]. This mechanism contributes to neutrophil infiltration, accumulation and adhesion to the liver sinusoids [165], a hallmark of inflammation and early reperfusion. The infiltrating neutrophils are activated by ROS and induce release of pro-inflammatory molecules, such as LTB_4 and *platelet activating factor* (PAF), themselves. LTB_4 amplifies the neutrophil response through well–characterized biological actions, including the promotion of leukocyte chemotaxis and the regulation of proinflammatory cytokines by binding to a GPCR termed *leukotriene B_4 receptor 1* (BLT1) (see section 1.4.1 and 1.4.2), whereas PAF can prime neutrophils for superoxide production resulting in drastic increase of ROS [166].

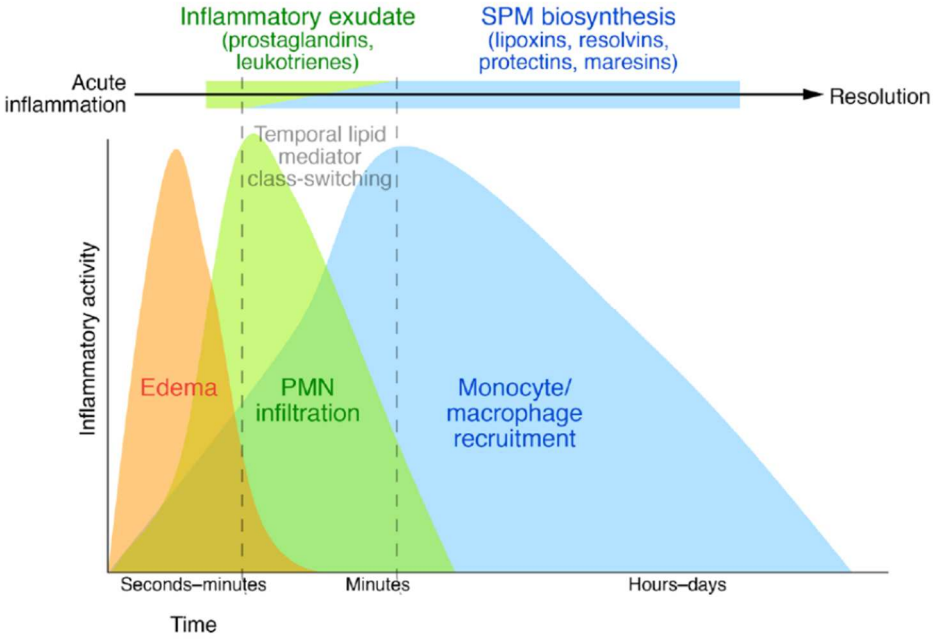

Figure 9: Steps in the acute inflammation. Edema formation, PMN infiltration and non-phlogistic monocyte-macrophage recruitment to inflammatory exudates. The reduction in PMN number coincides with the exudate appearance of lipid mediators and with the biosynthesis of lipoxins, resolvins (E- and D-series), protectins, and maresins in resolving exudates. (taken from Serhan and Levy [167]).

Furthermore, IL-1 and TNF-α are known to recruit and activate $CD4^+$ T cells, which then release *granulocyte-macrophage colony stimulating factor* (GM-CSF), *interferon gamma* (INF-γ) and lymphotoxin α, which in turn further activate/stimulate KCs. This forward loop amplifies KC activation and consequently also TNF-a and IL-1 release and can lead to an uncontrolled inflammatory response [168].

Zhang *et al.* [169] subjected mice to hepatic ischemia and performed lipidomic analysis of liver tissue obtained at different time points of reperfusion in comparison to sham-operated animals. They found an enrichment of *arachidonate 12-lipoxygenase* (ALOX12) and its intermediate *12-*

hydroxyeicosatetraenoic acid (12-HETE) in ischemic livers. Furthermore, they identified GPR31 to be the corresponding receptor involved in h I/RI, which exacerbates liver damage. Blocking the 12-HETE production inhibits ischemia-induced liver dysfunction, inflammation and cell death in mice and pigs [169], suggesting ALOX12 or 5-HETE as potential targets to prevent and treat I/R-induced liver damage.

Pharmacological agents that minimize effects of the reperfusion by reduction of the ROS burden and enhancing clearance of ROS-induced cellular damage are the most common strategy to avoid (hepatic) ischemia reperfusion injury [170]. In addition to pharmacologic agents, ischemic preconditioning is a method currently being under investigation. Here, organs such as the liver are subjected to short times of ischemia before a prolonged period of ischemia. In small animal models this method shows promising results, ameliorating the overall outcome and cellular damage [146, 171, 172]. However, translation into clinical practice showed mixed results [173] as some studies suggested beneficial effects, whereas others could not confirm this finding.

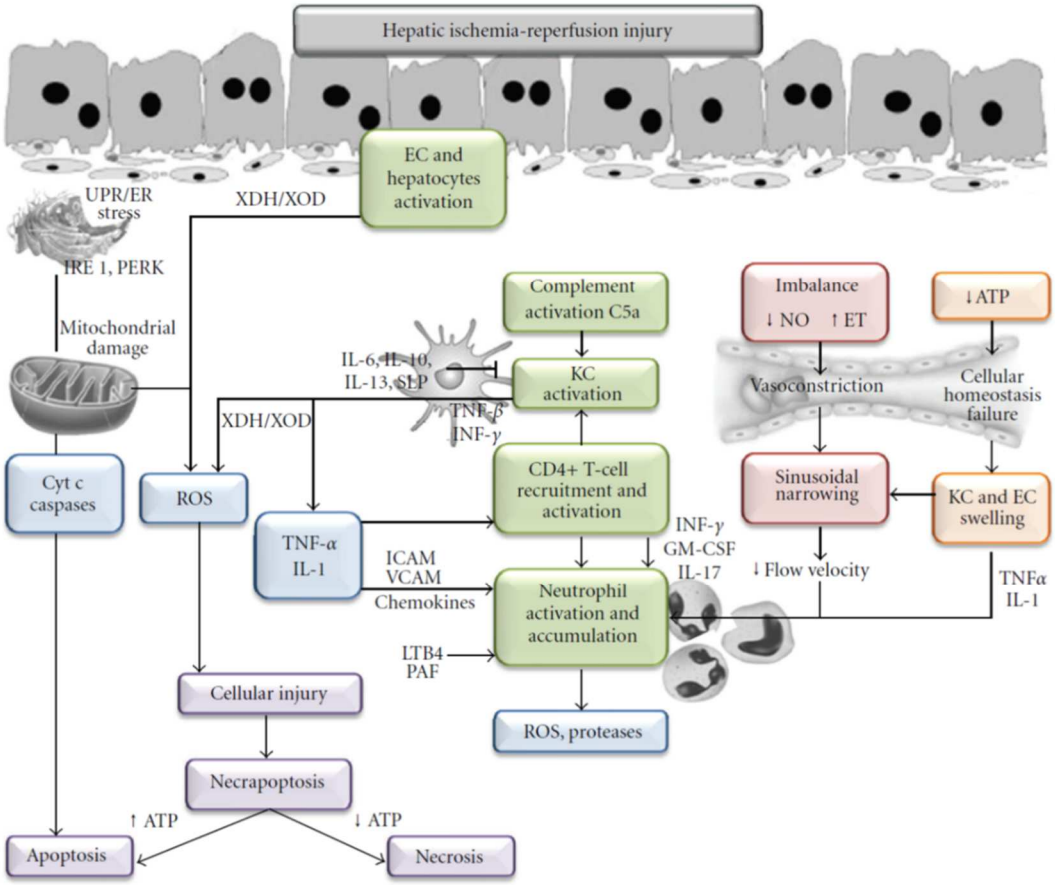

Figure 10: Mechanisms involved in hepatic ischemia reperfusion injury. EC, endothelial cell; ET, endothelin; UPR/ER, unfolded protein response/endoplasmic reticulum; IRE1, inositol-requiring enzyme 1; PERK, PKR-like R kinase; SLP, secretory leukocyte protease inhibitor; ICAM, intracellular cell adhesion molecule; VCAM, vascular cell adhesion molecule; GM-CSF, granulocyte-macrophage colony-stimulating factor; IL, interleukin; INF, Interferon; TNF, tumor necrosis factor; PAF, platelet-activating factor; LTB4, leukotriene B4; KC, Kupffer cell; X/XOD, xanthine/xanthine oxidase; Cyt c: cytochrome c [174].

1.3.3 The role of platelets in hepatic ischemia reperfusion injury

There are numerous studies investigating the role of immune cells in different settings of ischemia and although the role of platelets as immune modulating cells is emerging, more studies need to be performed to fully understand how they are involved and which interactions lead to progression of reperfusion injury.

The importance of the platelet GPIb-vWF axis in hepatic ischemia reperfusion injury is demonstrated by studies from Urisono *et al.* [175] who showed that vWF-deficient animals had significantly decreased levels of serum transaminases, which correlate with reduced neutrophil infiltration and overall decreased platelet-leukocyte interactions in the liver, showing profound protection from hepatic ischemia reperfusion [176].

Platelet aggregate formation, mediated by GPIIb/IIIa, causes impaired perfusion of the sinusoids that can be restored upon administration of anti-fibrinogen antibodies which effectively inhibit platelet aggregation [177, 178]. However, this treatment did not affect neutrophil infiltration. In some studies, platelet adhesion was also associated with increased thrombin activity, subsequent platelet activation and clearance from the circulation inducing thrombocytopenia [179]. Others report, that platelets adhere in the post-ischemic liver, but do not activate and degranulate [180].

Another study focused on the role of platelets, their function and platelet-derived serotonin in post-ischemic liver damage and regeneration. In this study, platelets were either inhibited by administering clopidogrel, an inhibitor of the ADP receptor $P2Y_{12}$ or depleted using anti-CD41 (αIIb, GPIIb) antibodies [181]. In addition, the impact of serotonin was assessed using tryptophan hydroxylase 1 deficient mice [181]. Nocito *et al*. showed that platelets have no direct impact on the pathogenesis of warm I/R injury as serum transaminase levels, leukocyte infiltration and tissue necrosis remained unaltered after both clopidogrel and CD41-treatment. Administration of anti-CD41 antibodies results in versatile immune reactions which might superimpose the effects of platelets. In addition, data from our laboratory (Stegner, Nieswandt unpublished) shows that CD41-opsonized platelets become located and trapped in the liver. According to Nocito *et al*., platelets mediate tissue repair and liver generation, since platelet depleted animals display impaired liver regeneration which is also reflected by impaired hepatocyte proliferation in serotonin-deficient mice [181]. However, these observations might result from overlapping effects during inflammation and resolution.

The degree of neutrophil infiltration into the post-ischemic liver is dependent on the inflicted liver damage determined by the ischemic phase. Induction of reperfusion injury following 30 minutes ischemia already shows neutrophil infiltration into the liver but to a lesser extend compared to induction by 90 minutes of ischemia. Platelet-neutrophil conjugate formation also

increases in a time-dependent manner [182]. Blockade of the main receptor pair for platelet-neutrophil interaction, P-selectin and its ligand PSGL-1 leads to reduced liver damage measured by serum transaminase levels [183, 184].

To study the role between platelet adhesion and neutrophil activation, neutrophil activation was selectively inhibited by administration of sivelestat, a selective inhibitor of the neutrophil elastase, before ischemia. Sivelestat leads to improved histological outcome and reduces levels of pro-inflammatory liver enzymes [185]. Furthermore, inhibition of neutrophil activation leads to significantly decreased numbers of adherent platelets in the post-ischemic phase [185].

Kupffer cells are the liver resident macrophages. They are the first responders towards the ischemia and their activation and subsequent ROS production causes platelet and leukocyte adhesion to the endothelium [186]. Early studies show that more than 50% of the adherent platelets are actually adhering to KCs [187]. Interestingly, the interaction of platelets and KCs in models of mild steatosis is reduced in contrast to healthy livers leading to attenuation of the liver damage. On the other hand, moderate steatosis increased platelet adhesion in contrast to mice with mild/normal steatosis following ischemia, thus aggravating liver damage [188].
In models of cold ischemia one third of the circulating platelets is rapidly sequestered in the liver after reperfusion. Adhesion of platelets to the endothelium mediates endothelial cell apoptosis [181] leading to increased graft injury. Single platelets adhere to the LSECs without morphological or dynamic evidence of impairment of microcirculation (Ref). Already one hour after reperfusion, a 6-fold increase in the number of LSECs is observed while hepatocyte necrosis or death is detected only after 3 hours of reperfusion [189].

1.4 The pancreas

The pancreas is an organ of the digestive system and located behind the stomach in the upper left part of the abdomen. The pancreas fulfils several endocrine and exocrine functions. The endocrine function regulates blood glucose levels by secretion of insulin, glucagon or somatostatin, whereas the exocrine function includes secretion of pancreatic juice which neutralizes gastric acid before entering the duodenum.

1.4.1 Structure and cellular organization of the pancreas

Macroscopically, the human pancreas can be distributed into three main parts: the head, the body and the tail (Fig. 11A). The head of the pancreas is defined by the superior mesenteric artery and aligned with the upper curvature of the duodenum. Body and tail are considered to

be separated at their midpoint, with the body lying underneath the stomach and the tail touching the hilum of the spleen. The human pancreas reaches a size of 14-18 cm in length and 2-9 cm in width and thickness, resulting in a weight of 50-100 g [190, 191].

The murine pancreas is less well defined and shows rather diffuse distribution in the mesentery of the small intestine [192]. Here, the three parts are called the duodenal, the gastric and the splenic part of the pancreas. The largest lobe in mice is the gastric lobe, which extends horizontally between duodenum and spleen and accounts for more than half of the total pancreas volume [193]. This part is considered to be homologous to the human body and tail of the pancreas whereas the duodenal part of the pancreas is homologous to the human head of the pancreas and is located at the mesenteries which surround the duodenum [194, 195]. The smallest part of the murine pancreas is the gastric lobe, protruding toward the stomach [196].

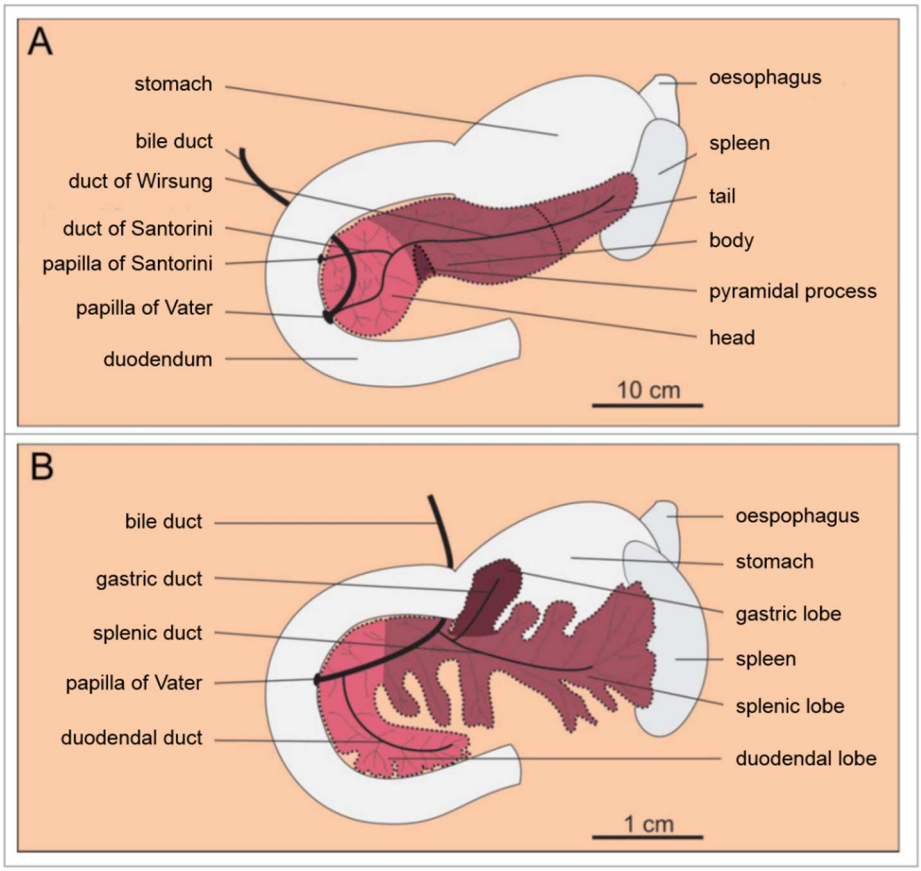

Figure 11: Anatomy of human and murine pancreas. **(A)**The human pancreas can be divided into head, body and tail, while the murine pancreas **(B)** is divided into duodenal duct, splenic duct and gastric duct. Color coding indicates homologous parts between humans and mice [197].

Microscopically, the pancreas can be further divided into the exocrine and the paracrine pancreas (Fig. 12). The exocrine pancreas can account for 96-99% of the total pancreatic mass, whereas the endocrine pancreas only covers 1-4% [190, 198].

The functional units of the exocrine pancreas are termed lobules and can measure 1-10 mm in diameter in humans and 0.5-1.5 mm in mice, respectively [199-201]. A pancreatic lobule is

formed of ascini, cluster of pyramidal cells forming dome-like structures. These ascini direct secretions from the apical poles toward the intercalate duct which further drains into intralobular ducts and finally into interlobular ducts. Interlobular ducts eventually converge into the main pancreatic duct which secretes into the duodenum just adjacent to the entrance of the common bile duct [202-204]. The exocrine pancreas secretes digestive enzymes such as proteases, lipases and amylase, water and bicarbonate to neutralize the stomach acid.

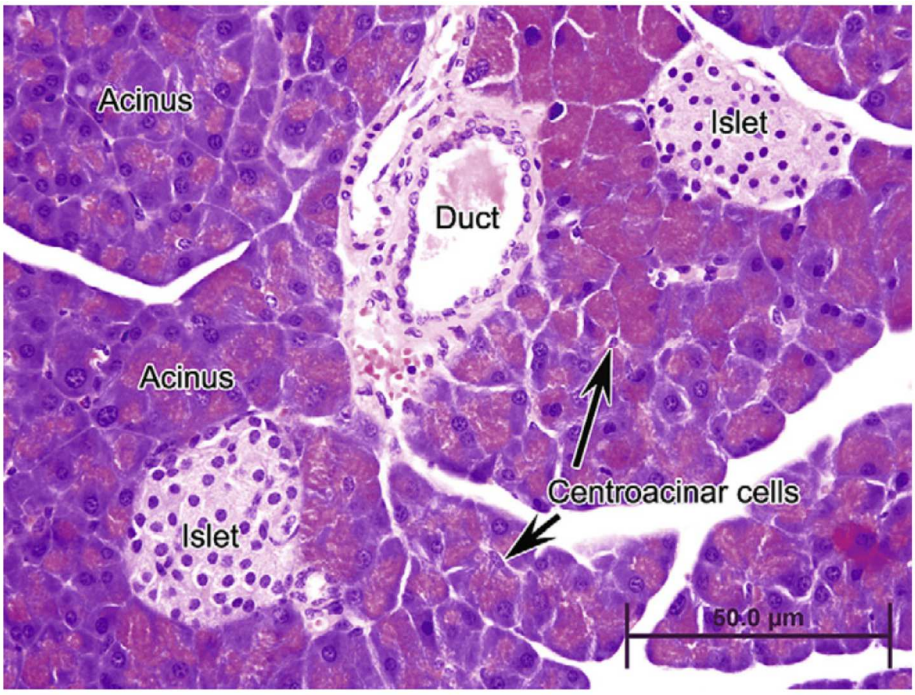

Figure 12: H&E staining of human endocrine and exocrine pancreas. Cellular structures of the exocrine pancreas (ascini - centroacinar cells and ducts) are shown. Endocrine pancreas is defined by Langerhans islets [205].

The endocrine pancreas consists of small areas termed islets of Langerhans [190, 198, 200, 204]. They show roundish to oval appearance, irregular profiles and consist of few to several thousand of cells. Size and distribution of Langerhans islets are comparable in humans and mice [200, 206-209], although single endocrine cells can be found throughout the ascinar tissue in both species. The islets consist of several hormone-secreting cells: α, β, δ, ε and *pancreatic polypeptide* (PP) cells. The insulin secreting β cells are the most abundant ones with 50-70% in humans and 60-80% in mice, respectively, while the α cells, with an abundance of 20-40% in humans and 10-20% in mice, secrete glucagon. Insulin regulates the uptake of glucose into cells and therefore reduces blood glucose levels while glucagon mediates the increase of blood sugar levels by conversion of glycogen into glucose. δ cells release somatostatin which can inhibit the growth hormone somatropin and the secretion of pepsin. PP cells release the pancreatic polypeptide and together with δ they account for only 10% of the pancreatic cells in humans and 5% in mice, respectively [207, 210-212]. The smallest population are the ε cells, which only account for 1% of the pancreatic cells and release the hormone ghrelin which for example induces the feeling of hunger [213].

1.5 Leukotrienes

Leukotrienes belong to the pro-inflammatory eicosanoids and can be divided into two major classes, the dihydroxy acid LTB_4 and the cysteinyl-leukotrienes (cys-LTs) which consist of LTC_4, LTD_4 and LTE_4 [214, 215].

They are produced in leukocytes and their name indicates this group of cells (leuko-) and the presence of three conjugated double bonds (-triene) which all leukotrienes share. Their production is usually accompanied by the production of histamine and prostaglandin which also act as inflammatory mediators [216].

1.5.1 Leukotriene biosynthesis

During leukotriene biosynthesis, arachidonic acid is cleaved from the nuclear membrane where it interacts with *5-lipoxygenase* (5-LO) and its *activating protein* (FLAP), resulting in the formation of 5-hydroperoxyeicosatetraenoic acid (5-HpETE). In addition to FLAP, *coactosin like protein 1* (COTL1), a regulator of the actin cytoskeleton, functions as a scaffold for 5-LO, increasing its activity [217]. In the next step, the 5-LO epoxide function transforms 5-HpETE into LTA_4 which contains the conjugated double bond characteristic for leukotrienes [218]. LTA_4 is an unstable intermediate which converted via *LTA_4 hydrolase* (LTA_4H) to form the potent chemotactic agent LTB_4. The conjugation of LTA_4 with a glutathione is catalyzed by the LTC_4 synthase, forming LTC_4 [219]. Sequential cleavage of LTC_4 ultimately leads to the formation of LTD_4 and LTE_4 (Fig. 13).

LTB_4 is able to activate neutrophils, allowing adhesion to the endothelium and mediating binding and transmigration into the surrounding tissue [220, 221]. Furthermore, it acts as a potent chemotactic agent and recruits neutrophils to areas of tissue damage where these produce ROS and promotes production of inflammatory cytokines in other immune cells [222].

Cys-LTs differ in their function in contrast to LTB_4. They act as potent bronchoconstrictors and show spasmogenic properties in the respiratory tract [223], exceeding the effect of histamine by far. In addition, they increase membrane permeability. These properties play crucial roles in allergic reactions, especially asthma bronchiale [224].

Leukotrienes signal via GPCRs. Four main receptors have been identified so far: BLT1 and BLT2 as receptors for LTB_4 as well as $CysLT_1$ and $CysLT_2$ as receptors for Cys-LTs. BLT1 was the first identified receptor and is highly expressed in inflammatory cells, such as neutrophils, dendritic cells or macrophages, B and T cells [225, 226]. As high affinity receptor of LTB_4, it mediates chemotaxis and calcium influx. Furthermore, BLT1 can activate different intracellular signaling pathways like MAPK, ERK or PI3K pathways inducing cellular activation [227]. BLT2 is the low affinity receptor of LTB_4, expressed on a variety of epithelial cells [228,

229], and mediates degranulation induced by LTB_4. The cysteinyl leukotriene receptor $cysLT_1$ is a high affinity receptor for LTD_4 and the main target for antagonists used for treatment of asthma. This receptor is highly expressed on blood leukocytes, the spleen as well as smooth muscle cells and interstitial macrophages of the lung. $CysLT_2$ binds with equal affinity to LTC_4 and LTD_4, although the binding towards LTD_4 is one log lower than its binding for $CysLT_1$. $CysLT_2$ is expressed on most cells, which also express cysLT1 and can furthermore be found in the heart, adrenal medulla and the placenta [230].

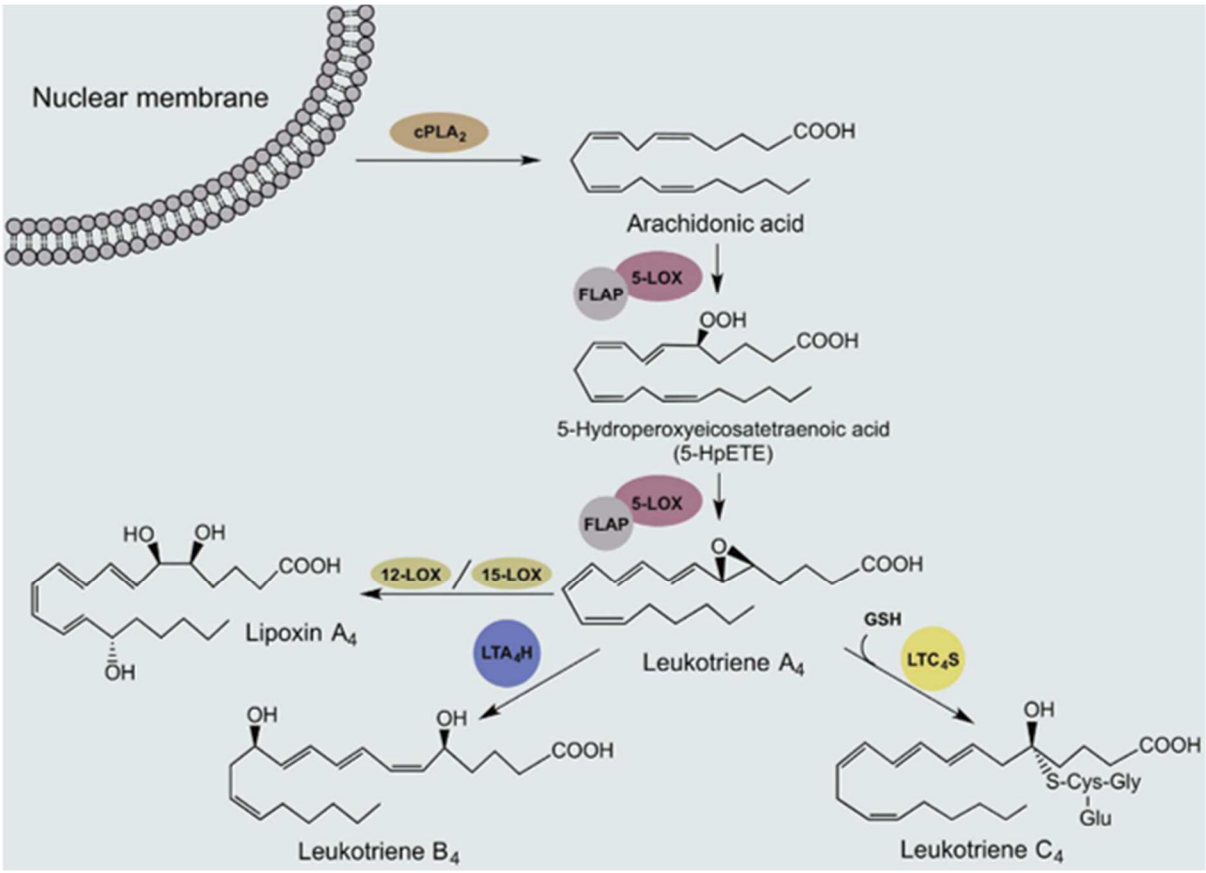

Figure 13: Model of leukotriene biosynthesis. Arachidonic acid is cleaved from the nuclear membrane by phospholipase A_2 and converted to 5HpETE and finally LTA_4 via 5-lipoxigenase (5-LO). LTA_4 can either be hydrolyzed to LTB_4 via LTA_4 hydrolase or conjugated with a glutathione to LTC_4 through LTC_4 synthase. Subsequent peptidase activity leads to the production of LTD_4 and LTE_4 [231].

1.5.2 The Leukotriene A_4 hydrolase (LTA_4H) and LTB_4

The Leukotriene A_4 hydrolase catalyzes the reaction from LTA_4 to LTB_4. LTA_4H has both hydrolase and aminopeptidase activity and is therefore a bifunctional zinc metalloenzyme. It has a size of 69 kDa and exists in four identified isoforms which are produced by alternative splicing. Isoform 1 and 2 are expressed in monocytes, lymphocytes, neutrophils, reticulocytes, platelets and fibroblasts.

LTA_4H is expressed/produced in a variety of tissues including intestine, lung and kidney, but can also be found in blood leukocytes, neutrophils, monocytes and erythrocytes [232].
LTA_4H is the rate limiting step in the biosynthesis of LTB_4 [233], a potent immune activating and chemotactic agent and can be found in a variety of tissues involved in acute and chronic inflammation [234], cardiovascular disorders [235, 236] as well as carcinogenesis [237] and PAF induced shock [238, 239]. In addition to its pro-inflammatory hydrolase activity, LTA_4H can exert anti-inflammatory action via its aminopeptidase activity, cleaving and thereby inactivating the peptide *Pro-Gly-Pro* (PGP) [240-242]. PGP is a Matrikine, a bioactive fragment of the ECM, that can potentially control a diverse array of physiological processes including paracellular permeability in endothelial cells or proliferation and radial spreading in lung epithelial cells [243]. It is a potent neutrophil chemoattractant, mimicking key sequences found in *glutamic acid, leucine, arginine+* (ELR+) chemokines and allows binding to *C-X-C chemokine receptor 1/2* (CXCR1/2).

Furthermore, LTA_4H serves as a checkpoint for lipid mediator biosynthesis and is able to mediate both, initiation and resolution phases of inflammation. LTA_4 is also a precursor for lipoxin production, a family of anti-inflammatory, pro-resolving lipid mediators. Depending on the mode of action, LTA_4H can shift the production from pro- to anti-inflammation [244, 245].

Mice being deficient for *5-lipoxygenase* (5-LO) appear healthy and show normal inflammatory response despite the lack of LTs [246]. In a model of lung fibrosis, pulmonary cells were protected from necrosis and showed decreased collagen deposition compared to controls [247]. Interestingly, these mice also showed an increase in cys-LTs, although synthesis pathways are blocked at early stages. In *Klebsiella* mediated bacterial infection models, 5-LO knockout mice were more susceptible for the bacteria, displaying increased mortality rates in comparison to controls [248]. Neutrophil infiltration into the lungs and BALF, however, was unaffected. Part of the high mortality rates could be explained by functional defects of macrophages that were unable to kill and clear bacteria effectively. This defect could be overcome by the administration of LTB_4 [249]. Similar results were obtained by fungal infection of the murine lungs [250].
Other studies investigated the role of LTB_4 receptor (BLTR) deficiency [229]. Mice were subjected to zymosan-induced peritonitis or arachidonic acid-induced ear inflammation. These mice showed decreased numbers of infiltrating neutrophils and macrophages into the peritoneum and almost abolished neutrophil infiltration to the inflamed ears. Neutrophils of BLTR deficient mice were able to respond normally to C5α and platelet activating factor, however, their response towards LTB_4 was affected, as indicated by decreased intracellular calcium signaling as well as completely abolished LTB_4 induced chemotaxis [251].

Mice being deficient for LTA_4H were shown to develop normally with no obvious defects. They were unable to produce LTB_4 which is responsible for neutrophil chemotaxis and display decreased edema formation following arachidonic acid-induced ear inflammation. Furthermore, *Lta4h*$^{-/-}$ mice show decreased sensitivity towards PAF-induced shock, identifying LTB_4 as one key mediator of this reaction [252].

1.6 Aim of this study

Platelets show an emerging role besides hemostasis and thrombosis. Especially their ability to interact and act in concert with other immune cells contributing to organ damage, termed the name thrombo-inflammation. With platelets being new players in the progression of inflammation, new possibilities for treatments arise, however the underlying mechanisms of platelet-mediated inflammatory responses remain to a large extent unclear. Consequently, studies on the role of platelets in different inflammatory settings and different organs are required to shed more light on these diverse, yet highly clinical-relevant processes.

Therefore, one part of this thesis was the establishment of a murine model of hepatic ischemia reperfusion injury, which resembles the clinical situation after liver surgery, transplantation or trauma. As part of the CRC/TR240, this project was carried out in collaboration with Prof. Valbona Mirakaj and her team at the University Hospital of Tübingen, who helped to establish the hepatic ischemia model [253] in our laboratory.

Using this model, we wanted to investigate the endpoints following hepatic ischemia and to understand the spatio-temporal events during reperfusion injury. Therefore, *in vivo* confocal intravital microscopy of the liver was established to visualize the processes following hepatic ischemia. Both methods, hepatic ischemia and intravital microscopy were (and are) used to study the role of platelets and identify relevant platelet surface receptors in the progression of hepatic ischemia reperfusion injury as well as their involvement in platelet-immune cell interactions.

Furthermore, we wanted to use and adapt the intravital microcopy for other organ systems, such as pancreas and subcutaneous tumors, to study and visualize the involvement of platelets in diabetes and tumor progression.

The course of inflammation is mediated by a variety of chemokines and other chemotactic molecules, which were recently shown to be released by activated platelets. One of them is LTA_4H, a molecule that catalyzes the last step of LTB_4 synthesis, a known strong chemoattractant for neutrophils. We wanted to investigate whether (platelet derived) LTA_4H influences thrombosis, hemostasis as well as the outcome of hepatic ischemia reperfusion injury with focus on neutrophil infiltration. Therefore, constitutive and platelet and

megakaryocyte specific conditional knockout mice for LTA_4H were generated. Platelets of these mice were studied in functional assays, both *in vitro* and *in vivo*.

The comparison of two bone marrow isolation strategies was a third project which was carried out in collaboration with Tobias Heib. Isolation of the bone marrow is a time consuming and variable process. A recent publication introduced a faster and way more yield efficient method- the spin-isolation method [254]. We wanted to compare the classical flushed isolation of bone marrow cells [255] with the rapid spin-isolation regarding yield and viability of primary cells as well as ploidy of primary MKs and the capacity of cultured MKs to form proplatelets. We plan to establish and validate the new spin-isolation method, to extract murine bone marrow in a standardized and time-efficient manner in further studies.

2. Materials and Methods

2.1 Materials

2.1.1 Chemicals and reagents

Adenosine diphosphate (ADP)	Sigma-Aldrich (Steinheim, Germany)
Agarose	Roth (Karlsruhe, Germany)
Ammonium persulfate (APS)	Roth (Karlsruhe, Germany)
Apyrase (grade III)	Sigma-Aldrich (Steinheim, Germany)
β-mercaptoethanol	Roth (Karlsruhe, Germany)
Bovine serum albumin (BSA)	Sigma-Aldrich (Steinheim, Germany)
Bromophenol blue (3',3",5',5"-tetrabromophenol-sulfonphthalein)	Sigma-Aldrich (Steinheim, Germany)
Chloroform	AppliChem (Darmstadt, Germany)
Collagen Horm® suspension + SKF sol.	Takeda (Linz, Austria)
Complete protease inhibitors (#11836153001)	Roche Diagnostics (Mannheim, Germany)
Convulxin (CVX)	Enzo Life Sciences (New York, USA)
Cryo-Gel	Leica Microsystems (Wetzlar, Germany)
4',6-diamidino-2-phenylindole (DAPI)	Invitrogen (Karlsruhe, Germany)
Dimethyl sulfoxide (DMSO)	Sigma-Aldrich (Steinheim, Germany)
DreamTaq DNA Polymerase (5 U L^{-1})	Life Technologies, Darmstadt, Germany)
DreamTaq Green PCR Master Mix, 2x	Life Technologies, Darmstadt, Germany
Dry milk, fat-free	AppliChem (Darmstadt, Germany)
Deoxynucleotide triphosphates (dNTP) mix	Life Technologies, Darmstadt, Germany
DNAse I	NEB (Frankfurt am Main, Germany)
Ethylenediaminetetraacetic acid (EDTA)	AppliChem (Darmstadt, Germany)
Eukitt® quick-hardening mounting medium	Sigma-Aldrich (Steinheim, Germany)
Enhanced chemiluminescence (ECL) detection substrate	MoBiTec (Göttingen, Germany)
Eosin	Roth (Karlsruhe, Germany)
Ethanol	Roth (Karlsruhe, Germany)
Fentanyl	Janssen-Cilag GmbH (Neuss, Germany)
Fetal calf serum (FCS)	Gibco (Karlsruhe, Germany)
Fibrinogen from human plasma (F3879+ F4883)	Sigma-Aldrich (Steinheim, Germany)
Fluorescein-isothiocyanate (FITC)	Molecular Probes (Oregon, USA)
Fluoroshield™	Sigma-Aldrich (Steinheim, Germany)
Fluorshield™ with DAPI	Sigma-Aldrich (Steinheim, Germany)
GeneRuler DNA Ladder Mix	NEB (Frankfurt am Main, Germany)
Hematoxylin	Sigma-Aldrich (Steinheim, Germany)
High molecular weight heparin	Ratiopharm (Ulm, Germany)
N-2-Hydroxyethylpiperazine-N'-2-ethane sulfonic acid (HEPES)	Roth (Karlsruhe, Germany)
Igepal® CA-630	Sigma-Aldrich (Steinheim, Germany)
Immobilon® PVDF transfer membrane	Merck Millipore (Darmstadt Germany)
Iron-III-chloride hexahydrate ($FeCl_3$ x 6 H_2O)	Roth (Karlsruhe, Germany)
Isofluran CP®	cp-pharma (Burgdorf, Germany)
Medetomidine (Dormitor)	Pfizer (Karlsruhe, Germany)

Methanol	Roth (Karlsruhe, Germany)
Midazolam (Dormicum)	Roche (Grenzach-Wyhlen, Germany)
Midori Green™	Biozym Scientific (Oldenburg, Germany)
Nonidet P-40 (NP-40)	Roche Diagnostics (Mannheim, Germany)
NuPAGE® LDS Sample Buffer (4x)	Life Technologies (Darmstadt, Germany)
PageRuler® Prestained Protein Ladder	Fermentas (St. Leon-Rot, Germany)
Paraformaldehyde (PFA)	Roth (Karlsruhe, Germany)
Phenol/chloroform/isoamyl alcohol	AppliChem (Darmstadt, Germany)
Poly-L-lysine	Sigma-Aldrich (Steinheim, Germany)
Prostacyclin (PGI_2)	Calbiochem (Bad Soden, Germany)
Proteinase K	NEB GmbH, Frankfurt am Main, Germany
RNase A (# R4875)	Sigma-Aldrich (Steinheim, Germany)
R-phycoerythrin (PE)	EUROPA (Cambridge, UK)
Sodium azide (NaN_3)	Sigma-Aldrich (Steinheim, Germany)
Sodium chloride (NaCl)	AppliChem (Darmstadt, Germany)
Sodium citrate	AppliChem (Darmstadt, Germany)
Sodium dodecyl sulfate (SDS)	Sigma-Aldrich (Steinheim, Germany)
Sodium hydroxide (NaOH)	AppliChem (Darmstadt, Germany)
Sodium orthovanadate (Na_3VO_4)	Sigma-Aldrich (Steinheim, Germany)
Sucrose	Sigma-Aldrich (Steinheim, Germany)
10x Taq Buffer (+KCl, -$MgCl_2$)	NEB (Frankfurt am Main, Germany)
Taq-Polymerase	NEB (Frankfurt am Main, Germany)
Tetramethylethylenediamine (TEMED)	Roth (Karlsruhe, Germany)
3,3,5,5-tetramethylbenzidine (TMB)	EUROPA (Cambridge, UK)
Thrombin from human plasma	Roche Diagnostics (Mannheim, Germany) Sigma-Aldrich (Steinheim, Germany)
Tris(hydroxymethyl)aminomethane (Tris)	Roth (Karlsruhe, Germany)
Triton X-100	Sigma-Aldrich (Steinheim, Germany)
TRIzol®	Invitrogen (Karlsruhe, Germany)
Tween 20®	Roth (Karlsruhe, Germany)
U46619	Alexis Biochemicals (San Diego, USA)
Vectashield hardset mounting medium	Vector Labs, Inc. (Burlingame, USA)
Water, nuclease-free	Roth (Karlsruhe, Germany)

Rhodocytin (Rhd) was kindly provided by J. Eble (University Hospital Frankfurt, Germany). *Collagen-related peptid*e (CRP) was synthesized by Genscript and cross-linked in-house.

2.1.2 Devices

Device	**Company**
Aggregometer (APACT)	APACT Laborgeräte und Analysensysteme (Hamburg, Germany)
Cryotom CM1900	Leica (Wetzlar, Germany)
Cauterizer	FST (Heidelberg, Germany)
Cube Unit	Life imaging services
Eppendorf centrifuge 5415C	Eppendorf AG (Hamburg, Germany)
Eppendorf centrifuge 5427R	Eppendorf AG (Hamburg, Germany)

FACS Calibur	BD Biosciences (Heidelberg, Germany)
FACS Celesta	BD Biosciences (Heidelberg, Germany)
Gene Touch Thermal Cycler	Biozym Scientific GmbH (Oldenburg, Germany)
Leica DMI 4000B	Leica (Wetzlar, Germany)
MultiImage® II FC Light Cabinet	Alpha Innotech corporation (Kasendorf, Germany)
Nikon ECLIPSE TS 100	Nikon GmbH (Düsseldorf, Germany)
scil Vet abc Plus+	scil animal care company GmbH (Viernheim, Germany)
Sysmex KX 21N	Sysmex GmbH (Norderstedt, Germany)
TCS SP5 CLSM	Leica (Wetzlar, Germany)
TCS SP8 CLSM	Leica (Wetzlar, Germany)
Zeiss Axiovert 200 inverted microsope	Zeiss (Jena, Germany)
Zeiss HBO 100	Zeiss (Jena, Germany)

2.1.3 Material

Material	**Company**
Canula (18G, 20G, 22G, 26G)	BD Biosciences (Heidelberg, Germany)
Cell strainer 100/70 µm	Corning GmbH (Kaiserslautern, Germany)
Coverslips #1.5	Thermo fisher scientific (Dreieich, Germany)
Dynabeads™ Untouched™ Mouse CD4 Cells Kit	Thermo fisher scientific (Dreieich, Germany)
Glass slide Superfrost Plus	Thermo fisher scientific (Dreieich, Germany)
Heparinized capillaries (100 µl)	Hartenstein (Würzburg, Germany)
PVDF membrane	GE Healthcare (Penzberg, Germany)
Micro Serrefine clips (60 g)	FST (Heidelberg, Germany)
Suture (Etilon 5.0)	(Wetzlar, Germany)
Syringe filters (70 µm)	Roth (Karlsruhe, Germany)
Syringes (1 ml)	Dispomed (Gelnhausen, Germany)
Ultrasonic flowprobe (Transonic Flowprobe 0.5)	Transonic systems (Maastricht, The Netherlands)
Well plates (96-well, 24-well, 6-well)	Greiner (Frickenhausen, Germany)

2.1.4 Antibodies

2.1.4.1 Commercial antibodies

Antibody	**Host**	**Cat.No**	**Manufacturer**
anti-LTA_4H	rat	STJ24431	St. John´s Laboratory (London, UK)
anti-Gapdh	rabbit	G5262	Sigma-Aldrich (Steinheim, Germany)
anti-rabbit IgG-HRP	goat	7074	Cell Signaling (Denver, USA)
anti-rabbit IgG-HRP	goat	7074S	Cell Signaling (Denver, USA)
platelet depletion antibody	rat	(R300)	Emfret Analytics (Eibelstadt, Germany)
Platelet depletion IgG control	rat	(K300)	Emfret Analytics (Eibelstadt, Germany)

Antibody (conjugate)	**Host organism**	**clone**	**Manufacturer**
anti-mouse CD3-BV786	armenian hamster	145-2C11	BioLegend (San Diego, USA)
anti-mouse CD4-BV605	rat	RM4-5	BioLegend (San Diego, USA)
anti-mouse CD8-PerCP-Cy5.5	rat	53-6.7	BioLegend (San Diego, USA)
anti-mouse CD11b-APC-Cy7	rat	M1/70	BioLegend (San Diego, USA)
anti-mouse CD19-BV650	rat	6D5	BioLegend (San Diego, USA)
anti-mouse CD45-AF700	rat	30-F11	BioLegend (San Diego, USA)
anti-mouse Ly6C-V450	rat	AL-21	BD Biosciences (Heidelberg, Germany)
anti-mouse Ly6G-AF647	rat	1A8	BioLegend (San Diego, USA)
anti-mouse NK1.1-PE	mouse	PK136	BioLegend (San Diego, USA)
anti-mouse CD16/32-PE-Cy7	rat	93	BioLegend (San Diego, USA)
anti-mouse CD34-PE	rat	SA376A4	BioLegend (San Diego, USA)
anti-mouse CD48-PacB	armenian hamster	HM48-1	BioLegend (San Diego, USA)
anti-mouse CD150-BV605	rat	TC15-12F12.2	BioLegend (San Diego, USA)
anti-mouse c-kit-AF700	rat	2B8	BioLegend (San Diego, USA)
anti-mouse Flk2/Flt3-PE-Cy5.5	rat	A2F10	BioLegend (San Diego, USA)

anti-mouse lin mixture-FITC	armenian hamster, rat	145-2C11; RB6-8C5; RA3-6B2; Ter-119; M1/70;	BioLegend (San Diego, USA)
anti-mouse Sca1-AF647	rat	D7	BioLegend (San Diego, USA)
anti-mouse Ter119-AF488	rat	TER-119	BioLegend (San Diego, USA)
anti-mouse F4/80-AF488 or AF594	rat	BM8	BioLegend (San Diego, USA)
anti-mouse CD31-AF647 or AF488	rat	390	BioLegend (San Diego, USA)
anti-mouse Exendin 4		#120214	Abcam (Cambridge, UK)

2.1.4.2 Monoclonal antibodies

The monoclonal antibodies (all rat IgG antibodies) listed below were generated in our laboratory and labeled with either *fluorescein isothiocyanate* (FITC), *phycoerythrin* (PE) or Alexa fluorophores using commercial kits following manufacturer's protocols.

Antibody	**Clone**	**Isotype**	**Antigen**	**Described in**
p0p4	15E2	IgG2b	GPIbα	[256]
p0p/B	57E12	IgG2b	GPIbα	[51]
DOM2	89H11	IgG2a	GPV	[256]
p0p6	56F8	IgG2b	GPIX	[256]
JAQ1	98A3	IgG2a	GPVI	[257]
INU1	11E9	IgG1	CLEC-2	[258]
ULF1	97H10	IgG2a	CD9	[256]
JER1	10B6	IgG1	CD84	[259]
LEN1	12C6	IgG2b	α2	[260]
MWReg30	5D7	IgG1	αIIb	[261]
EDL-1	57B10	IgG2a	β3	[256, 260]
JON/A	4H5	IgG2b	αIIbβ3	[260, 262]
JON6	14A3	IgG2b	αIIbβ3	unpublished
WUG 1.9	5C8	IgG1	P-selectin	unpublished
HB.197™	2.4G2	IgG2b	FcgR	[263]
Ly6G/Ly6C	RB6-8C5	IgG2b	Ly6G	[264]

CD11b	M1/70	IgG2b	Integrin αM subunit	[265]
CD4	GK1.4	IgG2b	CD4	[266]
CD105	MJ7/18	IgG2a	CD105	[267]

2.1.5 Kits

Kits	**Manufacturer**
Aspartate Aminotransferase (AST) Activity Assay Kit	Sigma-Aldrich (Steinheim, Germany)
Alanine Aminotransferase Activity (ALT) Assay Kit	Sigma-Aldrich (Steinheim, Germany)
Alexa Fluor labeling kits (A488, A546, A594 and A647)	Molecular Probes (Eugene, USA)
Dynal mouse T cell negative isolation kit	Invitrogen (Karlsruhe, Germany)
Lactate Dehydrogenase Assay Kit (LDH)	Abcam (Cambridge, UK)
LTB_4 Parameter Assay Kit	R&D Systems (Minneapolis, USA)
LIVE/DEAD™ Fixable Aqua Dead Cell Stain Kit	Thermo Fisher Scientific (Schwerte, Germany)

2.1.6 Buffers and media

All buffers were prepared using deionized water obtained from a MilliQ Water Purification System (Millipore, Schwalbach, Germany). pH was adjusted using HCl or NaOH.

Blocking Buffer (Western blot)

Washing Buffer (1x)	—
BSA or fat-free dry milk	5%

Blocking Buffer (Immunohistochemistry)

PBS (1x)	—
Tween 20®	0.1%
BSA	3%
Rat serum	0.3%

CATCH Buffer

PBS (1x)	—
HEPES	25 mM
EDTA	3 mM
BSA	3.5%

Coating Buffer, pH 9.6

Na_2CO_3	15 mM
$NaHCO_3$	85 mM

Decalcification Buffer, pH 7.4

PBS (1x)	—
EDTA	10%

FACS Buffer

PBS (1x)	—
FCS	1%
NaN_3	0.02%

Laemmli Buffer (for SDS-PAGE)

Tris base	40 mM
Glycine	0.95 M
SDS	0.5%

Lysis Buffer for DNA lysis

Tris base	100 mM
EDTA	5 mM
NaCl	200 mM
SDS	0.2%
added Proteinase K (20 mg mL^{-1})	100 µg mL^{-1}

PBS/EDTA (for platelet lysates)

PBS (1x)	—
EDTA	5 mM

PBS Fixation Buffer

PBS (1x)	—
PFA	4%

Phosphate-buffered saline (PBS), pH 7.14

NaCl	137 mM
KCl	2.7 mM
KH_2PO_4	1.5 mM
$Na_2HPO_4 \times 2H_2O$	8 mM

Sample Buffer for agarose gels, 6x

Tris base (150 mM)	33%
Glycerol	60%
Bromophenol blue	0.04%

SDS Sample Buffer, 4x

Tris base (1 M), pH 6.8	20%
Glycerol	40%
SDS	4%
β-mercaptoethanol (reducing conditions)	20%
Bromophenol blue	0.04%

Separating Gel Buffer (Western Blot), pH 8.8

Tris base	1.5 M

Stacking Gel Buffer (Western Blot), pH 6.8

Tris base	0.5 M

Stripping buffer (Western blot), pH 2.0

PBS (1x)	—
Glycine	25 mM
SDS	1%

Sodium-Citrate-Buffer, pH 7.0

Sodium Citrate	0.129 M

TAE, 50x, pH 8.0

Tris base	0.2 M
Acetic acid	5.7%
EDTA	50mM

TE-Buffer, pH 8.0

Tris base	10 mM
EDTA	1 mM

Transfer-Buffer (semi-dry blot)

Tris Ultra	50 mM
Glycine	40 mM
Methanol	20%

Tris-buffered saline (TBS), pH 7.3

NaCl	137 mM
Tris base	20 mM

Tyrode's Buffer, pH 7.3

NaCl	137 mM
KCl	2.7 mM
$NaHCO_3$	12 mM
NaH_2PO_4	0.43 mM
HEPES	5 mM
$CaCl_2$	2 mM
$MgCl_2$	1 mM
BSA	0.35%
Glucose	0.1%

Washing Buffer for immunoblotting (TBS-T)

TBS (1x)	—
Tween 20®	0.1%

2.1.7 Animals

C57BL/6JRj mice were obtained from Janvier Labs (Saint-Berthevin, France) or Charles River (Sulzfeld, Germany) and kept in the animal facility of the Rudolf Virchow Center Würzburg.

Lta4h$^{het/het}$ mice were purchased from KOMP Repository (University of California, Davis, USA). They were generated by injection of the embryonic stem cell clone *Lta4h*$^{tm1a(KOMP)Wtsi}$ into blastocysts. The *Lta4h* gene, located on chromosome 10, was targeted by a knockout first allele (KOMP Repository). The Knockout First allele is initially a non-expressive form but can be converted to a conditional allele via Flp recombination, which removes the *LacZ-p(A); BactP-p(A)* cassette. The resulting mice were intercrossed with *PF4-Cre* mice [268], to generate megakaryocyte and platelet specific knockout animals. *Lta4h*$^{het/het}$ mice were backcrossed with C57BL/6/J-mice.
PC.G5-tdT [269] mice were purchased from Jackson Laboratories (Jax-Nr.: 024477) and intercrossed with Cre-lines of interest.

Lys-eGFP mice were kindly provided by Thomas Graf (Barcelona, Spain [270].

Lta4h, PC.G5-tdT mice and Lys-eGFP mice were kept in the animal facility of the Center of Molecular Medicine (ZEMM), University Würzburg and/or at the Rudolf Virchow Center Würzburg.

Mice were kept in a temperature- and humidity-controlled environment. Food and water were accessible *ad libitum*. If not stated otherwise, 8- to 16-week-old mice of either sex were used in experiments. Animal studies were approved by the district government of Lower Franconia (Bezirksregierung Unterfranken) and carried out in accordance with local regulations.

2.2 Methods

2.2.1 Genotyping of mice

2.2.1.1 Isolation of genomic DNA from mouse ears

A 1 mm^2 piece of mouse ear was incubated o/N at 56°C and 900 rpm or for 3 h at 56°C and 1,400 rpm in 500 µL of lysis buffer. Cellular proteins and lipids were removed by the addition of 500 µL of phenol/chloroform/isoamyl alcohol (25:24:1). Samples were mixed well and centrifuged for 10 min at 9,391 xg in an Eppendorf 5417R tabletop centrifuge at RT. After centrifugation, the aqueous nucleic acid containing upper phase was transferred into a new cap containing 500 µL isopropanol to precipitate the DNA. Subsequently, the nucleic acids were spun down by centrifugation for 15 min at 18,406 xg and 4°C. The pellet was washed and dehydrated by the addition of 500 µL 70% ethanol with subsequent centrifugation for 10 min at 18,406 xg. Before dissolving the pellet in 50 µL TE buffer, the pellet was dried for 30 min at 37°C.

2.2.1.2 Genotyping by *Polymerase chain reaction* (PCR)

The original construct of the Lta4h knockout-first allele, including primer binding sites, is depicted in Fig. 14.

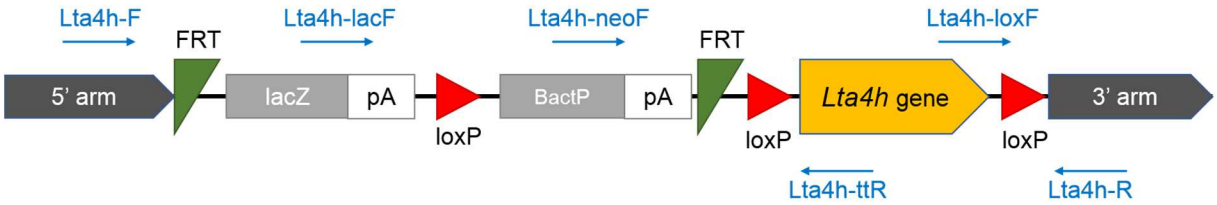

Figure 14: Knockout-first construct for generation of constitutive and conditional Lta4h knockout mice.

PCR mix for Lta4h WT/TG and Flox PCR

0.5 µL	DNA sample
2.5 µL	10x DreamTaq green Buffer
2.6 µL	$MgCl_2$ [25 mM]
1 µL	dNTPs [10 mM]
1 µL	forward Primer [1 µg mL^{-1}]
1 µL	reverse Primer [1 µg mL^{-1}]
1 µL	DreamTaq-Polymerase [5 U $µL^{-1}$]
15.4 µL	H_2O

PCR Program WT-PCR

Temperature [°C]	Time [s]	Repeats
94	300	1
94	20	
65	30	10
72	40	
94	15	
55	30	30
72	50	
72	300	
22	∞	1

Primer Lta4h WT

Lta4h-F: 5' GAC TTA TTT GGC CAT CGG GAA AGG 3'
Lta4h-ttR: 5' CGC ATG TCT GCC TTT TCT ACT GAG G 3'
Expected band sizes: 544 bp for WT and 744 bp for Post-Flp.

Primer Lta4h TG

Lta4h-neoF: 5' GGG ATC TCA TGC TGG AGT TCT TCG 3'
Lta4h-ttR: 5' CGC ATG TCT GCC TTT TCT ACT GAG G 3'
Expected band sizes: no band for WT and 566 bp for Pre-Cre.

Primer Lta4h flox

Lta4h-loxF: 5' GAG ATG GAG CAA CGC AAT TAA TG 3'
Lta4h-loxR: 5' ACT AAG ACG ATA GCA AGC CCA GAC C 3'
Expected band sizes: no band for WT and 239 bp for floxed and 537 bp for Post-Cre.

PCR mix for Lta4h Flp-PCR

1 µL	DNA sample
2 µL	10x DreamTaq green Buffer
2 µL	$MgCl_2$ [25 mM]
0.5 µL	dNTPs [10 mM]
0.1 µL	oIMR0042 [1 µg mL^{-1}] – internal control fw
0.1 µL	oIMR0043 [1 µg mL^{-1}] – internal control rev
0.1 µL	oIMR1348 [1 µg mL^{-1}] – fw
0.1 µL	oIMR1349 [1 µg mL^{-1}] – rev
0.1 µL	DreamTaq-Polymerase [5 U $µL^{-1}$]
14.3 µL	H_2O

PCR Program Flp-PCR

Temperature [°C]	Time [s]	Repeats
94	180	1
94	20	30
58	30	
72	40	
72	120	1
22	∞	1

Primer Flp

oIMR0042: 5' CTA GGC CAC AGA ATT GAA AGA TCT 3'
oIMR0043: 5' GTA GGT GGA AAT TTC TAG CAT CAT CC 3'
oIMR1348: 5' CAC TGA TAT TGT AAG TAG TTT GC 3'
oIMR1349: 5' CTA GTG CGA AGT AGT GAT CAG G 3'
Expected band sizes: 324 bp for WT (internal control) and 324 bp + 725 bp for Flp.

PCR mix for PF4-PCR

1.0 µL	DNA sample
2.5 µL	DeramTaq green Buffer
2.5 µL	$MgCl_2$ [25 mM]
1 µL	dNTPs [10 mM]
1 µL	forward Primer [1 µg mL^{-1}]
1 µL	reverse Primer [1 µg mL^{-1}]
0.25 µL	DreamTaq-Polymerase [5 U $µL^{-1}$]
15.75 µL	H_2O

PCR program PF4

Temperature [°C]	Time [s]	Repeats
94	300	1
94	30	30
58	30	
72	45	
72	30	1
22	∞	1

Primer Pf4

Pf4_for: 5´ CCC ATA CAG CAC ACC TTT TG 3´
Pf4_ rev: 5´ TGC ACA GTC AGC AGG TT 3´
Expected band size: 450 bp for positive samples.

2.2.2 Molecular biology and biochemistry

2.2.2.1 Agarose gel electrophoresis

The PCR products were separated on agarose gels with different densities. In parallel, a marker with a range from 100 to 10,000 bp was run on the gels to control the size of the products. For a 1% agarose gel, 1 g of agarose per 100 mL TAE buffer was boiled in a microwave until it was dissolved. The cooled (60°C) agarose was supplemented with the DNA marker Midori Green™ [50 µL L^{-1}] and poured into a sleigh containing a comb. The cast gel was then laid into a chamber filled with 1x TAE buffer. The samples were separated for 30-45 min at 140V, for 1% agarose gels. 2% agarose gels, used for Flp PCR samples, were separated at 120V-140V for 30 min. For big gels 4 g agarose in 400 mL 1x TAE buffer were used to prepare 1% agarose gels. The big gels were run at 160V. Finally, the DNA/Midori Green™ was visualized under *ultra violet* (UV) light and pictures were taken with a camera (Herolab GmbH, Germany).

2.2.2.2 Sodium Dodecyl Sulfate (SDS)-Polyacrylamide Gel Electrophoresis (PAGE)

For denaturing SDS-PAGE, samples were mixed with an equal volume of reducing 2x loading dye and boiled for 5 min at 95°C. Samples were then separated by their molecular weight according to the protocol by Laemmli [271]. Molecular weight marker and protein samples were loaded to the gel in the electrophoresis chamber. Electrophoresis was performed at 25 mA per gel.

2.2.2.3 Immunoblotting

Samples were separated by SDS-PAGE as described above and blotted onto *polyvinylidene difluoride* (PVDF) membranes and incubated with the primary antibodies of interest o/N at 4 °C. For visualization, horseradish peroxidase (HRP)-conjugated secondary antibodies were used and membranes were developed using an *enhanced chemiluminescence* (ECL) detection system with autoradiography films or digitally on a MultiImage® II FC Light Cabinet device.

2.2.3 In vitro analyses of platelet function

2.2.3.1 Serum preparation

Mice were bled under isoflurane anesthesia from the retro-orbital plexus. 700 µL blood were collected into a 1.5 mL Eppendorf tube using non-heparinized capillaries. The blood was left to coagulate for 30 min at RT and then centrifuged at 736 xg at RT for 5 min. The supernatant

was transferred into a new tube and centrifuged at 18,406 xg for 5 min. The supernatant (serum) was collected and stored at -80°C.

2.2.3.2 Platelet isolation from whole blood of mice

Mice were bled under isoflurane anesthesia up to 1 mL in 300 µL heparin [20 U mL^{-1}]. 300 µL of heparin [20 U mL^{-1}] were added and the samples were centrifuged for 6 min at 60 xg. Subsequently, the upper phase and the buffy coat with some erythrocytes were transferred to new tubes containing 300 µL heparin [20 U mL^{-1}]. To further purify the platelets, the centrifugation was repeated (6 min, 60 xg) and only the upper phase without any erythrocytes was pipetted into a new Eppendorf tube. Platelets were spun down for 5 min at 736 xg, resuspended in 1 mL of Tyrode's buffer without Ca^{2+}, containing 2 µL of apyrase [0.02 U mL^{-1}, f.c.] and 5 µL PGI_2 [0.1 µg mL^{-1}, f.c.] and allowed to rest for 5 min at 37°C. The washing step was repeated twice, before the pellet was resuspended in an appropriate volume of Tyrode's buffer containing apyrase [0.02 U mL^{-1}, f.c.]. The platelets were allowed to rest for 30 min prior to experiments.

2.2.3.3 Determination of platelet size, count and glycoprotein expression

50 µL of blood was withdrawn from the retro-orbital plexus in 300 µL heparin [20 U mL^{-1}]. 650 µL Tyrode's buffer without Ca^{2+} were added to the samples (1:20 dilution). 50 µL of the diluted blood were incubated with fluorophore-conjugated antibodies directed against platelet-specific epitopes and subsequently analyzed using flow cytometry (FACSCelesta, BD Biosciences). *Forward scatter* (FSC) and the counts per 30 seconds were determined. Alternatively, platelet count and size were measured in EDTA-blood using a scil Vet abc Plus+ hematology analyzer (scil animal care company GmbH). The expression levels of the most prominent platelet glycoproteins were determined by incubating heparinized blood with fluorophore-conjugated monoclonal antibodies and *mean fluorescence intensities* (MFI) were analyzed by flow cytometry.

2.2.3.5 Platelet integrin activation and degranulation

50 µL of blood were withdrawn from the retro-orbital plexus of mice under isoflurane anesthesia, diluted in 300 µL heparin [20 U mL^{-1}] and washed twice (5 min, 736 xg) with 1 mL of Ca^{2+}-free Tyrode's buffer. Afterwards, the washed blood was resuspended in 650 µL Ca^{2+}-containing Tyrode's buffer. Washed blood of *wild-type* (WT) and KO mice was incubated with fluorophore-conjugated antibodies directed against activated αIIbβ3 integrins (JON/A-PE) and against P-selectin (WUG 1.9-FITC). Subsequently, the samples were activated with different agonists to trigger different signaling pathways. While CVX and CRP activate platelets via

GPVI, Rhd signals through CLEC-2. ADP, U46619 and thrombin on the other hand signal via GPCRs. The reaction was stopped after an incubation for 7 min at 37°C and 7 min at RT by addition of 500 µL PBS.

2.2.3.6 Aggregation studies

In aggregometry, light transmission of a washed platelet suspension was monitored over time (10 min) using a four-channel aggregometer (APACT, Laborgeräte und Analysensysteme, Hamburg). Platelets were washed according to the protocol described in 2.2.3.2. Platelet count was adjusted to 0.5 x10^6 platelets µL^{-1} in Ca^{2+}-free Tyrode's buffer containing 0.02 U mL^{-1} apyrase. Platelets were rested for 30 min at 37°C to prevent pre-activation.
0.5 x10^6 platelets per µL in 160 µL Ca^{2+}-containing Tyrode's buffer supplemented with 100 µg mL^{-1} human fibrinogen were activated with different concentrations of agonists (1.6 µL, 100x concentrated), such as collagen, CRP, CVX, or ADP, U46619 and thrombin. For stimulation with thrombin, Ca^{2+}-containing Tyrode's buffer without human fibrinogen was used. Aggregation studies with ADP were performed in platelet-rich plasma (0.5 x10^6 platelets µL^{-1}). The aggregation was expressed as arbitrary units with the light transmission of 160 µL Tyrode's buffer with Ca^{2+} and fibrinogen set as 100%.

2.2.3.7 Western Blot analysis of platelets

For Western blotting, platelets were prepared as described in section 2.2.3.2 but washed twice in PBS/EDTA [5 mM] to remove residual serum albumin. Platelet counts were adjusted to 1x 10^6 platelets per µL in IP Buffer supplemented with Igepal, protease inhibitor cocktail and Na_2VO_3 using a Sysmex KX 21-N cell analyzer (Sysmex Deutschland GmbH). Samples were incubated 30 min on ice, then mixed with an equal volume of reducing 2 x loading Dye and boiled for 5 min at 95°C. Samples were directly subjected to SDS-PAGE and immunoblotting or stored at 4°C.

2.2.3.8 Platelet adhesion under flow conditions

For flow chamber experiments on collagen, rectangular coverslips (24 x 60 mm) were coated o/N at 37°C with 70 µg mL^{-1} fibrillar type I collagen (Horm) and blocked for 1 h with 1% BSA prior to the experiment. Mice were bled up to 1 mL in 300 µL heparin [20 U mL^{-1}], the blood was diluted 3:1 with Ca^{2+}-containing Tyrode's buffer and incubated for 5 min at 37°C with a DyLight-488-conjugated anti-GPIX derivative [0.2 µg mL^{-1}]. A transparent flow chamber with a slit depth of 50 µm was covered with a collagen-coated and blocked cover slip and perfused for 4 min with the prepared blood using a pulse-free pump at shear rates of 1,000 s^{-1}, reflecting the blood flow in different vessel types. Subsequently, the chamber was washed for 4 min and

same shear conditions with Ca^{2+}-containing Tyrode's buffer while at least five phase-contrast and fluorescent pictures were taken using a Zeiss Axiovert 200 inverted microscope (40 x/0.60 objective) equipped with a CoolSNAP-EZ camera (Photometrics). The recorded phase-contrast and fluorescence pictures were analyzed off-line using Metavue software.

2.2.3.9 Platelet spreading on fibrinogen

The ability of platelets to adhere and form filo- and lamellipodia on a fibrinogen-coated surface in response to thrombin, was investigated by a spreading assay. Rectangular coverslips (24 x 60 mm) were coated with 10 µg human fibrinogen [100 µL of 100 µg mL^{-1}] o/N at 4°C in a humid chamber. The slides were blocked with 1% BSA for 1 h at RT. 30-50 µL of washed platelets [3 $x10^5$ per µL] were mixed with 50-70 µL Ca^{2+}-containing Tyrode's buffer, activated with 0.01 U mL^{-1} thrombin and immediately allowed to spread on the fibrinogen-coated coverslips at RT on a heating mat. After different time intervals (5, 15 and 30 min), the adherent platelets were fixed with 300 µL 4% PFA in PBS for 5 min and *differential interference contrast* (DIC) microscopy pictures were taken using an inverted microscope Zeiss HBO 100 (Axiovert 200M, Zeiss). For analysis, the phase abundance of the different spreading stages (1, resting; 2, formation of filopodia; 3, formation of filopodia and lamellipodia; 4, fully spread) was determined. In addition, for visualization of the spreading process, time-lapse videos were recorded by taking pictures every 5 seconds for 20 min.

2.2.4 In vivo analyses of platelet function

2.2.4.1 Anesthesia (Triple narcotics)

Mice were anesthetized by intraperitoneal injection of a combination of Midazolam, Medetomidine and Fentanyl [5, 0.5 and 0.05 mg kg^{-1} body weight]. Mice were placed on a heating mat to prevent hypothermia. After 5 min corneal and inter-toe reflexes were tested to assure proper anesthesia. For hepatic ischemia reperfusion injury, mice were tested after 25 min, to ensure a proper depth of anesthesia for the surgery (stage III – surgical tolerance).

2.2.4.2 Tail bleeding time

Mice were anesthetized by intraperitoneal injection of triple narcotics and a 1 mm segment of the tail tip was cut with a scalpel. Bleeding time was monitored by gently absorbing drops of blood on filter paper at 20 seconds intervals without touching the wound site. Bleeding was determined to have ceased when no blood was observed on the paper. Experiments were stopped after 20 min by euthanasia.

2.2.4.3 $FeCl_3$-induced injury of mesenteric arterioles

The mesentery of 3- to 4-week old anesthetized mice (triple narcotics) was exteriorized by a midline abdominal incision. Endothelial damage in mesenteric arterioles was induced by application of a 3 mm^2 filter paper soaked with 20/13% $FeCl_3$. Arterioles were visualized using a Zeiss Axiovert 200 inverted microscope equipped with a 100-W HBO fluorescent lamp source and a CoolSNAP-EZ camera (Visitron). Digital images were recorded and analyzed using the Metavue software. Adhesion and aggregation of fluorescently labeled platelets (DyLight-488-conjugated anti-GPIX derivative) was monitored until complete occlusion occurred (blood flow stopped for > 2 min). Experiments were performed by Dr. Sarah Beck (Department of Experimental Biomedicine I).

2.2.4.4 Hepatic ischemia reperfusion injury

Hepatic ischemia was induced in 8- to 10-week-old mice. Mice were anesthetized with an intraperitoneal injection of triple narcotics (10 µL g^{-1}). Briefly, a midline incision was made to open the peritoneum and expose the liver lobes of the mouse. An atraumatic clip (micro serrefine clip, FST) was used to occlude the portal triad, consisting of the *V.portae, A.hepatica, ductus hepaticus.* To assess the role of platelet and neutrophil surface receptors in hepatic ischemia reperfusion injury, blocking antibodies against GPIb (50 µg p0p/B-F(ab)), αIIbβ3 (50 µg JON/A-$F(ab)_2$), P-selectin (100 µg WUG 1.9) and Mac-1 (50 µg Mac-1) were injected i.v. 25 minutes into ischemia. After clip removal, the wound was closed using surgical knots (Etilon suture 5.0) and fluid depletion was compensated by injection of 200 µL 0.96% NaCl *i.p.* Then, 3 hours of reperfusion were allowed. Liver damage was assessed using AST, ALT and LDH activity measurements in serum of the mice. Cryo sectioning of the median liver lobe was used to determine immune cell infiltration into the tissue by immunofluorescence staining.

2.2.4.5 Hot needled injury

Hot needle injury was induced in 8- to 10-week-old mice. Mice were anesthetized with in an intraperitoneal injection of triple narcotics (10 µL g^{-1}). Briefly, a midline incision was made to open the peritoneum and expose the liver lobes of the mouse. The median lobe was exposed, and a cauterizer tip was used to burn the liver tissue (1 mm diameter). Directly afterwards, mice were prepared for intravital microscopy (2.2.4.6).

2.2.4.6 Intravital microscopy of the liver

Intravital microscopy was performed using a Leica TC SP8 inverted confocal microscope. The microscope was equipped with a Cube Unit to allow a temperature-controlled environment for

the mice. For intravital microscopy the mice were anesthetized with in an intraperitoneal injection of triple narcotics (10 µL g^{-1} body weight). Before the operational procedure, mice were injected *i.v.* with fluorescently labelled antibodies directed against platelets (5 µg anti-GPIX), neutrophils (5 µg anti-Ly6G) and endothelial cells (7.5 µg anti-CD105). Briefly, the operational field was shaved and cleaned before midline incision. The vessels in skin and peritoneal muscle were cauterized before removal. Connecting ligaments were cut carefully to allow exposure of the left medial lobe. The liver lobe was covered with kimwipe tissue soaked in warm saline, to avoid desiccation of the liver and allow small adjustments to minimize breathing movements.

2.2.5 MK analyses

2.2.5.1 Sample preparation for histology

Number, localization and structure of MKs were assessed using conventional histology. Spleen and femora of adult KO and WT mice were isolated and fixed o/N in 4% PFA in PBS at 4°C. The femora were decalcified for 3 days in decalcification buffer. Afterwards, spleens and femora were dehydrated in an automated tissue processor (Leica ASP200S) and embedded in paraffin.

2.2.5.2 Hematoxylin and Eosin (H&E) staining of paraffin sections

After embedding in paraffin, 3 µm thick sections of the spleens and femora were prepared, fixed on glass slides and dried o/N at 37°C. Sections were deparaffinized and rehydrated using xylene (2 x 5 min) and a graded alcohol series (100%, 96%, 90%, 80% and 70%, 2 min each). Finally, the slides were transferred to H_2O bidest (2 min), stained with hematoxylin for 15 sec and washed intensively (~10 min) with tap water. 0.05% Eosin was used for counterstaining (2 min). Slides were washed once with H_2O bidest and dehydrated by a graded alcohol series (70%, 80%, 90%, 96% and 100%, each 2 min) followed by xylene (2 x 5 min). Sections were mounted with Eukitt®, a xylene-based mounting medium. Analysis was performed with an inverted Leica DMI 4000 B microscope.

2.2.5.3 Isolation of MKs from bone marrow of adult mice- flush method

Femora and tibiae of adult mice were dissected and cleaned from remaining muscle tissue. The bones were cut at both ends and the bone marrow was flushed out into a sterile 6 well plate using 2 mL modified CATCH buffer. The bone marrow was homogenized by repeated drawing up the syringe with a 23G needle and filtered through a 70 µm cell strainer. The cell

strainer was washed with 8 mL CATCH buffer. Cells were counted and used for further experiments.

2.2.5.4 Isolation of MKs from bone marrow of adult mice- spin method

0.5 mL Eppendorf tubes were introduced with a hole at the bottom, made by a 18G needle and then placed into a 1.5 mL Eppendorf tube containing 100 µL DEMEM. Femora and tibiae of adult mice were dissected and cleaned from remaining muscle tissue. The bones were cut at one end and placed with the cut end downwards into the prepared Eppis. The bones were flushed by centrifugation for 50 sec at 2,500 xg at RT. The pellet was resuspended with 900 µL CATCH buffer and filtered through a 70 µm cell strainer. Cells were counted and used for further experiments.

2.2.5.5 Culture of MKs from bone marrow of adult mice

Bone marrow was isolated according to one of the methods described above (2.2.5.3 or 2.2.5.4). To obtain pure MKs, the cell suspension was purified using negative selection. The Dynal mouse T cell negative isolation kit was used according to the manufacturers´ instructions and contains anti-B220, anti-GR-1 (Ly-6G/C), anti-CD3, anti-Ter-119 and anti-Mac1 antibodies. These antibodies are directed against B cells, monocytes and neutrophils as well T cells, erythrocytes and macrophages to eliminate these cells and subsequently enriching the MK population. The cells were centrifuged for 10 min at 300 xg and resuspended with PBS to a concentration of 100 $x10^6$ cells mL^{-1}. The cell suspension was incubated with antibodies and magnetic beads for 20 min at RT with gentle agitation. Beads were washed three times with PBS using a magnetic rack. Elution fractions were collected, counted and centrifuged for 10 min at 300 xg, RT. MKs were then used for further experiments.

2.2.5.6 Proplatelet formation of cultured bone marrow derived MKs

The cells were resuspended in 2 mL MK medium, divided into 2 wells of a 12-well plate and incubated at 37°C, 5% CO_2. At day 3 of culture, MKs were purified by a BSA gradient following the protocol of Shivdasani *et al.* [272] and the isolated MKs were resuspended in 1 mL MK medium. For analysis of proplatelet formation, appr. 3,000 cells/well were cultured in 96-well plates (triplicates) for one additional day and the percentage of proplatelet-forming MKs per visual field (20x objective) was determined. The remaining cells were cultured in one well of a 12-well plate for further analysis.

2.2.5.7 Determination of MK ploidy by flow cytometry

Bone marrow was isolated as described above. 200 µL of the cell suspension were transferred to FACS tubes and centrifuged for 5 min at 300 xg (RT). Cells were resuspended in a 1:1 mixture CATCH/PBS 5% FCS and incubated with anti-RFc (2.4G2- 1:50) for 15 min to saturate unspecific binding sites. MKs were stained with an anti-GPIIb/IIIa antibody (MWReg30-FITC) in a 1:2.5 dilution for 20 min on ice. For washing 1 mL of the 1:1 CATCH/PBS 5 % FCS was added and centrifuged for 5 min at 300 xg, RT. Cells were resuspended in 250 µL PBS 0.1% EDTA and fixed with addition of 250 µL 1% PFA in PBS, and kept on ice for 10 min. Afterwards, cells were washed by addition of 3 mL PBS and centrifugation for 5 min at 300 xg, RT. The pellet was resuspended in 500 µL PBS 0.1% TritonX, to permeabilize the membrane. Then, the cells were washed by addition of 3 mL PBS and centrifugation as before and either resuspended in 500 µL Propidium iodide solution (PI) or 500 µL PBS with 1 µL of a 1:200 dilution of sytox orange. Samples were incubated o/N at 4 °C in the dark and analyzed using a FACSCalibur (Becton Dickinson) or FACS Celesta (Becton Dickinson). For analysis, the GPIIb/PI-positive population was gated and the mean ploidy of the different ploidy stages was determined.

2.2.5.8 Flowcytometry of stem cells and immune cells

Bone marrow cells were isolated according to the isolation method above (2.2.5.4), resuspended in 990 µL FACS buffer and poured through a 70 µm cell strainer. 50- 75 µL of this suspension were used per staining. The cells were mixed with an equal volume of antibody mixture and incubated 30 min at 4 °C in the dark. The antibody mix for immune cells is supplemented with the 2.4G2 antibody to saturate unspecific binding sites. The cells were then centrifuged 5 min at 300 xg and resuspended in 50 µL PBS/dead cell marker (1:500) mix and incubated for another 30 min at 4 °C in the dark. After centrifugation (5 min, 300 xg, RT) the pellet is resuspended in 100 µL FACS buffer and transferred to FACS tubes. Volume was adjusted to 500 µL with PBS and measured on a FACS Celesta (BD Biosciences).

2.2.6 In vitro analysis of neutrophil migration

2.2.6.1 Neutrophil isolation from bone marrow

Bone marrow of adult mice was isolated according to 2.2.5.4. The cells were resuspended in 1 mL RPMI medium with 10% FCS and filtered over a cell strainer (70 µm). To isolate the neutrophils, a histopaque gradient (5 mL histopaque 1119 and 5 mL histopaque 1077). The bone marrow was placed on top of the gradient and centrifuged for 35 min at 1.100 xg (Heraeus Multifuge 3S-R, Thermo Scientific, Waltham USA) with slow acceleration (1) and without

deceleration. Neutrophilic phase was removed and washed with 40 mL RPMI with 10 % FCS and centrifuged for 10 min at 300 xg with acceleration/deceleration 9. The resulting pellet was resuspended in 1 mL RPMI with 10 % FCS and 1 % penicillin and streptavidin. Cells were counted in a Neubauer chamber (1:10 with trypan blue). Neutrophils were kept on ice for further experiments.

2.2.6.2 Neutrophil transmigration assay

Neutrophils were isolated according to the above protocol (2.2.6.1). 6.5 mm trans-wells (Corning, Kennebunk, USA) with a pore size of 3 µm were used. The lower chamber contained 500 µL serum-free RPMI medium and was supplemented with different chemo-attractants. 250,000 neutrophils in 100 µL RPMI medium were seeded in the upper chamber. Platelet supernatant was diluted 1:1 in RPMI medium, to serve as chemoattractant. 250.000 neutrophils in 100 µL RPMI medium were used as quality control. Cells were cultured in the incubator (HERAcell 240, Thermo Fisher Scientific, Waltham, U.S.A) for 16 hours at 37°C and 5% CO_2.

The medium from the upper and lower chamber was collected and neutrophils were counted (1:2) in a Neubauer chamber. Inserts were washed twice by dipping into PBS and removing the liquid. Neutrophils were fixed with application of 500 µL 4% PFA in the lower chamber and 200 µL in the insert for 5 min. Inserts were washed with PBS and cells permeabilized with 500 µL 100% methanol. Inserts were washed with PBS twice and stained with Giemsa solution (1:20 in H_2O distillation) for 15 min at RT with 500 µL in the lower chamber and 200 µL in the insert. Inserts were washed twice with PBS. To scrape off neutrophils, that have not migrated, the inserts were cleaned with cotton sticks. The inserts were imaged with the Leica DMI4000B microscope (Leica Microsystems, Wetzlar, Germany) and five pictures were taken of each insert, and the transmigrated neutrophils were counted.

2.2.7 Histology

5 µm-thick sections of formalin-fixed paraffin-embedded spleens of male and female mice were prepared, deparaffinized and stained with hematoxylin and eosin. Number of MKs was analyzed with an inverted Leica DMI 4000 B microscope.

2.2.8 Statistical data analysis

The presented results are mean ± *standard deviation* (SD) from at least three independent experiments per group, if not stated otherwise. Differences between WT and KO mice were statistically analyzed using the Mann-Whitney-U-test. Differences between more than two groups were analyzed by one-way analysis of variance (ANOVA) with Dunnetts T3 as post-hoc test. *P*-values < 0.05 were considered as statistically significant: ***$P < 0.001$; **$P < 0.01$; *$P < 0.05$. Results with a *P*-value > 0.05 were considered as non-significant (NS).

3. Results

3.1 Establishment of the hepatic ischemia reperfusion model (h I/RI)

Since recent publications provided evidence for a role of platelets during hepatic reperfusion injury independent of their classical role in hemostasis and thrombosis including thrombo-inflammation, innate immunity as well as host defense and tissue regeneration, the aim of the present study was to establish a model of hepatic ischemia reperfusion injury (h I/RI) to study the role of platelets and (interacting) immune cells in the progression of h I/RI.

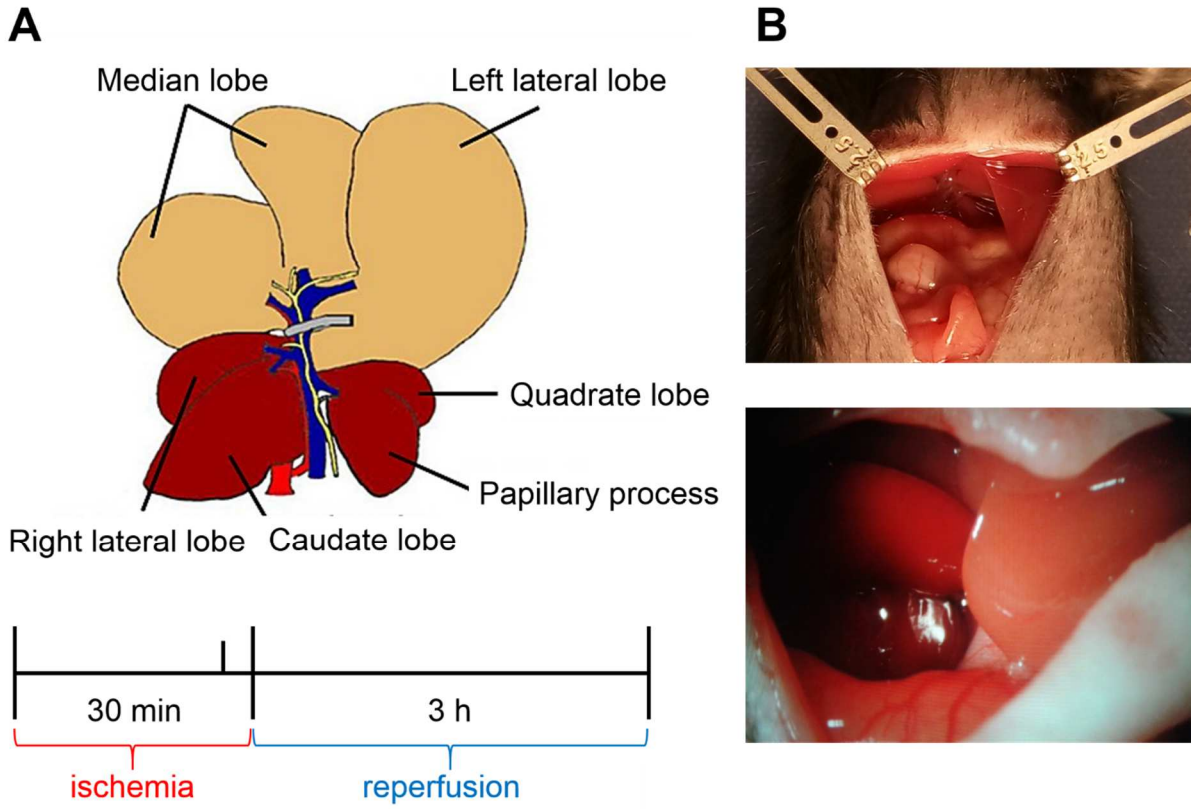

Figure 15: Model of hepatic ischemia. (A) Upper panel shows a scheme of the murine liver with occluded (ocher) and perfused liver lobes (red). 30 minutes of ischemia are followed by 3 hours of reperfusion (lower panel). Any treatment is applied before the end of the ischemic phase. **(B)** Mouse liver *in vivo*. Upper panel shows a perfused liver (red). Lower panel shows occluded liver lobes (whitish color).

Hepatic ischemia is induced by clip application as shown in Fig. 15A. The hepatic artery and portal vein as well as the bile duct are occluded for 30 minutes inducing ischemia in ~70% of the liver. The correct placement of the clip can be observed immediately, as the parenchymal color shifts from dark reddish/brown to light brown (Fig. 15B). If the color change does not occur, the clip needs to be readjusted. In our setting, ischemia was induced for a period of 30 minutes, followed by 3 hours of reperfusion. Any treatment to assess platelet function, was performed at the end of the ischemic phase.

3.2 Establishment of confocal intravital microscopy

The role of immune cells, platelets as well as their interactions with each other have been under investigation for some years. There is evidence that platelets alter immune cell activity and therefore influence the progression of inflammation. However, the underlying mechanisms are still incompletely understood.

Confocal intravital microscopy allows the spatio-temporal resolution of processes taking place following hepatic ischemia. Together with the possibility to interfere with receptors on the platelet surface, intravital microscopy gives new insights to the kinetics of platelet-immune cell interactions.

3.2.1 Liver IVM

In order to study the role of platelets following hepatic ischemia reperfusion injury by confocal-IVM, an *in vivo* imaging protocol had to be established. Crucial steps in the establishment of the confocal-IVM protocol involved the immobilization of the mouse, proper exteriorization of the liver for imaging, characterization of fluorescent markers and reporter mice and visualization of dynamic processes.

Inlays for the inverted microscope were built using cell culture lids. Circles of 2-3 cm were removed and replaced by coverslips, making them suitable for microscopy. This way, the mouse could be placed on the lid and the liver imaged from below providing an even surface Fig. 16A, B). In addition, the microscope was connected to a cubic unit allowing temperature adjustments to prevent the mouse from cooling out through the imaging session.

For the *in vivo* imaging set-up, several methods were tested to isolate and exteriorize the liver with minimal damage and bleeding complications [273]. Incision of connecting ligaments, such as the ligament *falciforum* and the *xiphoid process* provided best results in term of exteriorization. The breathing artefacts were diminished by application of NaCl soaked tissues, allowing gentle stretching of the liver without additional need of direct contact to the tissue. As the liver is quite sensitive for any kind of touch, repetitive direct contact to adjust the liver leads to micro lesions and can trigger platelet adherence and neutrophil activation. Furthermore, the soaked tissue prevented desiccation (Fig. 16C, D).

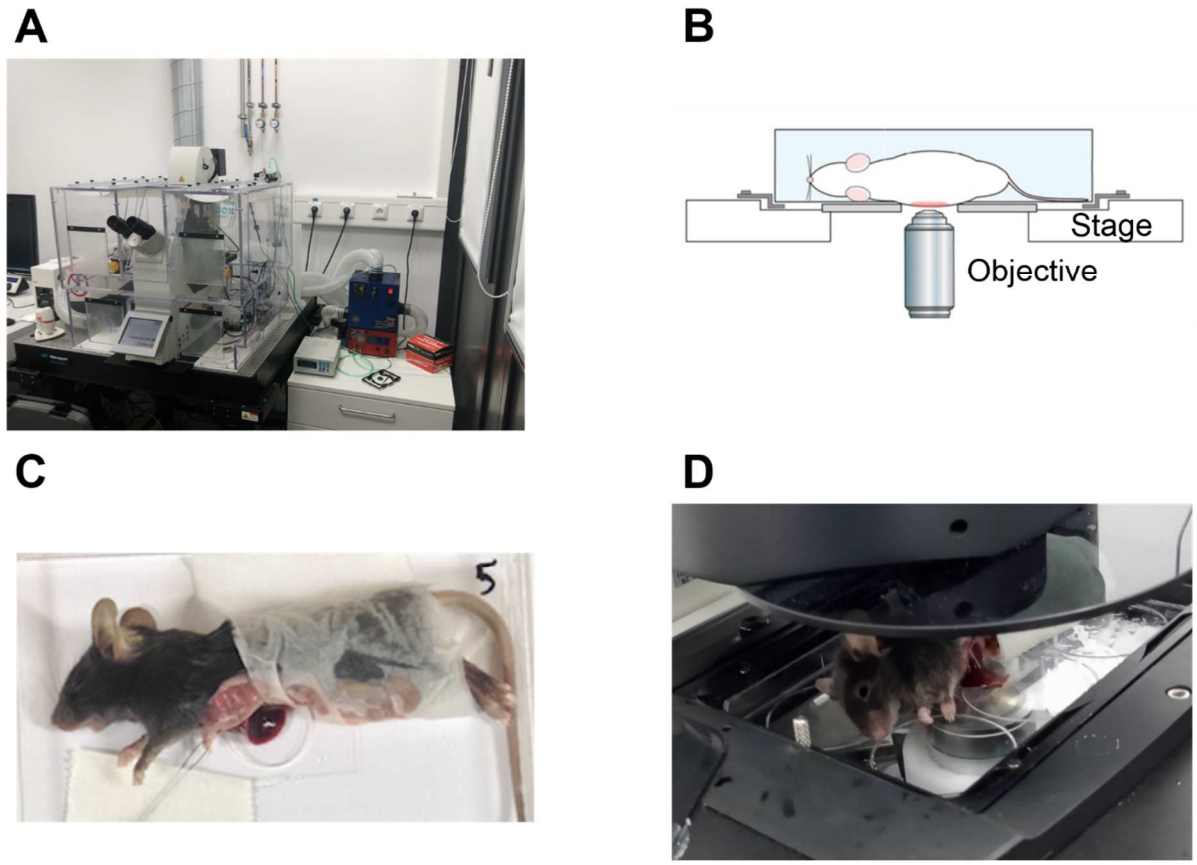

Figure 16: Intravital microscopy set-up. (A) The inverted microscope is equipped with a cubic unit that maintains environmental stable conditions (35°C) for the mouse. **(B)** Scheme of a mouse on the microscopic stage. **(C)** The exposed liver lobe is placed on the imaging device and the intestines are wrapped in tissue soaked in 0.96 % NaCl, followed by placement of the mouse in the microscopy chamber **(D)**. B and D taken from Marques *et al.* [273].

Several markers were tested to stain the sinusoidal lumen, such as BSA or *tetramethylrhodamindextran* (TRITC). However, these stainings failed since liver sinusoids consist of a fenestrated, discontinuous endothelial lining, allowing both BSA and dextran to enter the surrounding tissue, thereby staining hepatocytes. The endothelium was stained using an anti-endoglin (CD105) or anti-*platelet endothelial cell adhesion molecule* (PECAM1= CD31) antibody. With the anti-PECAM1 antibody a weak staining of platelets could also be observed following ischemia, which might indicate moderate platelet degranulation. Platelets were visualized by using an anti-GPIX antibody derivative (Fig.17A, B). Besides establishment of cell-specific stainings, the obstacle of breathing movements (Fig. 17C) had to be overcome preferably without affecting liver function.

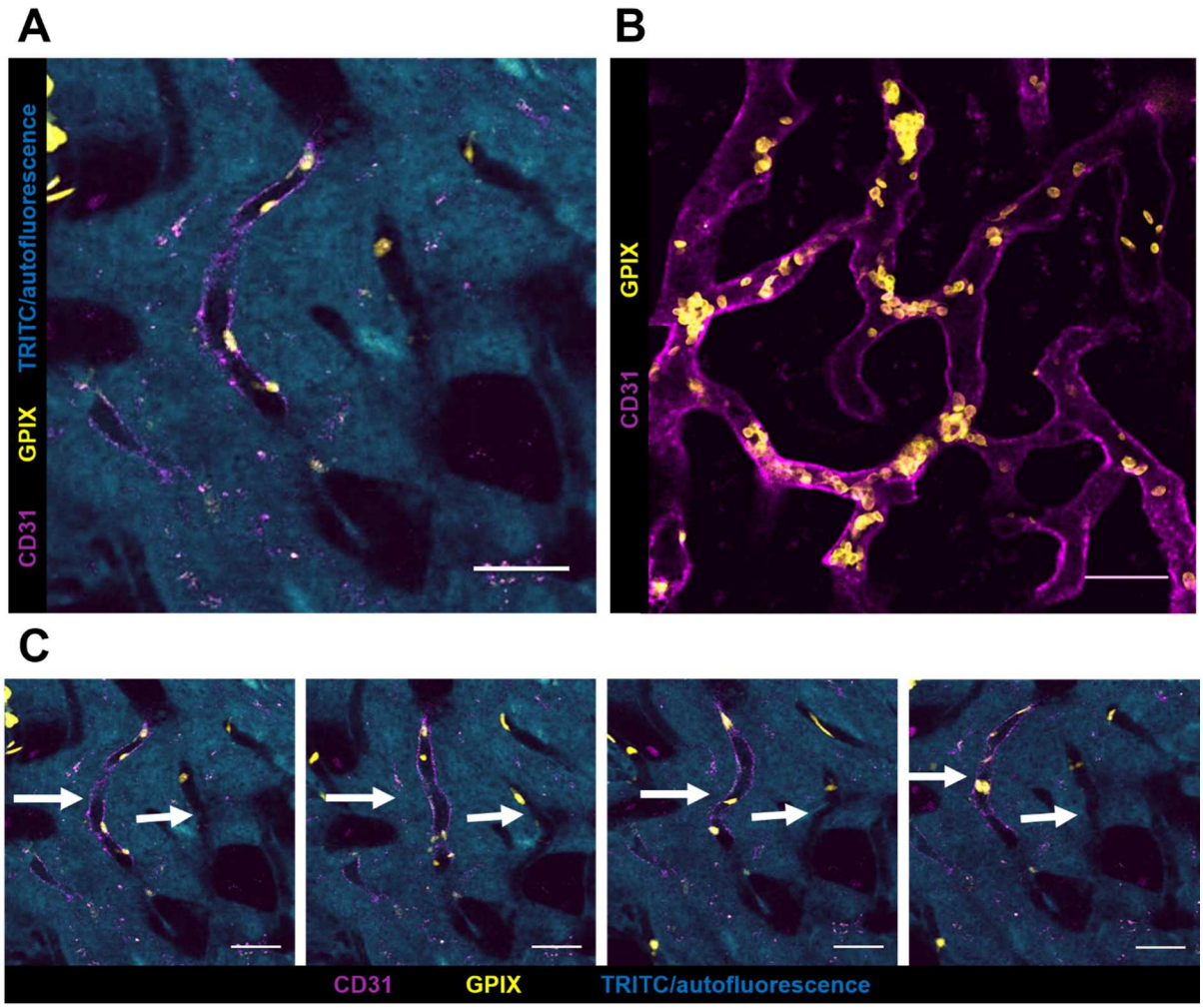

Figure 17: Confocal intravital microscopy (IVM) of the murine liver. (A) First attempts show a combination of autofluorescence and failed intra-sinusoidal staining using tetramethylrhodamindextran (cyan) and staining of blood vessels (magenta), platelets (yellow). **(B)** Without TRITC leaking into the surrounding tissue, the signal for platelets and endothelial cells becomes much clearer. **(C)** Breathing artefacts (indicated by white arrows) were disturbing and needed to be overcome. Scale bars: 10 µm.

The antibodies used to visualize the different cell types were tested using a variety of Alexa Fluor conjugates and alternating concentrations to determine the best combination to yield strong signals with least bleaching effects. The best results were obtained with platelets being labelled with a concentration of 5 µg/mouse anti-GPIX Alexa Fluor 546, neutrophils with 5 µg/mouse anti-Ly6G Alexa Fluor 488 and the endothelium with either 7 µg/mouse anti-endoglin or anti-PECAM1 or a mixture (1:1) coupled to Alexa Fluor 647 (Fig. 18A). CD4, a marker for T helper cells, worked best with 7 µg/mouse coupled to Alexa Fluor 546 (Fig. 18B), while the Kupffer cell marker F4/80 worked well when coupled to Alexa Fluor 594 or Alexa Fluor 488 with 7 µg/mouse (Fig. 18C). CD11b served as a pan-marker for myeloid cells, since its expression in BM cells is induced upon differentiation into the granulocyte-monocyte lineage. It worked best at a concentration of 7.5 µg/mouse and when coupled to Alexa Fluor 647 (Fig. 18D).

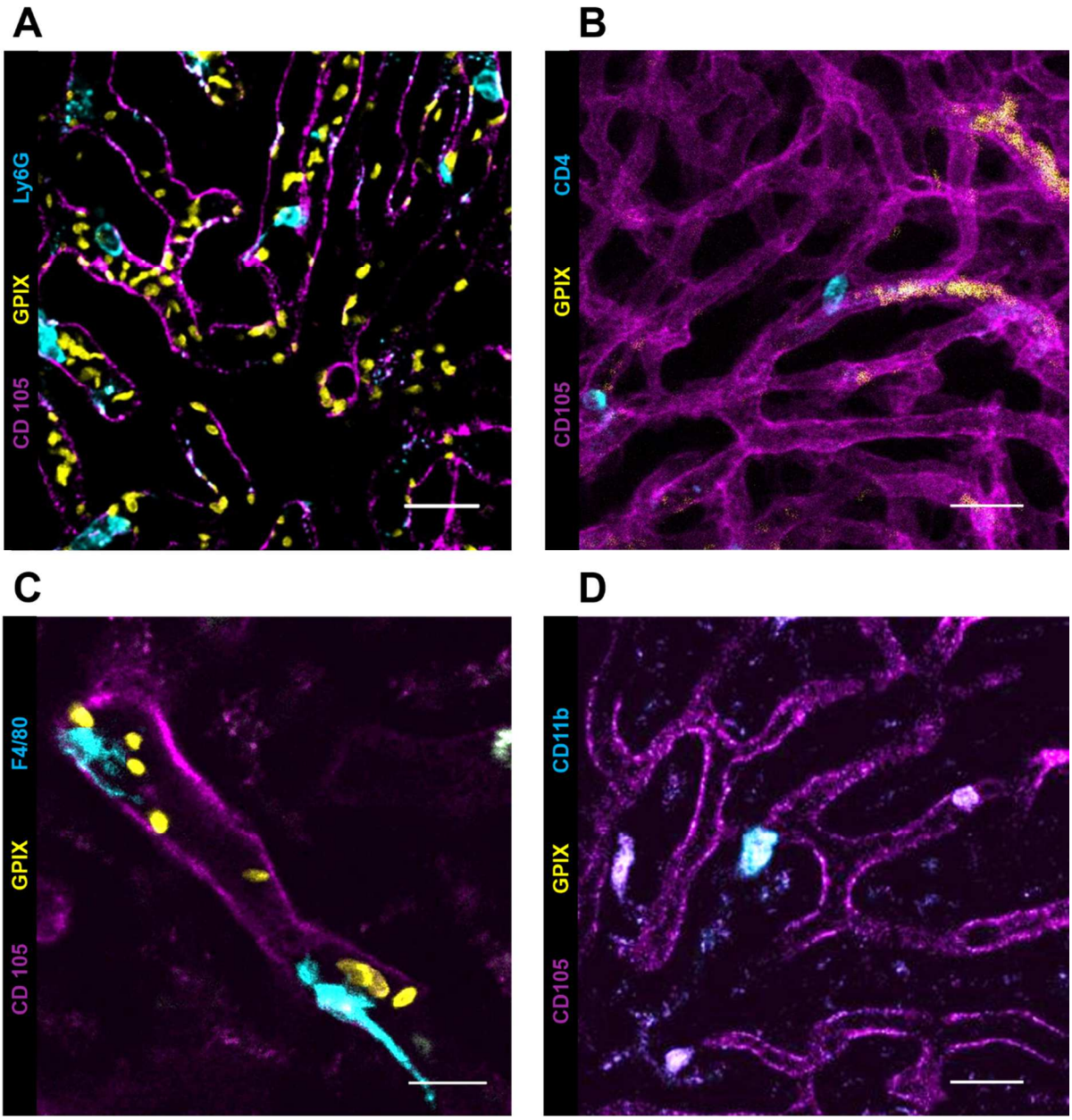

Figure 18: IVM of different immune cell populations in the murine liver. A-D staining of platelets (yellow) and endothelium (magenta) Additional staining of **(A)** neutrophils (cyan), **(B)** Maximum projection of T cells (cyan) in the liver vasculature, **(C)** Macrophages/Kupffer cells (cyan) Scale bar: 5 µm and **(D)** myeloid cells (cyan). Scale bar: 10µm.

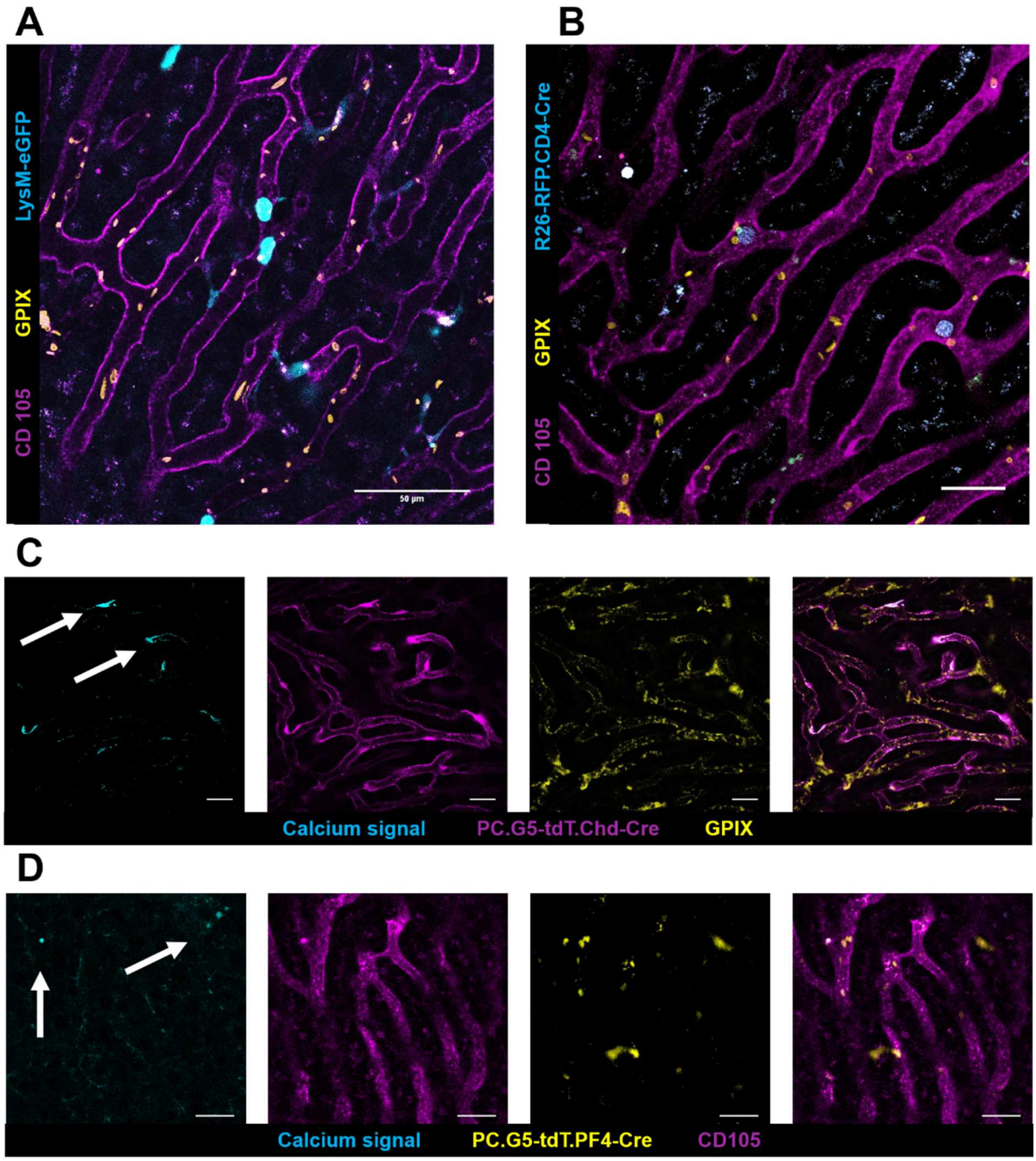

Figure 19: Intravital microscopy of reporter mice. (A-B) platelets (yellow) and endothelium (magenta). **(A)** Neutrophil specific LysM-eGFP mouse (cyan). Scale bar 50 µm. **(B)** R26-RFP.CD4-Cre reporter mouse (cyan). Scale bar 25 µm. **(C)** and **(D)** calcium reporter mouse lines. **(C)** PC.G5-tdT.Cdh-cre reporter mouse shows endogenous expression of tdTomato in endothelial cells and **(D)** PC.G5-tdT.PF4-cre, with endogenous expression of tdTomato in platelets. Upon calcium signaling, additional GFP signals can be observed (as indicated by white arrows in the first picture). Scale bars: 15 µm.

In addition to antibody-mediated visualization of specific cell types, reporter mice were analyzed (Fig. 19). These mice express fluorescent proteins under the control of cell type specific promoters and allow the visualization of the fluorescent cells without additional antibody application. Reporter mice for neutrophil/granulocytes (Lys-eGFP$^{+/-}$), platelets

(PC.G5.tdT Pf4-Cre), CD4$^+$ T cells (R26-RFP.CD4-Cre$^{+/-}$) and endothelial cells (PC.G5.tdT Cdh-Cre) have been studied by *intravital microscopy* (IVM) (Fig. 19A-D). Of note, the CD4 reporter mouse is not completely specific for CD4$^+$ T cells alone, as cytotoxic CD8$^+$ T cells are double positive for CD4 and CD8 during their maturation process.

The PC.G5.tdT reporter mouse lines were developed to visualize calcium fluxes in the specific cell types, allowing conclusions in terms of cellular activation. These mice show constitutive expression of tdTomato positive platelets or endothelial cells. Upon calcium signaling, a conformational change allows the additional detection of a GFP signal (Fig. 19). Calcium signaling could be observed in endothelial cells (C) and platelets (D).

3.2.2 IVM of the pancreas

To image the pancreatic tissue *in vivo*, only small adjustments had to be made from the liver set-up. The pancreas was exteriorized similar to the liver and fixed with NaCl soaked tissue (Fig. 20A).

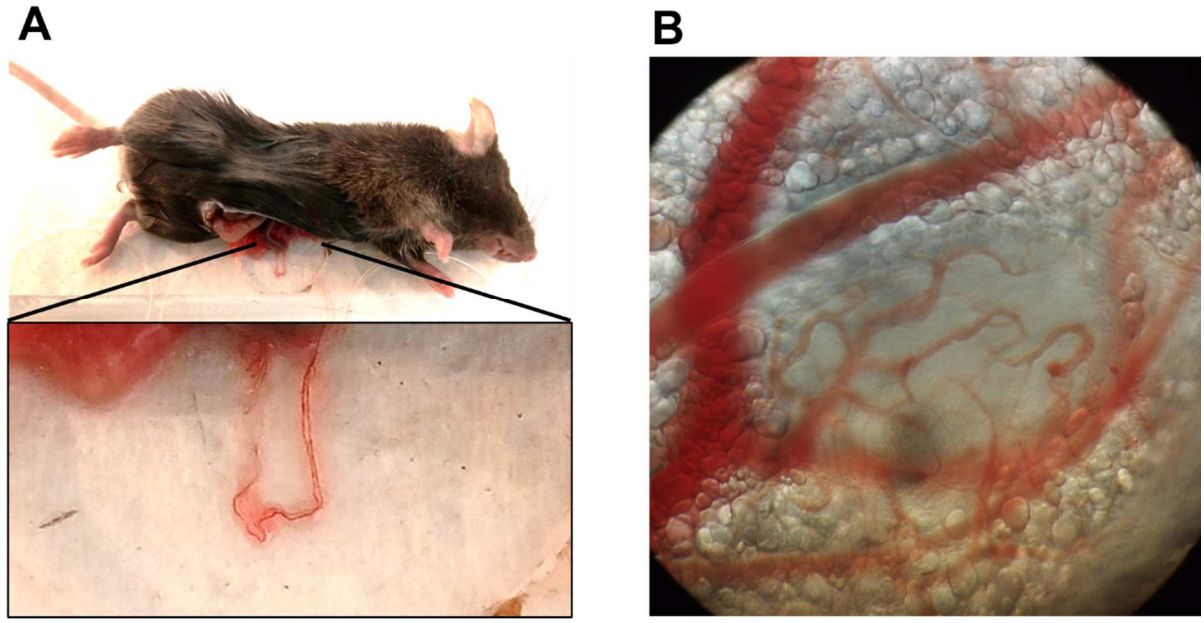

Figure 20: Preparation of the pancreas for intravital microscopy. (A) Preparation and exteriorization of the pancreatic loop for intravital microscopy. **(B)** Brightfield image of a pancreatic islet.

To distinguish between the endocrine from the exocrine pancreas, Exendin-4 was used (Ref; Fig. 21A) Exendin-4 is a peptidomimetic of the endogenous ligand receptor for glucagon-like peptide-1 (GLP-1) and specific for β cells. Especially the role of immune cells, most importantly CD4$^+$ T cells and platelets, in terms of diabetes development and progression was investigated

in WT and GPVI-deficient mice. Best staining results were obtained with 5 µg/mouse anti-GPIX Alexa 546, 5 µg/mouse anti-Exendin4 Alexa 488 and a 1:1 mixture of total 7 µg/mouse anti-PECAM1 and anti-endoglin conjugated to Alexa 647.

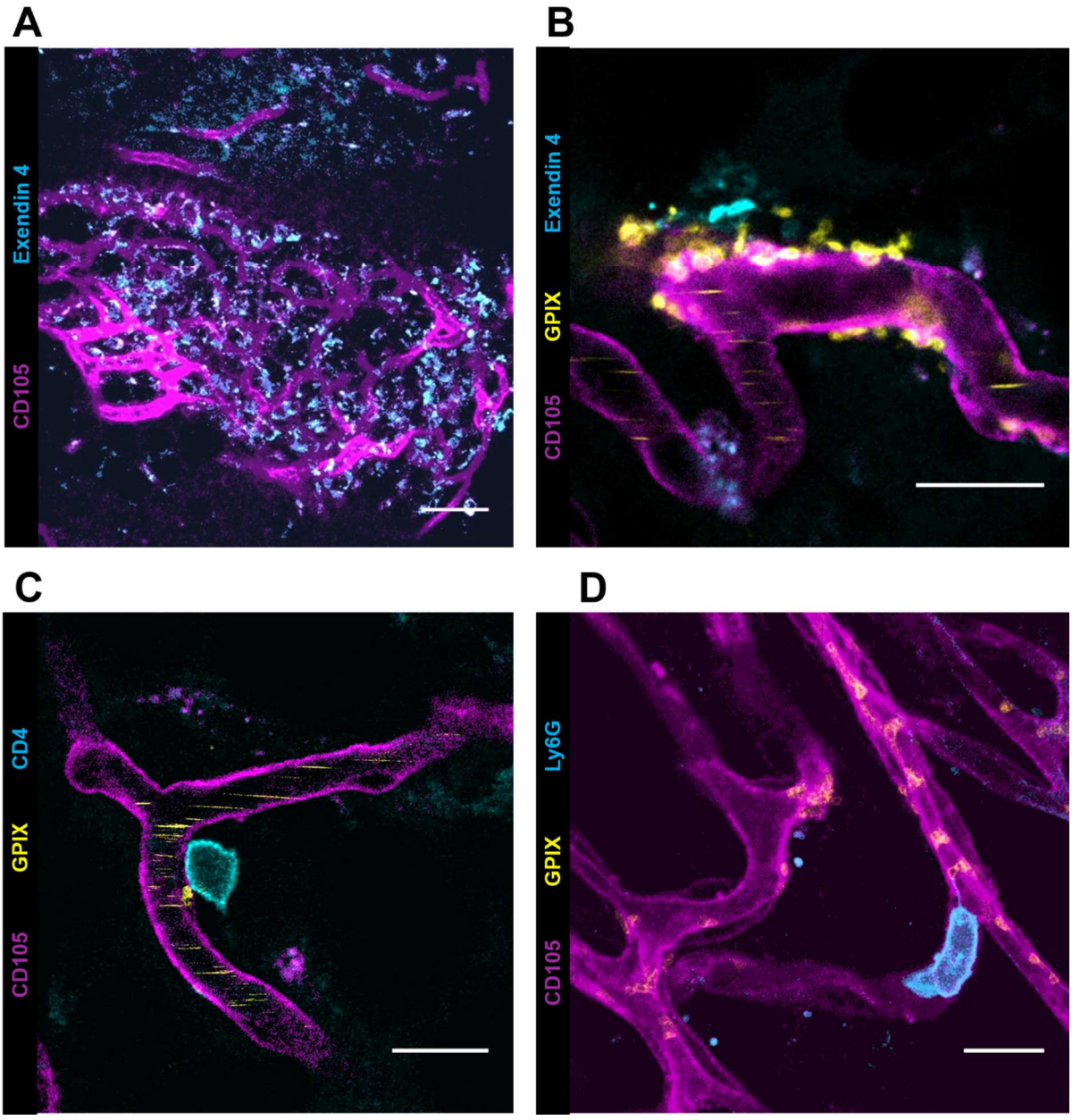

Figure 21: Establishment of intravital microscopy of the pancreas. (A-D) Staining of the endocrine pancreas with endothelium (magenta) and platelets (yellow). **(A)** Maximum projection of a whole islet, where β-cells are stained with Exendin4 (cyan). Scale bar: 25 µm. **(B)** Zoom-in shows platelets localized outside the vasculature. **(C)** T cell (cyan) residing outside the vessel in the vasculature of an islet **(D).** Maximum projection of a neutrophil (cyan) patrolling vessels of the endocrine pancreas. Scale bars (B-D): 10 µm.

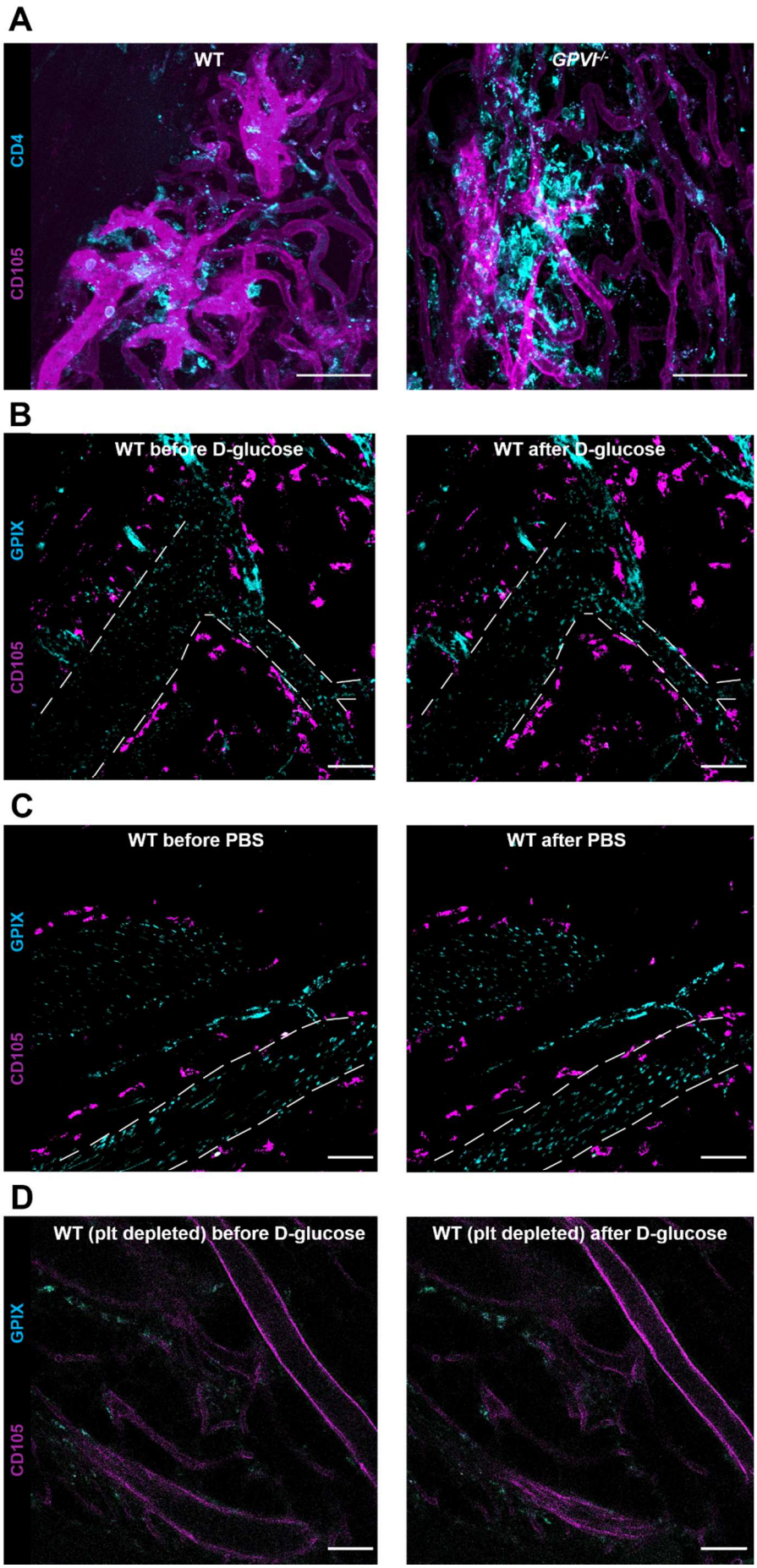

Figure 22: IVM of the endocrine pancreas. (A) Maximum projection of complete islets of WT and GPVI deficient mice with staining of vessels (magenta) and $CD4^+$ T cells (cyan). **(B-D)** vessels = magenta and platelets = cyan. **(B)** WT mice before and after injection of D-glucose. Right panel: narrowing of sinusoidal lumen (big vessel: 79 µm to 75 µm and small vessel 35 µm to 26 µm. **(C)** WT mice before and after injection of PBS. Right panel: no narrowing was observed. **(D)** Platelet-depleted mice before and after injection of D-glucose. Right panel: no narrowing was observed. Scale bar: 50 µm.

We compared the number of $CD4^+$ T cells in WT and GPVI deficient mice and found their number significantly increased in *Gp6*$^{-/-}$ mice (Fig. 22A)

To investigate whether and how platelets respond to high levels of glucose, WT mice were injected with 150 µL of 30% D-glucose while under the microscope. Already at basal conditions, considerable numbers of platelets resided at the pancreatic vasculature, which did not seem to increase after glucose administration. However, we often observed a moment of vasoconstriction at around 1-minute post-injection, in which the blood flow seemed to stop. The blood flow was mostly restored after 2 additional minutes (Fig. 22B) and vessel diameter normalized, again. To rule out, that injection of a large volume or the osmolarity accounts for the observed effect, control mice were injected with 150 µL PBS or L-glucose. No vasoconstriction and stopping of the blood flow could be observed for either case (Fig. 22C). To exclude a platelet independent effect, WT mice were injected with an anit-GPIbα antibody mix to deplete platelets from the circulation and were later injected with 150 µL of D-glucose. Also, in this case no vasoconstriction and stagnation of the blood flow could be observed (Fig. 22D). This data indicates, that platelets are somehow involved in this process, but the underlying mechanism remains to be elucidated.

3.2.3 IVM of subcutaneous tumors

Tumors are known to display high angiogenic capacity, since the growing tumor needs to be supplied with all necessary nutrients. Studies by our group and others have suggested an involvement of platelets in tumor progression and metastasis, respectively [89]. Although end point analysis verified an involvement of platelets, the immediate effects of targeting distinct platelet receptors on the tumor vasculature needed to be investigated. Therefore, IVM of tumor-bearing mice was established.

For this, tumor cells were injected subcutaneously, and mice were imaged, when the tumors reached a size of about 0.5 - 0.8 cm. The skin was removed, and the mouse was placed on the imaging table in a way that the tumor had contact with the cover slip. To visualize the different cell types potentially involved in the process of tumor progression, several markers were tested. Neutrophils, which have potent anti-inflammatory potential were stained with an antibody directed against Ly6G (5 µg/mouse Alexa Fluor 488). In contrast to control healthy tissue, neutrophils were found to be present in the surrounding tissue/vasculature in addition to the vessel lumen in tumor-bearing mice. (Fig. 23B). Moreover, to address the question, whether platelet receptor targeting affects tightness of the tumor vasculature, the vessel lumen was stained with *bovine serum albumin* (BSA) coupled to *fluorescein isothiocyanate* (FITC) (25 µg/mouse). Intact vessels only showed FITC fluorescence in the lumen, whereas increased intensities BSA-FITC signals in the surrounding tissue pointed towards a disruption

of the endothelial lining (Fig. 23C). Maximum projections of larger tumor areas which were captured by tile scans reflected the high, errant angiogenic capacity of tumors, as vessel thickness and structure were altered. Normally, vessels develop in a directed, straight manner and their thickness is usually consistent. The tile scan analysis further managed to display aberrant blood flow and different velocities as platelets appear as smears in some areas of the picture (Fig. 23D).

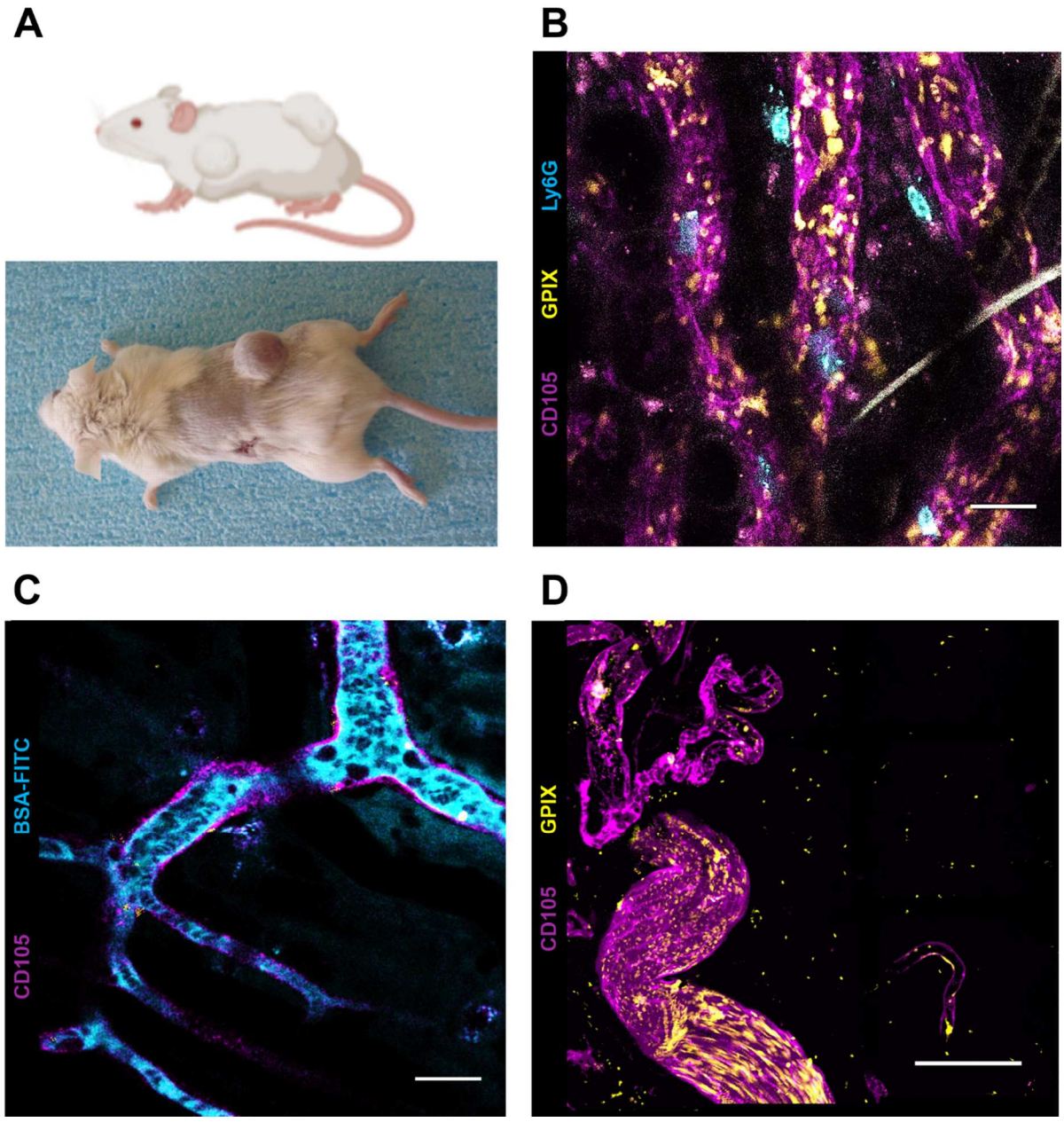

Figure 23: Intravital microscopy of subcutaneous tumors at the back of the mouse. Tumor cells were injected subcutaneously and prepared for IVM, when they reached a size of 0.5-0.8 cm **(A)** Tumor vasculature was highly heterogeneous, with normal appearing vessel structures (magenta) and neutrophils (cyan) patrolling them [274]. **(B)** Scale bar: 10 µm. Other areas show less condensed vessel structures. **(C)** Due to leaking vessels, fluorescently labelled BSA enters the surrounding tissue, which leads to a slight cyan background staining. Inside the vessel, negative staining of erythrocytes and immune cells is visible. Scale bar: 20 µm. **(D)** The maximum projection shows the heterogeneity of the blood flow. Some areas have increased velocities and shear rates than others, as demonstrated by the different staining pattern for platelets. Scale bar: 50 µm.

3.3 Platelets in hepatic ischemia reperfusion injury (h I/RI)

3.3.1 Platelet depletion reduces liver damage following h I/RI

To address the question, whether platelets are also involved in hepatic ischemia reperfusion injury, first experiments have been performed with our collaborators from the group of Prof. Valbona Mirakaj at the University Hospital in Tübingen. To assess the role of platelets in the acute phase (onset of inflammation), platelets were depleted with a single injection of 50 µg/mouse of an anti-GPIbα antibody mixture (R300, Emfret) at the end of the ischemic phase before allowing three hours of reperfusion. Control mice were injected with the same amount of a rat IgG. ELISA measurements of *aspartate transaminase* (AST), *alanine transaminase* (ALT) and *lactate dehydrogenase* (LDH), markers used in human liver diagnostics, were used to evaluate tissue damage. Mice treated with the platelet depletion antibody showed significantly reduced liver damage (Fig. 24A). As it is known that platelets are trapped in spleen and liver following platelet depletion and to rule out, that the population still present in the vasculature alters the outcome of the experiment, depletion experiments with subsequent platelet transfusion were performed. These experiments confirmed that the time of depletion had no influence on the outcome. The presence of platelets, however, exacerbated the damage (Fig. 24B).

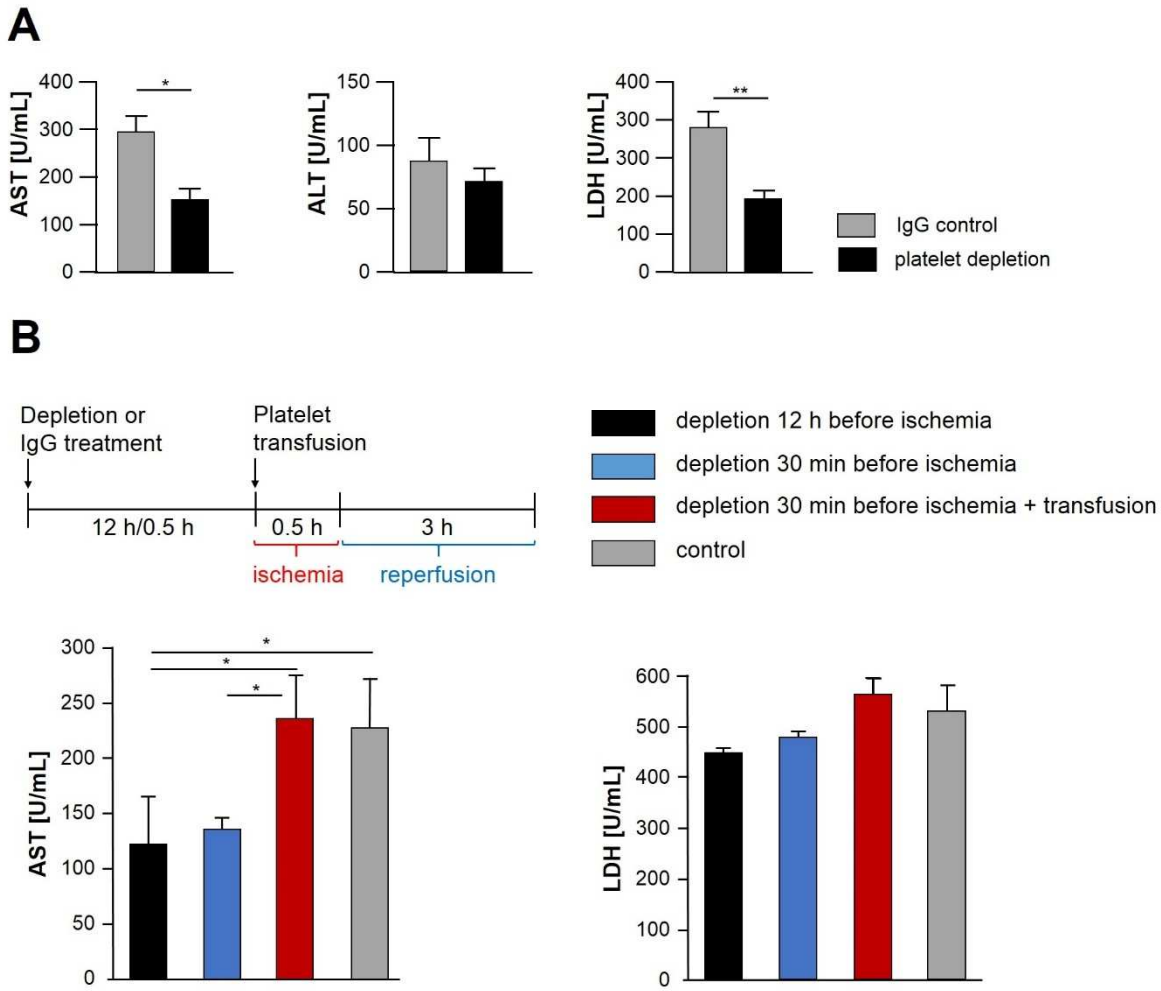

Figure 24: Serum analysis of platelet-depleted animals following liver ischemia. Mice were subjected to 30 min ischemia and treated with platelet depletion or IgG antibody (control). Three hours of reperfusion were allowed. Serum was analyzed for aspartate transaminase (AST), alanine transaminase (ALT) and lactate dehydrogenase (LDH) **(A)**. Platelet depletion at different time points before ischemia reduced liver damage. Even low platelet counts after transfusion abrogated the positive effect of platelet depletion **(B)**.

Furthermore, flow cytometric analysis of single cell suspensions from the post ischemic liver revealed reduced numbers of infiltrating neutrophils into the tissue (Fig. 25A). These findings were supported by confocal intravital microscopy. Here, the numbers of infiltrating neutrophils were also reduced in platelet-depleted animals (Fig. 25B).

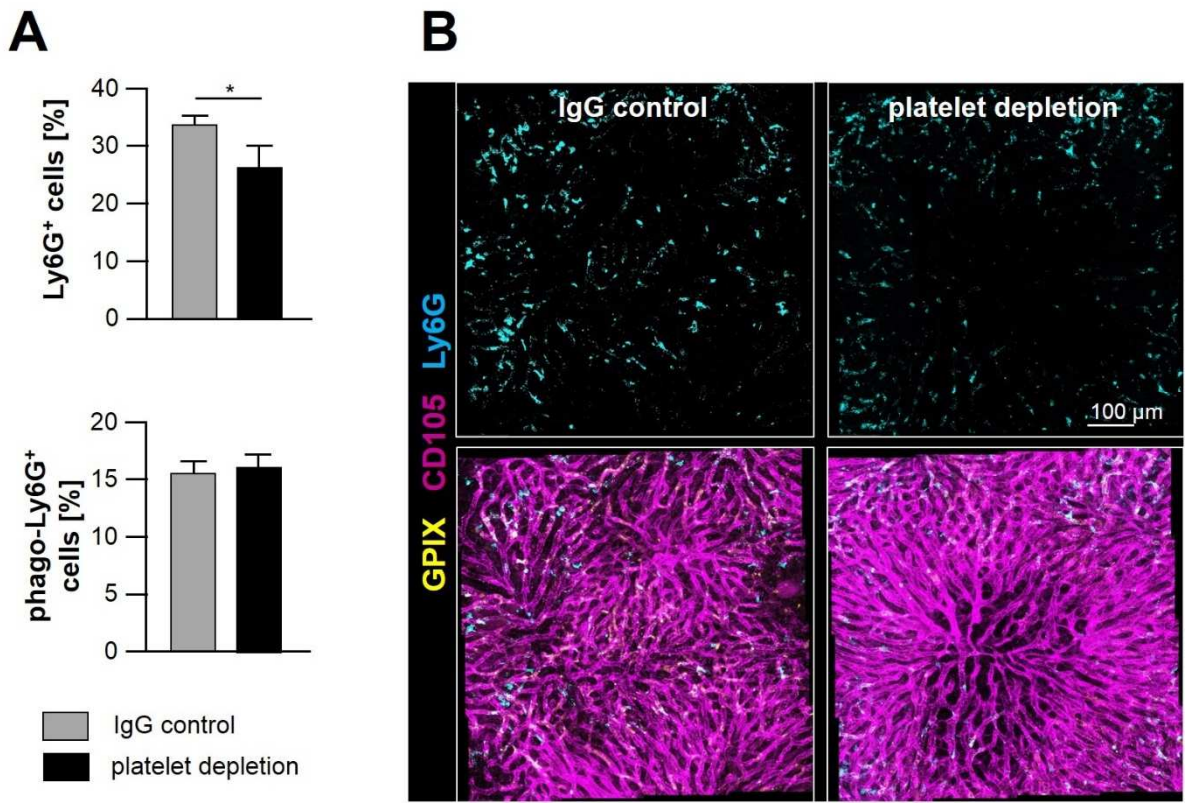

Figure 25: Neutrophil recruitment to the post-ischemic liver. (A) Flow cytometric analyses of single cell suspensions reveal reduced numbers of neutrophils in the post-ischemic liver. Data kindly provided by our collaborators Prof. Dr. Valbona Mirakaj and her team. **(B)** Intravital microscopy after three hours of reperfusion show reduced numbers of neutrophils in the liver. Vessels: magenta, platelets: yellow and neutrophils: cyan.

3.3.2 General platelet parameters are unaltered after hepatic ischemia

It is known that some diseases lead to altered platelet function or platelet reactivity (Hermansky-Pudlak syndrome or Glanzmann thrombasthenia, [275, 276]). To assess whether hepatic ischemia reperfusion injury alters platelet size and count or their functionality in terms of activation or degranulation, mice were subjected to 30 minutes ischemia and three hours of reperfusion.

After three hours of reperfusion platelet size, count and common platelet surface receptors were analyzed by flow cytometry. Interestingly, all tested parameters were undistinguishable between operated and naïve mice (Fig. 26A, B). Next, agonist-induced αIIbβ3 integrin activation was determined using the JON/A-PE antibody, which only binds to activated αIIbβ3. Flow cytometric analysis of antibody binding verified comparable integrin activation in operated and naïve mice in response to all tested agonists in line with similar degranulation kinetics assessed by determining the exposure of the α-granule marker P-selectin (Wug1.9) (Fig. 26C) suggesting normal platelet functionality following ischemia.

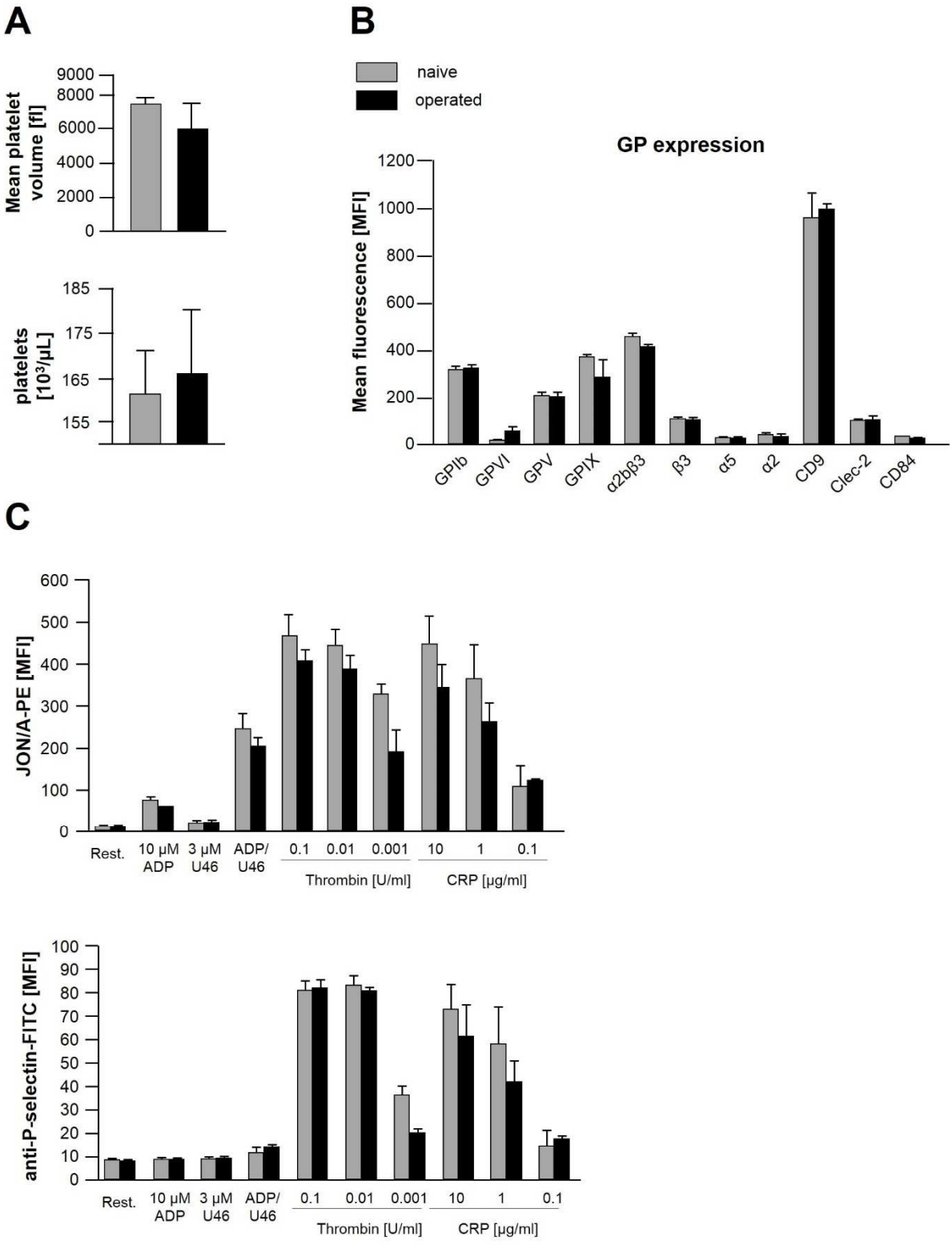

Figure 26: General platelet parameters are unaffected in post-ischemic mice. Flow cytometric analyses of whole blood to determine platelet size and count **(A)** as well as major platelet glycoprotein expression **(B)**. Washed blood was analyzed regarding αIIbβ3 integrin activation (binding of JON/A-PE, upper panel) and degranulation-dependent P-selectin exposure (lower panel) in response to the indicated agonists from naïve (grey) or operated (black) mice.

3.3.3 Platelet aggregation is dispensable for neutrophil infiltration following h I/RI

Since we were able to show an involvement of platelets in h IR/I, we wanted to assess the underlying signaling pathways leading to the protective effect seen in platelet-depleted animals. First, the role of platelet aggregation was assessed by injection of 50 µg/mouse JON/A. The $F(ab)_2$ fragment binds to the fibrinogen binding site on integrin αIIbβ3 and thereby prevents platelet aggregation [277].

The $F(ab)_2$ fragment was injected at the end of the ischemic phase and three hours of reperfusion were allowed. Serum analyses revealed no protective effect after blocking of αIIbβ3 integrins. The number of infiltrating neutrophils into the liver as well as the levels of the liver damage markers AST, ALT and LDH were indistinguishable from control mice (Fig. 27) suggesting that platelet aggregation is dispensable following h I/RI.

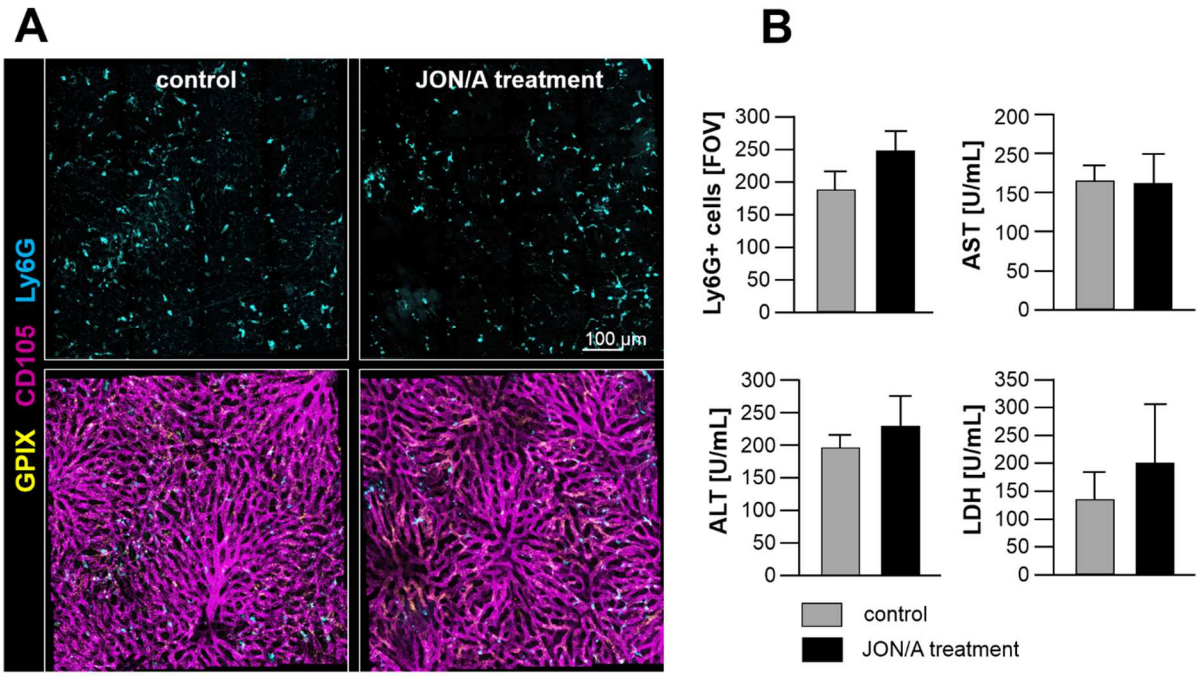

Figure 27: Intravital microscopy and serum analysis following αIIbβ3 integrin blockade. (A) Intravital microscopy after three hours of reperfusion with platelets (yellow), endothelium (magenta) and neutrophils (cyan). **(B)** Quantitative analysis of neutrophil infiltration to the liver and serum analysis with control animals (grey) and integrin-blocked animals (black).

3.3.4 GPIbα-blockade (p0p/B treatment) protects from neutrophil infiltration and reduces cellular damage following ischemia

GPIbα is part of the GPIb-V-IX complex and interacts with vWF, thrombin, P-selectin, Mac-1 and some coagulation factors [60]. This receptor is required for initial tethering and adhesion of platelets, especially under high shear conditions. Genetic GPIbα deficiency results in lack of the entire receptor complex and severe macrothrombocytopenia [278], however, application of p0p/B-F(ab) blocks the thrombin and vWF binding site of GPIbα [51], thus preventing the interaction with its main ligand without affecting platelet count. Therefore, application of 50 µg/mouse of p0p/B-F(ab) was used to study the role of GPIbα in h I/RI.

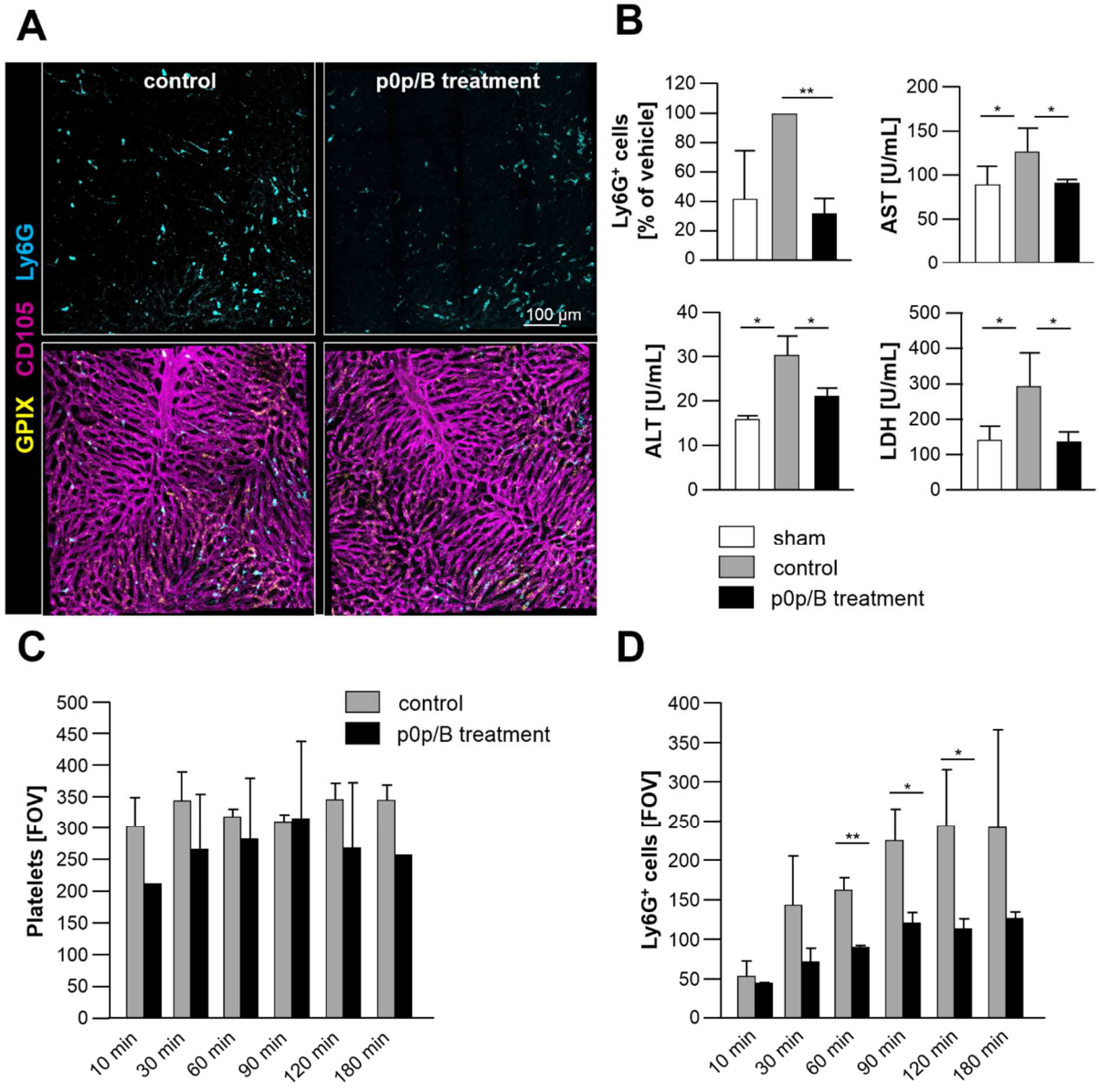

Figure 28: Intravital microscopy and serum analysis following blockade of the vWF-GPIb interaction upon p0p/B-F(ab) administration. (A) IVM after three hours of reperfusion with platelets (yellow), endothelium (magenta) and neutrophils (cyan). **(B)** Quantitative analysis of neutrophil infiltration and liver damage. Serum analysis with control treated animals (grey) and GPIbα-blocked animals (black). Kinetics of platelet **(C)** or neutrophil **(D)** accumulation in the post-ischemic liver**.**

Strikingly, neutrophil infiltration into the liver following ischemia was markedly reduced under these conditions (Fig. 28A). In line with these findings, serum parameters revealed significantly decreased levels of damage markers suggesting a role of platelet adhesion in the progression of h I/RI (Fig. 28B). Since opening of the peritoneal cavity might already induce small amounts of liver damage, sham-operated mice, which underwent the surgery without occlusion of the liver, were used to set the degree of p0p/B mediated liver protection into perspective. Administration of p0p/B showed comparable liver damage to sham operated animals, indicating that p0p/B is able to reduce inflammation to a minimum level.

To assess at which point of time following ischemia GPIbα is important, time course analyses were performed and the number of platelets and neutrophils during three hours of reperfusion were evaluated (Fig. 28C, D). No differences were observed for the number of platelets in the observation area. However, a significant reduction in neutrophil numbers accompanied by a reduced slope was observed in p0p/B-treated animals. These findings suggest that platelet adhesion mediated by GPIbα might affect neutrophil recruitment.

3.3.5 GPIb-IL-4R mice behave like p0p/B-treated animals following h I/RI

To exclude the possibility that the observed effects upon GPIbα blockade are a result of the antibody application itself a transgenic mouse model was used. The GPIb-IL-4R mouse line expresses a modified version of GPIb, where the extracellular domain is replaced by the human IL-4 receptor α [279], thus abolishing interaction with native ligands without affecting the formation of the GPIb-V-IX complex suggesting normal downstream signaling.

These mice were subjected to 30 minutes ischemia and three hours of reperfusion. As seen for GPIbα blockade using p0p/B-F(ab), transgenic mice showed reduced serum parameters thus supporting the role of GPIb in liver damage progression following ischemia and arguing against unspecific antibody-mediated effects in p0p/B-F(ab)-treated mice (Fig. 29).

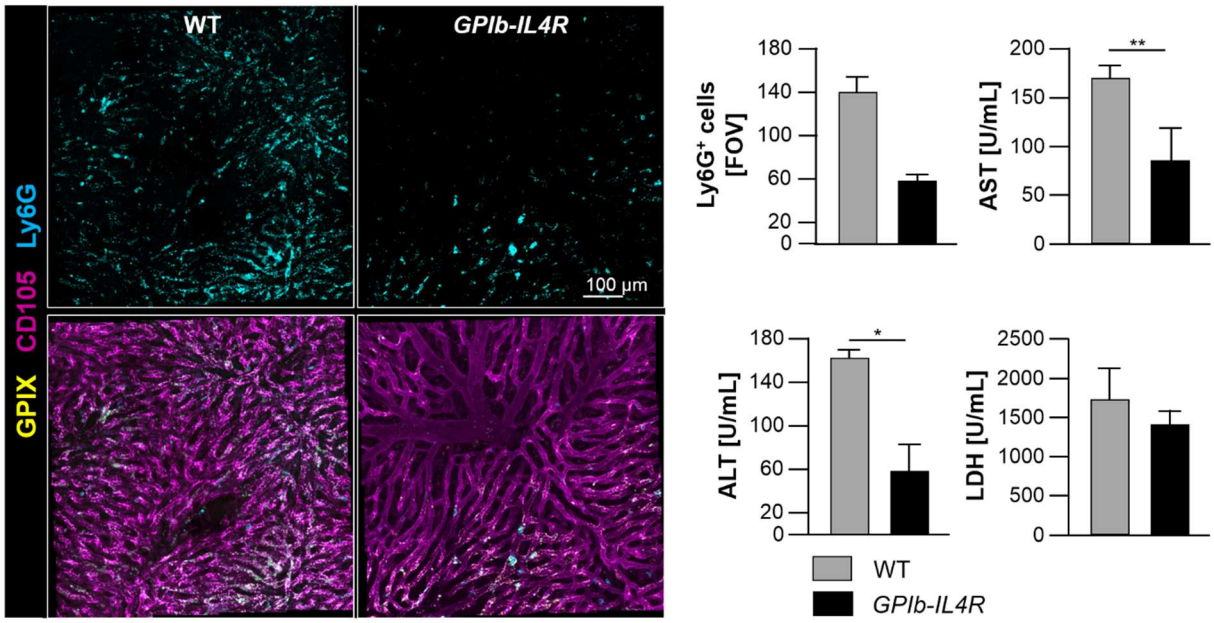

Figure 29: Intravital microscopy and serum analysis of GPIb-IL-4R mice after h I/RI. (A) Intravital microscopy after 3 hours of reperfusion with platelets (yellow), endothelium (magenta) and neutrophils (cyan). **(B)** Quantitative analysis of neutrophil infiltration to the liver and serum analysis with control treated animals (grey) and GPIb-IL-4R animals (black).

3.3.6 *vWF*$^{-/-}$ mice display a comparable phenotype to p0p/B-treated animals following h I/RI

vWF is the major GPIb ligand and necessary for initial tethering to the endothelium after tissue damage (ref). It is released by a broad range of cells, including platelets. Recent publications were able to demonstrate a liver-protective effect in the absence of vWF [175].

By using *vWF*$^{-/-}$ mice in the h I/RI model we were able to show reduced neutrophil infiltration into the post-ischemic liver using intravital microscopy (Fig. 30A), which is in line with the above-mentioned publication. Furthermore, serum parameters indicated reduced liver damage, thus suggesting a better outcome and decreased inflammation (Fig. 30B).

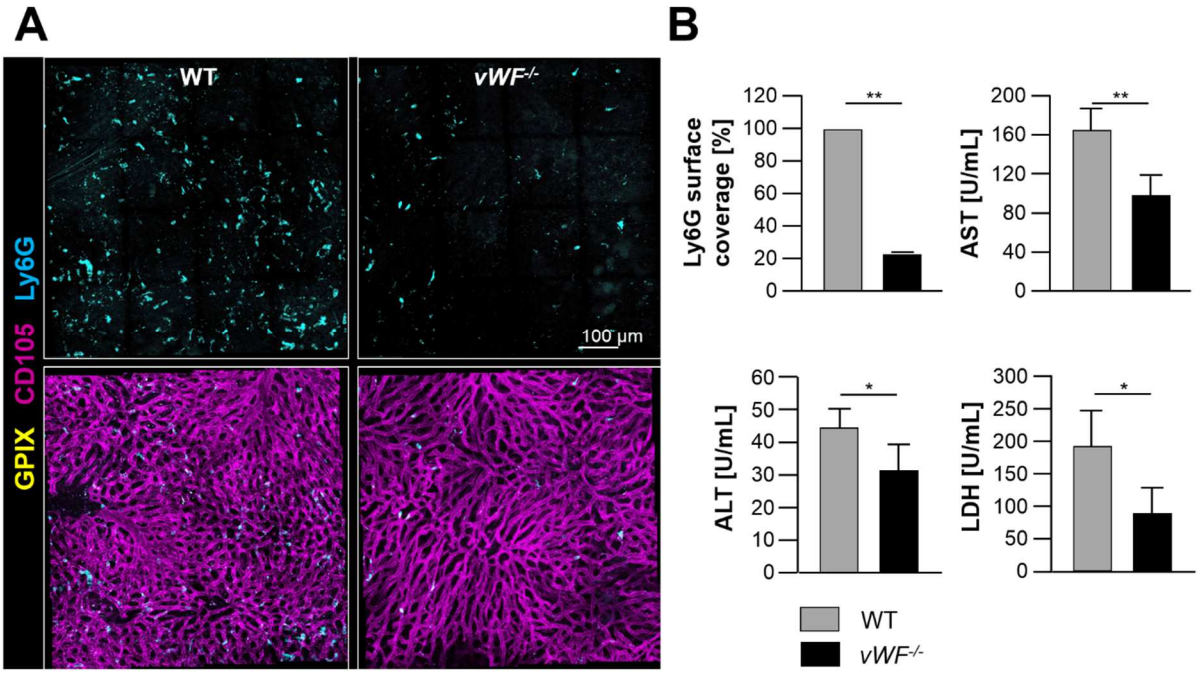

Figure 30: Intravital microscopy and serum analysis of vWF-deficient animals following h I/RI. (A) Intravital microscopy after three hours of reperfusion with platelets (yellow), endothelium (magenta) and neutrophils (cyan). **(B)** Quantitative analysis of neutrophil infiltration to the liver and serum analysis with control treated mice (grey) and *vWF*$^{-/-}$ mice (black).

3.4 Characterization of the LTA_4H knockout mice

3.4.1 LTA_4H knockout mice are viable and healthy

Constitutive *Lta4h* knockout mice (*Lta4h*$^{-/-}$) were viable and born at normal Mendelian ratio. They were fertile and did not show any signs of spontaneous bleeding. Western blot analysis confirmed the expression of LTA_4H in control mice and its absence in samples from *Lta4h*$^{-/-}$ mice (Fig. 31A).

A

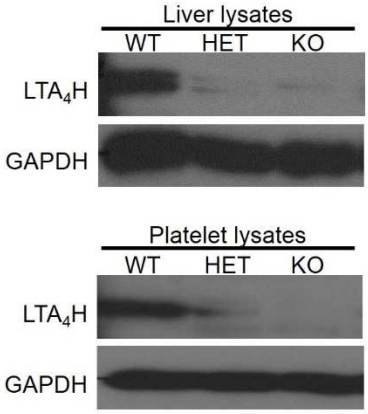

B

	wt	*Lta4h*$^{-/-}$	p-value
PLT [x10^3/µL]	1033.1 ± 141.2	1073.2 ± 253.1	0.68
MPV [µm^3]	5.7 ± 0.3	5.5 ± 0.2	0.08
RBC [x10^6/µL]	9.8 ± 1.4	9.3 ± 1.6	0.46
WBC [x10^3/µL]	6.8 ± 2.3	6.5 ± 2.4	0.79
HCT [%]	48.1 ± 6.6	45.2 ± 8.1	0.42
MCV [µm^3]	48.9 ± 1.4	49.0 ± 0.6	0.85
MCH [pg]	15.3 ± 0.6	15.3 ± 0.2	0.69
MCHC [g/dL]	31.2 ± 0.4	31.2 ± 0.5	0.96

C

	wt	*Lta4h*$^{-/-}$	p-value
α-GPIb [MFI]	5975.2 ± 139.4	5981.6 ± 185.9	0.95
α-GPVI [MFI]	925.6 ± 66.5	1063.3 ± 369.6	0.40
α-GPV [MFI]	4286.8 ± 225.7	4323.8 ± 282.4	0.83
α-GPIX [MFI]	7690.0 ± 164.5	7617.0 ± 404.5	0.72
α-a2 [MFI]	817.4 ± 15.1	841.4 ± 39.8	0.26
α-α5 [MFI]	468.2 ± 30.0	454.4 ± 23.3	0.46
α-αIIbβ3 [MFI]	8837.4 ± 362.2	8760.4 ± 222.1	0.70
α-CD9 [MFI]	17870.8 ± 502.4	18870.2 ± 912.0	0.07
α-Clec2 [MFI]	3035.2 ± 388.1	2968.6 ± 912.0	0.77
α-CD84 [MFI]	584.4 ± 32.3	612.4 ± 65.3	0.42

Figure 31: Unaltered basal blood parameters in *Lta4h*$^{-/-}$ mice. (A) Western blot analysis confirmed the absence of LTA4H in knockout mice**.** GAPDH served as loading control. **(B)** Basal blood parameters were determined using an automated hematology analyzer. **(C)** Abundance of major platelet glycoproteins was measured by flow cytometry.

Basic blood parameters as well as platelet size and count were indistinguishable from control animals, suggesting that LTA_4H is not essential for hematopoiesis (Fig. 31B). The abundance of major platelet surface receptors was analyzed using flow cytometry. Platelet glycoprotein expression was unaffected by the loss of LTA_4H (Fig. 31C).

3.4.2 Unaltered integrin activation in platelets of *Lta4h*$^{-/-}$ mice

Agonist-induced αIIbβ3 integrin activation using the JON/A-PE antibody [262] as well as degranulation-dependent surface exposure of P-selectin, a marker for α-granule release, were determined by flow cytometry. *Lta4h*$^{-/-}$ platelets displayed an unaltered αIIbβ3 integrin activation in response to all tested agonists as well as an indistinguishable agonist-induced P-selectin exposure (Fig. 32A, B).

In line with this experiment, platelet aggregation upon stimulation with different agonists was comparable between WT and LTA_4H-deficient platelets (Fig. 32C). In order to test GPCR-dependent responses, ADP, the thromboxane A_2 analogue U46619 and thrombin were used. GPVI-dependent aggregation was tested using collagen and *collagen related peptide* (CRP). Only high doses of ADP showed slightly delayed response in *Lta4h*$^{-/-}$ platelets, however, same levels of aggregation were reached. These data suggest, that LTA_4H is dispensable for inside-out signaling.

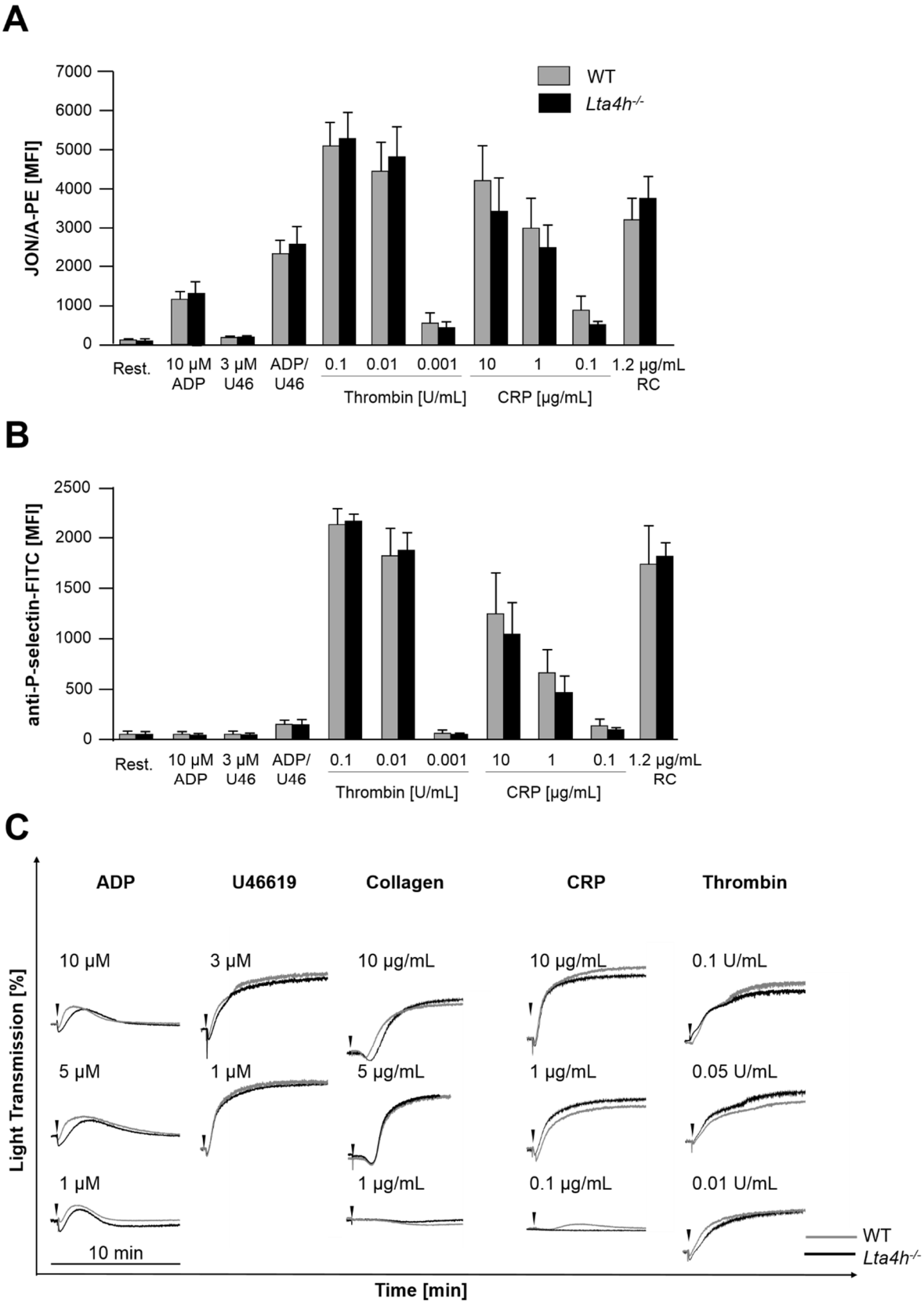

Figure 32: Unaltered integrin activation in *Lta4h*$^{-/-}$ mice. (A) Activation of platelet αIIbβ3 integrin (JON/A-PE) and **(B)** degranulation (α-P-selectin-FITC) in *Lta4h*$^{-/-}$ platelets as determined by flow cytometry. **(C)** For aggregation studies with thrombin, collagen-related peptide (CRP), collagen and U46619, washed platelets were used; aggregation studies with ADP were performed in platelet-rich plasma.

3.4.3 Platelet outside-in signaling is unaffected in Lta4h knockout mice

To test whether integrin outside-in signaling was affected by the loss of LTA_4H, knockout and control platelets were allowed to spread on a fibrinogen-coated surface in the presence of thrombin (0.01 U mL^{-1} final concentration). The filopodia formed were indistinguishable between WT and *Lta4h*$^{-/-}$ platelets (Fig. 33). Furthermore, the kinetic of platelet spreading was comparable between the groups. This data demonstrates that LTA_4H is not required for platelet spreading on fibrinogen.

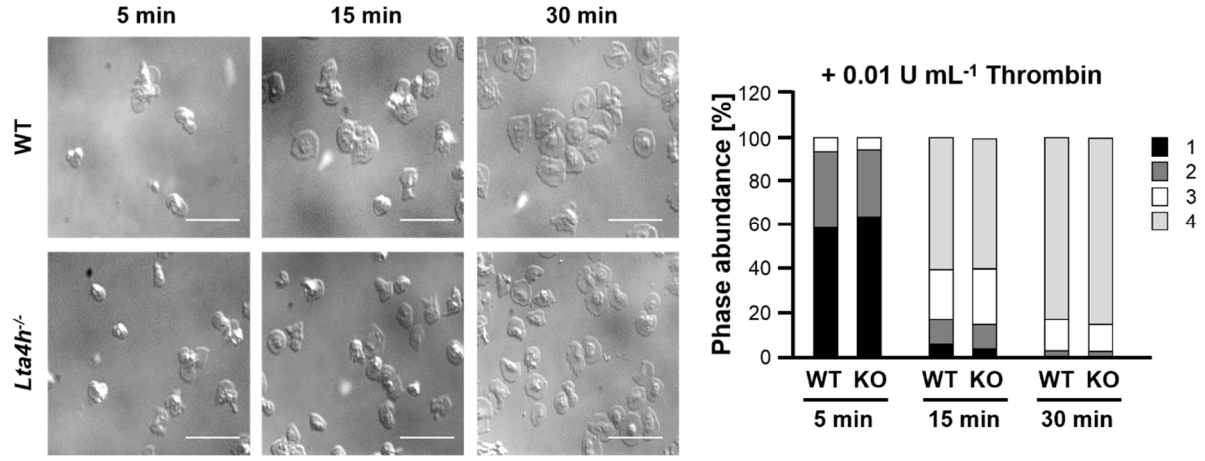

Figure 33: Integrin outside-in signaling is indistinguishable in *Lta4h*$^{-/-}$ platelets. Platelets were stimulated with 0.01 U mL^{-1} thrombin and spread on fibrinogen (100 µg/ml) coated surfaces. Representative *differential interference contrast* (DIC) images (left panel) and quantification of abundancy of different spreading phases (right panel) revealed unaltered spreading capacity of *Lta4h*$^{-/-}$ platelets.

3.4.4 Unaltered aggregate formation of *Lta4h*$^{-/-}$ platelets under flow

Next, Lta_4h deficient platelets were tested for their capacity to form aggregates on collagen-coated surfaces under flow conditions. Both thrombus volume and surface coverage were unaltered in *Lta4h*$^{-/-}$ mice as compared to controls (Fig. 34).

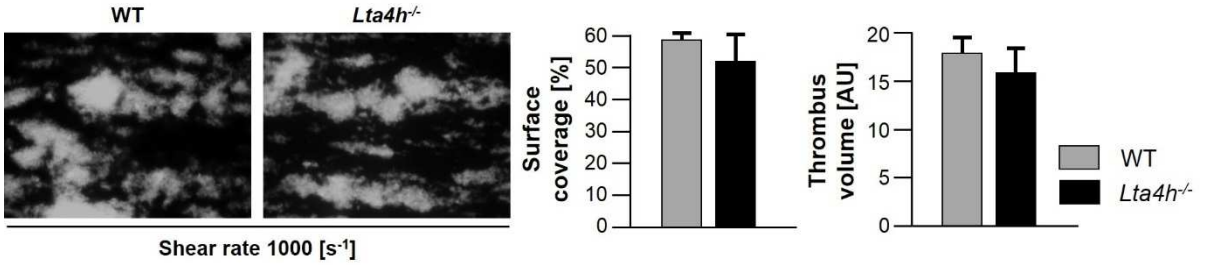

Figure 34: Unaltered adhesion and thrombus formation of *Lta4h*$^{-/-}$ platelets on collagen under flow. Whole blood was perfused with shear rates of 1000 s^{-1} over collagen-coated surface. Representative fluorescence images are shown (left panel). Quantification of surface coverage and the relative thrombus volume (right panel) show no differences of *Lta4h*$^{-/-}$ compared to WT thrombus formation.

3.4.5 *Lta4h*$^{-/-}$ mice show unaltered arterial thrombus formation and tail bleeding times as compared to control animals

Pathological thrombus formation was assessed by intravital microscopy upon $FeCl_3$-induced injury of mesenteric arterioles. Both the point of thrombus initiation as well as the time to full occlusion was comparable between WT and *Lta4h*$^{-/-}$ animals (Fig. 35A). However, a slight delay in the appearance of first thrombi could be observed in *Lta4h*$^{-/-}$ mice.

To study the effect of LTA_4H-deficiency on the hemostatic function of platelets, tail bleeding experiments were performed. One millimeter of the tail tip of the anesthetized animals was cut and the time to cessation of the blood flow was measured using a filter paper. In line with platelet activation and aggregation experiments, knockout and control animals stopped bleeding within the observed time window of 20 minutes. Mean bleeding times were indistinguishable between the groups, although bleeding times were quite heterogenous (Fig. 35A). These findings suggest, that LTA_4H is dispensable for thrombosis and hemostasis.

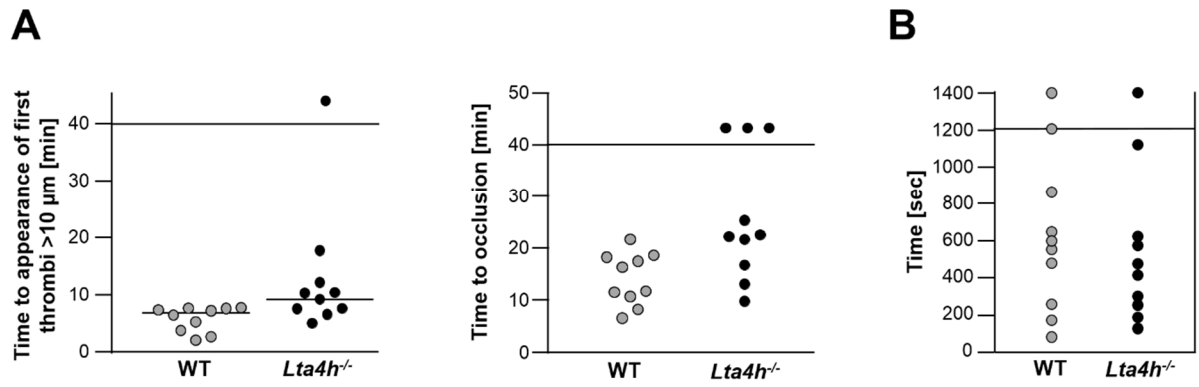

Figure 35: *In vivo* thrombus formation and hemostasis was unaffected in *Lta4h*$^{-/-}$ animals. (A) Mice were subjected to the $FeCl_3$ induced thrombosis model and thrombus formation was monitored. Time to appearance of first thrombi and full vessel occlusion; experiments performed by Dr. Sarah Beck. **(B)** Hemostasis was assessed in a tail bleeding assay. No significant differences between WT and ko mice were detectable.

3.4.6 LTB_4 and platelet supernatant induce neutrophil transmigration *in vitro*

LTB_4 is a known chemoattractant for neutrophil migration. To study whether platelets devoid of the Lta_4 hydrolase are unable to produce LTB_4 and thereby less potent in attracting neutrophils, a transwell assay was performed in which neutrophils were stimulated with different agents: *fetal calf serum* (FCS), LTB_4, platelet *supernatant* (SN) and CRP. Quantification of neutrophils on the porous membrane showed a dose dependent chemotactic property of LTB_4, with a high number of neutrophils per field of view. Platelet supernatant and 10 % FCS were also able to induce neutrophil recruitment, but to a lesser extent. 10 µg mL^{-1} CRP, however, had no chemotactic effect. Determination of transmigrated neutrophils into the lower chamber showed highest numbers for stimulation with platelet supernatant and the high

concentration of LTB_4, indicating that platelet supernatant is able to act as a chemotactic agent, as well (Fig. 36).

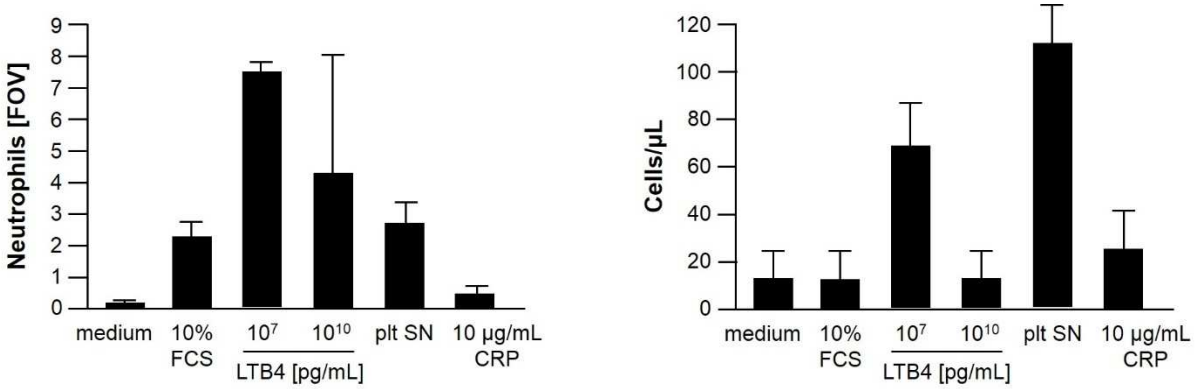

Figure 36: Transwell assay shows chemotactic capacity of platelet supernatant. Neutrophils were seeded into a transwell chamber and exposed to different potentially chemotactic agents. After 16 hours at 37 °C and 5 % CO2, neutrophil numbers in the porous membrane (left panel) and the medium in the lower chamber (right panel) were determined.

3.4.7 *Lta4h*$^{-/-}$ mice are not protected from hepatic ischemia reperfusion injury

Since LTB_4 acts as a powerful substance in neutrophil recruitment, we wanted to investigate whether the absence of LTA_4H leads to reduced neutrophil infiltration ultimately resulting in a protection from ischemia reperfusion injury. WT and knockout mice were subjected to 30 minutes ischemia followed by three hours of reperfusion. Blood was collected after 3 hours of reperfusion. The serum was tested in ELISA measurements for AST, ALT and LDH to determine liver damage. Surprisingly, we found no differences between the two groups (Fig. 37A), indicating that the absence of LTA_4H does not ameliorate cellular damage in the reperfusion phase. We then continued to analyze neutrophil infiltration into the post-ischemic liver. After three hours of reperfusion, we found significantly reduced numbers of neutrophils in *Lta4h*$^{-/-}$ animals (Fig. 37B), with unaffected liver damage markers. This data suggests, that LTA_4H deficiency leads to reduced neutrophil infiltration into the liver. However, liver damage is only partially caused by infiltrating neutrophils.

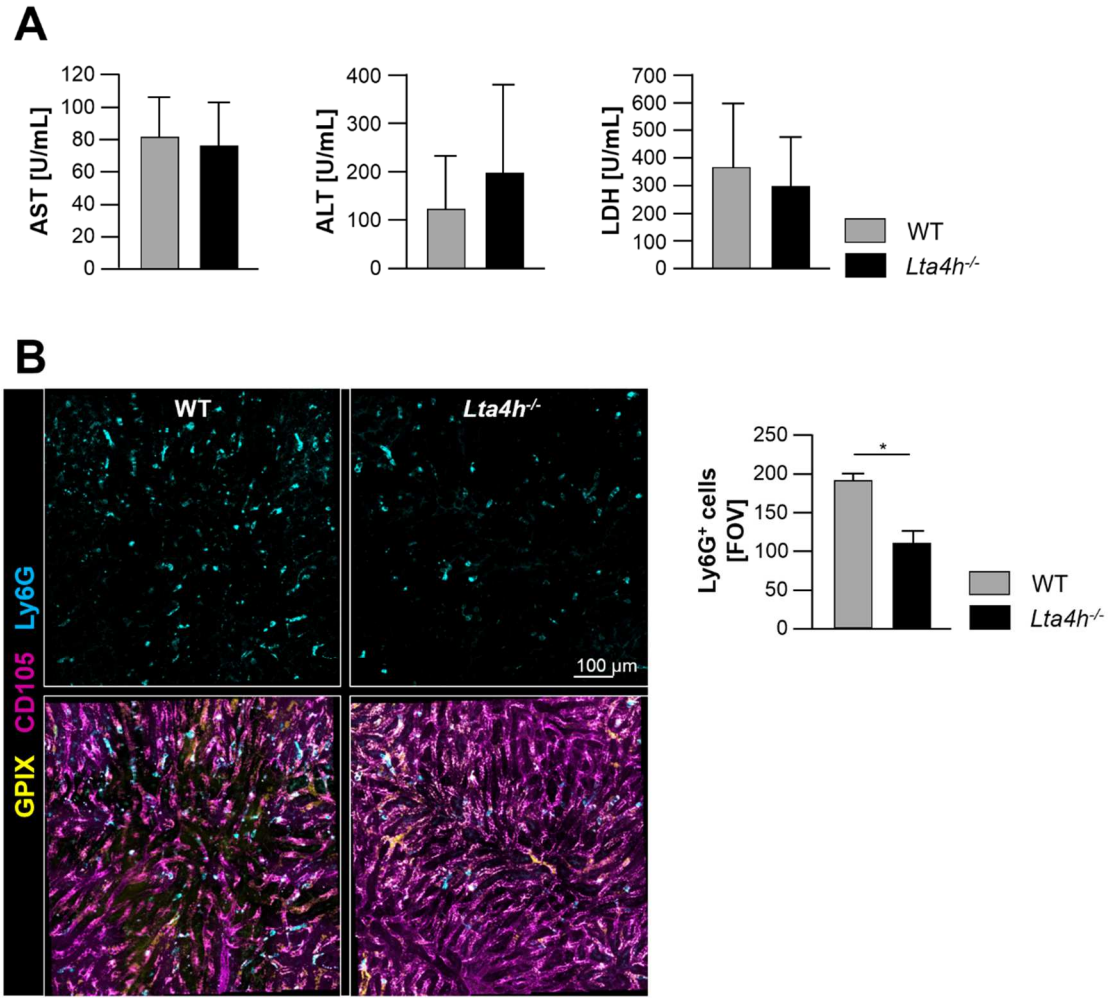

Figure 37: *Lta4h*$^{-/-}$ mice are not protected from hepatic ischemia reperfusion injury. After three hours of reperfusion, serum was collected and analyzed for liver damage markers **(A)** with WT (grey) and *Lta4h*$^{-/-}$ (black) mice. **(B)** IVM after three hours of reperfusion with platelets (yellow), endothelium (magenta) and neutrophils (cyan) show reduced neutrophils infiltration to the tissue, quantified on the right panel.

3.4.8 *Lta4h*$^{-/-}$ mice show reduced neutrophil infiltration following the hot needle injury

We next wanted to validate the results from hepatic ischemia in a setting that is known to be neutrophil-driven. Therefore, we chose the hot needle injury, where the inflammation response is localized to one spot making it a model of sterile inflammation. Confocal IVM was used to observe platelet and neutrophil recruitment over a period of three hours. We found that the number of adhering platelets was comparable between WT and *Lta4h*$^{-/-}$ animals (Fig. 38A). However, at the end of the observed time window, the number of neutrophils was significantly decreased in *Lta4h*$^{-/-}$ mice (Fig. 38B). These findings were in line with the results obtained from h I/RI.

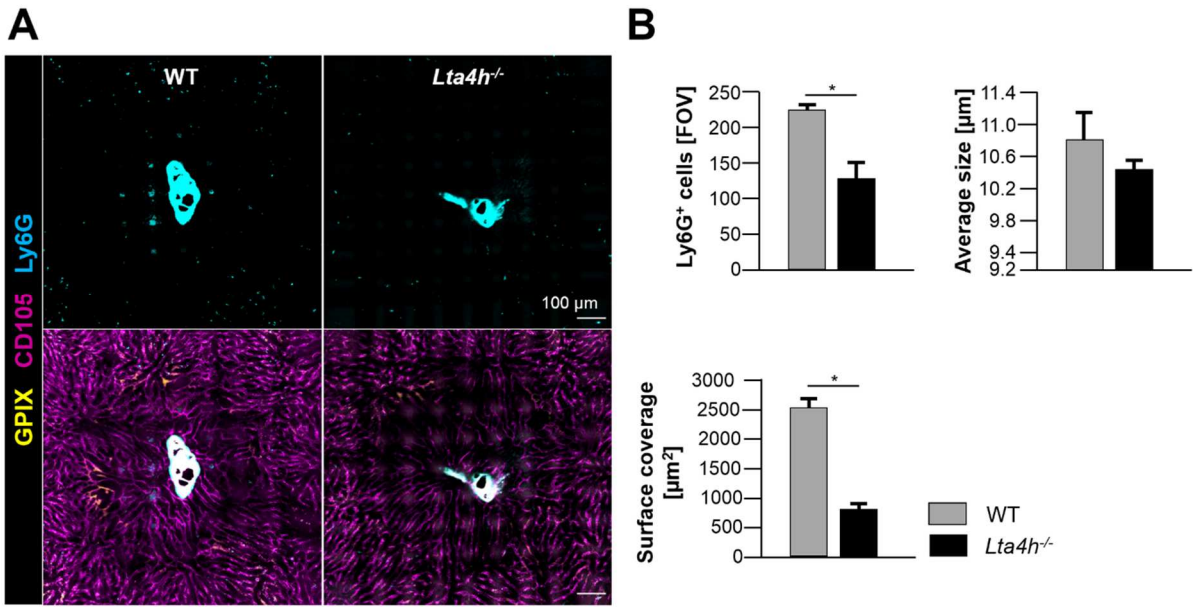

Figure 38: Hot needle injury with *Lta4h* knockout mice. After injury of the liver with a thermal probe, the recruitment of neutrophils was monitored over a period of 3 hours **(A)**. Platelets (yellow), endothelium (magenta) and neutrophils (cyan) show reduced neutrophils infiltration to the tissue of WT (grey) and *Lta4h*$^{-/-}$ animals (black). **(B)** Quantification.

3.5 Spin isolation of murine BM is time efficient and suited for analysis of HSCs, immune cells and MKs

Isolation of BM-derived cells has been a time-consuming process where quite some shear stress is applied to the cells by repeated flushing through a 23 G needle [255]. A recent publication introduced a new method to isolate BM cells [254]. This second method completely lacks processing of the cells through a needle and flushes the bone marrow using centrifugation. We were interested in a comparison of both methods in quantitative (stem and immune cell FACS analysis, MK ploidy) and qualitative (culture of BM MKs and pro-platelet formation) experiments. This study was performed jointly with Tobias Heib from our department.

3.5.1 The spin-flush method results in a higher yield of cells

As mentioned above, the biggest difference between the two isolation methods is the repeated flushing of the bone marrow with a 23G needle in contrast to centrifugation of the complete bone. The centrifugation-based spin-method is not only faster (Fig. 39A) but also results in bigger cell pellets (Fig. 39B) and ultimately higher cell yields. Of note, the cell viability was indistinguishable between both isolation methods (Fig. 39C).

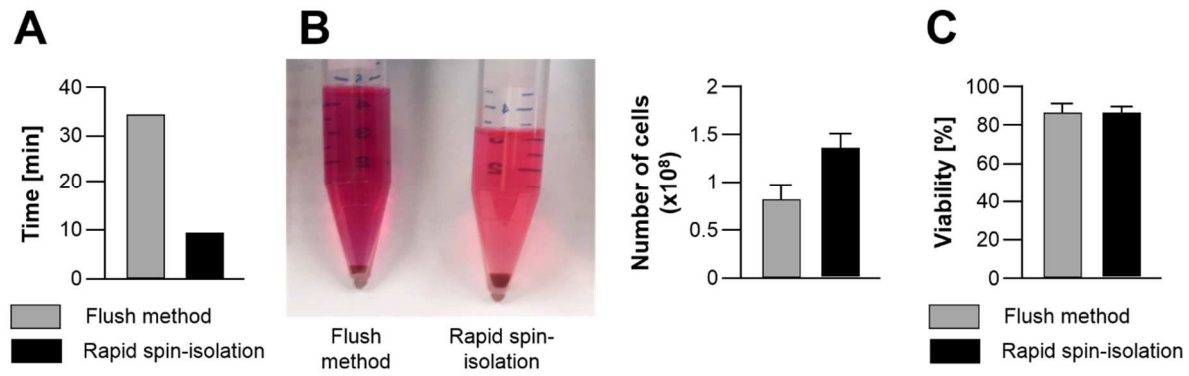

Figure 39: Cell yield after two bone marrow isolation methods. (A) Time saving effect of the rapid spin-isolation method. **(B)** Representative images of obtained cell pellets. Number of cells were quantified using a countess with a cut-off of 7-50 µm. **(C)** Viability was determined by flow cytometry using a dead cell marker kit (Heib, Gross *et al.*, accepted).

3.5.2 Both isolation methods result in comparable distribution of HSCs and multipotent progenitor populations

Since HSCs as such cannot be isolated as a pure cell type, flow cytometric analysis was used to determine the subpopulations and their distribution. As HSCs lack the expression of mature surface markers of blood cells, these cells are characterized by their lack of lineage mix (lin-)

markers of mature blood cells such as B220 (CD45R), Mac-1 (macrophages) or Ter119 (erythrocytes). Moreover, they were further characterized by their expression of c-kit and Sca-1 [3, 280]. The latter is lost during differentiation into *common myeloid progenitors* (CMPs), but still present in short- and long-term HSCs as well as *multipotent progenitors* (MPPs). The gating strategy is displayed in Fig. 40.

Quantification of single cell suspensions showed comparable numbers for cell aggregate formation and cell viability, using a dead cell marker (Fig. 41A). Analyzing the different progenitor populations (Fig. 41B), we found an overall increased cell number in the rapid-spin isolation method, however lin^- $cKit^+$ cell populations were indistinguishable between both isolation methods. The expression of *Stem cell antigen 1* (Sca-1) distinguishes between stem cell progenitors ($Sca\text{-}1^+$) and lympho-myeloid lineage populations ($Sca\text{-}1^-$). We found the *granulocyte-macrophage progenitor* (GMP) subpopulation of $Sca\text{-}1^-$ cells to be increased in rapid spin-isolated samples, while all other subpopulations remained unaltered. Stem cell progenitors showed no differences after isolation with either method.

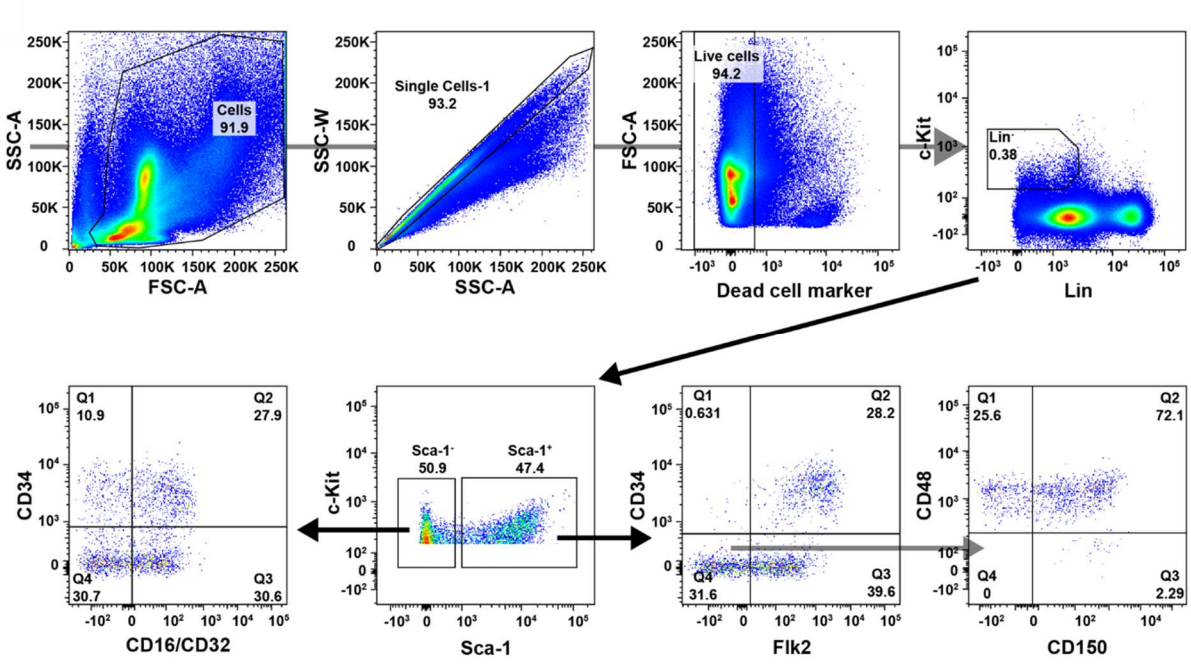

Figure 40: Gating strategy for progenitor cell populations in the murine bone marrow. Bone marrow HSCs were analyzed in a reverse manner. The living cell population was analyzed with regard to mature cell type specific markers. After exclusion of positive cells, expression of cKit and Sca-1 was analyzed. $Sca\text{-}1^-$ cells give rise to common myeloid progenitors (CMPs) and further differentiate into megakaryocyte/erythrocyte progenitors (MEPs) and granulocyte/monocyte progenitors (GMPs). $Sca\text{-}1^+$ cells are separated by expression levels pf CD34 and Flk2. Short term HSCs are $CD34^+Flk2^-$, whereas long-term HSCs are $CD34^-$ $Flk2^-$. Heib, Gross *et al.*, accepted).

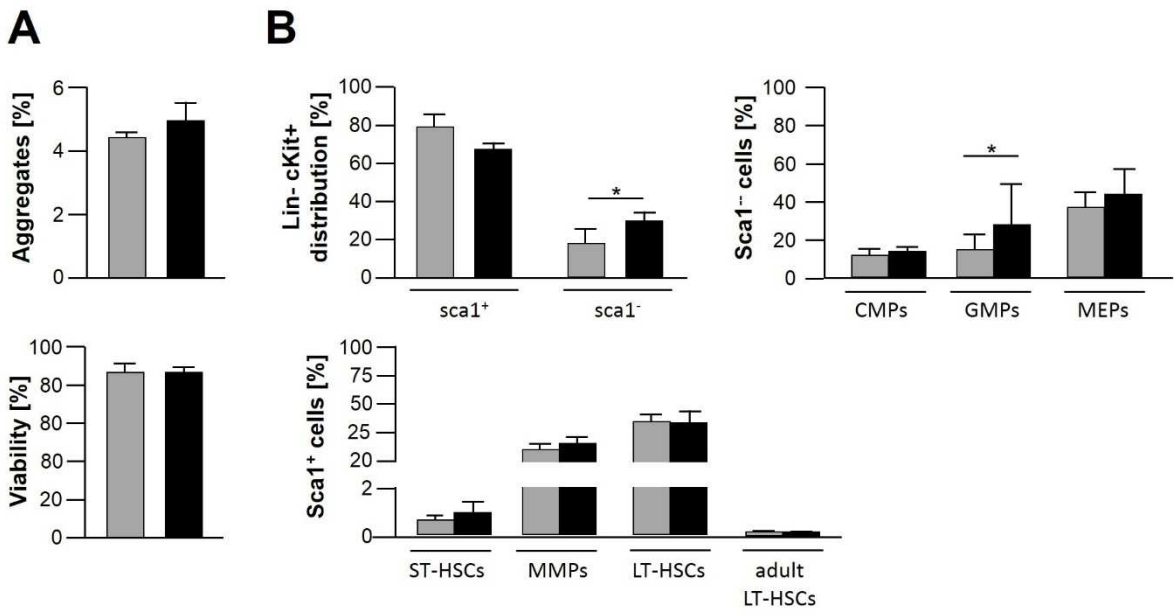

Figure 41: Flow cytometry of hematopoietic stem cells the murine bone marrow. (A, *upper panel***)** Forward scatter (FSC)-area vs FSC-height is used to determine the amount of aggregates. **(A,** *lower panel***)** cell viability was determined using a dead cell marker kit. Dying cells become positive for this membrane impermeable marker. **(B)** Stem cell progenitor distribution displayed in % as frequency of parent. Minor differences were observed for rapid spin-isolated cells in Sca-1 expression. (Heib, Gross *et al.*, accepted).

3.5.3 Rapid spin isolation results in increased lymphoid cell yields without affecting cell viability

To determine immune cell populations by flow cytometry, the lymphoid pan marker CD45 (leukocyte common antigen) was used [281]. There are at least four known isoforms of this glycoprotein and all leukocytes express at least one version of it [282].

Leukocyte populations were determined directly after cell isolation. A gating strategy for the tested leukocyte subpopulations can be seen in Fig. 42. After gating for CD45-positive cells, immune cell populations were further distinguished by their expression of the myeloid pan marker CD11b. CD11b+ cells differentiate into granulocytic cell populations giving rise to neutrophils (Ly6G) and monocytes (Ly6C), whereas CD11b- cells differentiate into lymphoid cell populations, giving rise to T cells (CD3, CD4, CD8), NK cells (NK1.1) as well as B cells (CD19).

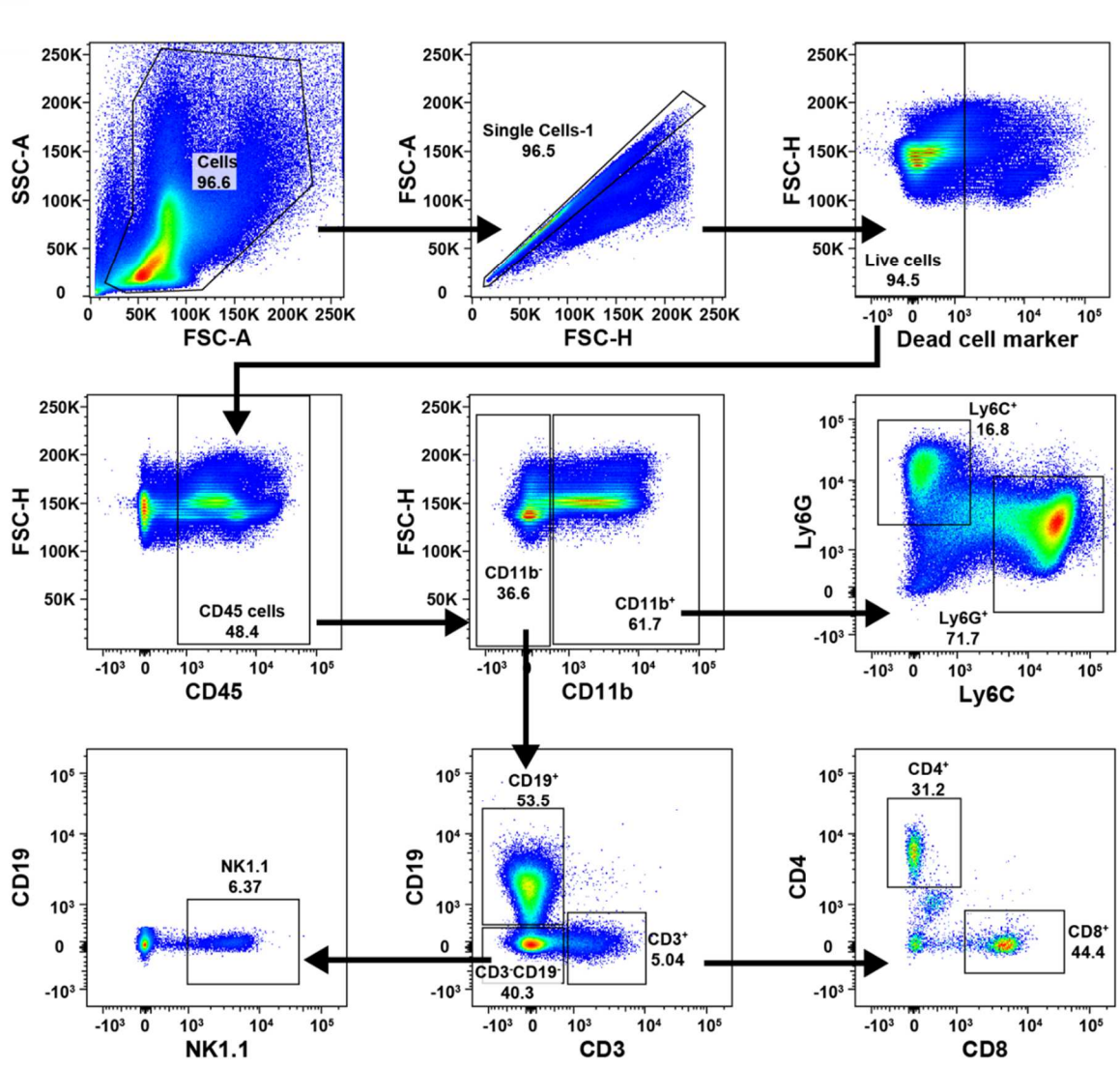

Figure 42: Gating strategy for immune cell populations in the murine bone marrow. Immune cell populations were distinguished by expression of the pan marker CD45. Immune cells can be divided by their expression of CD11b. CD11b positive cells give rise to myeloid cell populations (neutrophils, monocytes), whereas CD11b- cells give rise to all lymphoid cell populations (CD3, NK cells). (Heib, Gross *et al.*, accepted).

In line with data derived for stem cell progenitor determination, aggregate formation and cellular viability was indistinguishable for both tested isolation methods (Fig. 43A), whereas aggregate formation was similar for both isolation methods. In line with the overall increased cell yield for spin-isolated cells, an increase in subpopulations of individual immune cells can be observed (Fig. 43B).

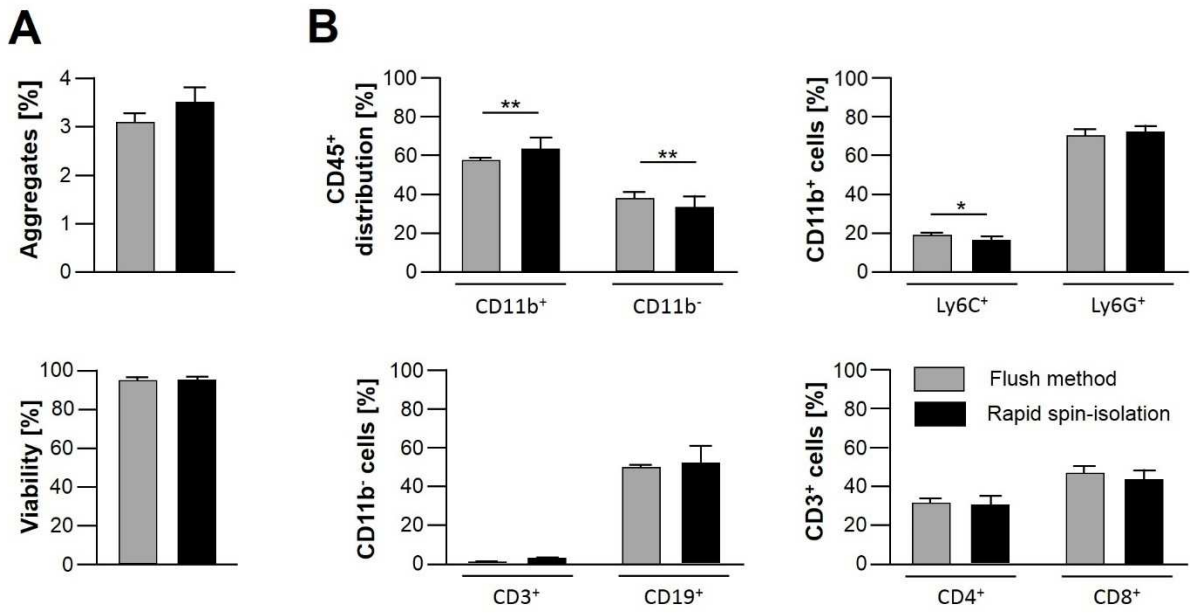

Figure 43: Increased granulocytic immune cell populations in the murine BM after rapid spin-isolation. (A, *upper panel***)** Forward scatter (FSC)-area vs FSC-height was used determine aggregate formation. **(A,** *lower panel***)** The dead cell marker was used to determine viability. **(B)** Immune cells were determined by CD45 expression. Immune cell subpopulation distribution is displayed in % as frequency of parent. (Heib, Gross *et al.*, accepted).

4. Discussion

To limit blood loss at sites of vascular injury proper platelet activation, coagulation and subsequent aggregate formation are essential. Decreased platelet activity or coagulation defects can result in severe bleeding disorders, while overshooting platelet activation can lead to complete vessel occlusion as found in myocardial infarction or ischemic stroke. These cardiovascular diseases are among the leading causes of death worldwide [283]. Therefore, platelet signaling pathways and thrombus formation need to be understood better in order to identify new potential targets to prevent disease onset. In addition to their classical role in hemostasis, platelets have been recognized as cells of the immune system [284]. As such, they are able to influence the course and severity of inflammation either directly or indirectly via interaction with other immune cells [48]. Therefore, a comprehensive picture of classical platelet function and their role in inflammatory settings needs to be drawn.

In this thesis, the role of platelets was investigated in hepatic ischemia reperfusion injury, a model of sterile inflammation. Our results showed, that initial platelet tethering (via GPIbα and vWF) but not platelet aggregation (via GPIIb/IIIa) is relevant for the resulting liver damage. Furthermore, the role of LTA_4H in platelet function and inflammation was investigated in constitutive knockout mice. It was demonstrated that platelet function is completely unaltered in these animals and the degree of liver damage following ischemia was comparable to WT animals. However, these mice showed reduced neutrophil infiltration, most likely as a result of missing LTB_4.

In the last part of this thesis, two isolation methods of murine bone marrow, the classical flush and the rapid spin-isolation method, were compared. We found the rapid-spin isolation to be superior, as it was not only time-saving, but also resulted in significantly increased cell yield and higher reproducibility.

4.1 Choice of the hepatic ischemia reperfusion injury model

Ischemia reperfusion injury in the liver is a major complication of trauma, hemorrhagic shock, resection and transplantation. It is a dynamic process that determines the viability of the hepatic tissue after resection and of the grafted organ. Ischemic periods can vary from a short time as found in tumor resection to durations of several hours as during liver transplantation.
To mimic the various scenarios in humans, quite a number of rodent models for hepatic ischemia are available. The inflicted damage is dependent on the duration and percentage of the ischemia. However, other parameters such as age or steatosis can also affect the outcome.

In the literature, ischemic periods from 30-90 minutes and reperfusion times of 1, 3, 6 and 24 hours of reperfusion have been investigated extensively in rodents [142]. The effects of 30 minutes ischemia are summarized below.

Table 1: Periods of 70% warm ischemia and their effects on cytokine expression and inflammation- and damage markers (modified from Karatzas *et al.*) [142].

70% warm ischemia	Upregulation/Increase of
30 minutes	AST, ALT, LDH, ET-1, NOS, TNF-α, IL-1β, MDA, LOOH, HO-1, oxidative stress, caspase 3 activity, tissue lipid peroxidation, MPO, ICAM-1, B7-1, B7-2
60 minutes	AST, ALT, LDH, TNF-a, MPO, RANKL
90 minutes	AST, ALT, LDH, TNF-a, MAP, HMGB1, RAGE, TLR4, IL-6

70% ischemia is achieved by interruption of the blood flow towards the left lateral and median lobe. 30 minutes of ischemia are sufficient, to trigger a full-blown immune response (table 1). Ischemic periods of 30-60 minutes should be favored when mechanisms of hepatic ischemia or protective roles of antibody administration are studied, as these periods of ischemia have a high survival rate (30-60 minutes >90%; [285]. When expanding the time of occlusion to 90 minutes, survival is already decreased to ~50% after 24 hours and decreased even further to ~30% after 7 days [146, 147]. This data is in line with our findings, that WT mice subjected to 30 minutes ischemia followed by three hours of reperfusion show increased levels of serum damage markers and neutrophil infiltration into the tissue Fig. 24. However, our histological data failed to show an increase in apoptotic or necrotic areas (data not shown). This might be a result of using frozen tissue instead of paraffin embedded tissue. The advantage of paraffin sections is the preservation of tissue morphology and the absence of crystal formation that might occur during the freezing procedure. Of note, paraffin embedding can mask epitopes and is therefore not suitable for enzyme- and antigen-dependent observations. Furthermore, 30 minutes of ischemia followed by three hours of reperfusion might just not be enough in our hands to trigger morphological changes. Nevertheless, infiltration of multi-lobulated cells into the tissue were observed (data not shown), which again, is in line with the literature. We could extend the ischemic time used for our experiments from 30-60 minutes to get a more clear-cut result in terms of histology and serum parameters used for liver damage. The extension of the ischemic phase would also allow to study more animals in one surgical period. When animal numbers are increased, liver samples could be distributed to paraffin embedding or cryo-conservation and therefore enhance H&E staining quality while still allowing for immunofluorescence stainings.

4.2 Platelets are able to alter the progression of hepatic ischemia reperfusion injury

Thrombo-inflammation refers to pathological responses in the vasculature induced by vessel wall injury, pathogen invasion as well as non-infectious (sterile) inflammatory triggers. Thus, diseases such as ischemic stroke, myocardial infarction as well as bacteremia, viremia or tumor metastasis are associated with thrombo-inflammation, although they belong to other categories in their classical sense. The mechanism of inflammation and the inflammatory response is modulated by a plethora of cells and their interplay with each other. Some of the cells involved in the progression of inflammation are platelets [286]. During the last decade an advancing number of studies uncovered a role for platelets, besides their classical role in hemostasis and thrombosis, in the progression of inflammation [287, 288].

In some of these studies platelets were shown to have protective roles, while in other studies and under different inflammatory settings they were able to exacerbate damage [85, 289]. Although liver inflammation and platelets have been studied, little is known about hepatic ischemia and the role of platelets as focus was set on historical relevant cell types such as granulocytes or lymphocytes [290, 291].

In this study, we focused on the role of platelets and their role to recruit neutrophils into the inflamed tissue, as neutrophil infiltration is a hallmark of inflammation [49, 117, 292]. We were able to show that platelets are involved in the progression of hepatic ischemia reperfusion as platelet depletion reduced liver damage markers and neutrophil infiltration into the inflamed tissue. We wanted to address, whether platelet function is affected after three hours of reperfusion and found general platelet parameters from platelet count and size to activation and degranulation to be completely unaltered (Fig. 26). Liver damage was confirmed by increased serum transaminase levels which are used to determine liver damage (Fig. 24) and were in the expected range [175]. These findings were in line with other studies that could show that platelets do not become activated and therefore do not release their granules following mild ischemia [180].

To investigate how platelets affect the outcome of reperfusion injury, we started to target well-studied platelet signaling pathways. Initial tethering is mediated by platelet GPIbα and immobilized vWF on endothelial cells. To target this pathway, the blocking Fab-fragment p0p/B, directed against GPIbα, was used. In line with data derived from ischemic stroke, GPIbα blockade resulted in decreased cellular damage (Fig. 28, [47]. In hepatic ischemia reperfusion injury neutrophil numbers were also significantly decreased, while unaffected in ischemic stroke, indicating different mechanisms of cellular damage. Our data was confirmed in vWF-deficient animals. We (Fig. 30) and others [175] showed that vWF is important for cellular

damage inflicted by neutrophils, as both numbers of neutrophils and serum transaminase levels were significantly reduced in vWF-deficient animals subjected to liver ischemia. To rule out any antibody mediated effects of p0p/B administration, the transgenic GPIb-IL-4R mouse in which the extracellular part of GPIb was replaced by the human IL-4 receptor was used (Fig. 29). Notably, we observed a similar protection from neutrophil recruitment in the transgenic mice, thus verifying that the observed decrease in liver damage in p0p/B-treated animals is due to the impaired GPIbα-vWF interaction. It is known, that neutrophils can directly and indirectly interact with the endothelial cells. Direct interaction is mediated by endothelial vWF or P-selectin with neutrophil Mac-1 or PSGL1, respectively. Indirect binding via platelets is mediated via platelet GPIbα or GPIIb/IIIa and neutrophil Mac-1 and results in integrin activation and intracellular signaling in neutrophils. To dissect whether neutrophils prefer (in)direct binding, flow adhesion assays could be performed, where isolated neutrophils are perfused over either adhesive platelets or a vWF matrix. Furthermore, the relevance of GPIb could be investigated by blockade of the receptor post aggregate formation in the flow chamber and before perfusion of isolated neutrophils. To validate the *in vitro* findings, intravital microscopy could be performed. Platelet-neutrophil interactions could be quantified in WT and GPIbα-blocked animals following hepatic ischemia. There, the questions of when and where binding of platelet-neutrophils and endothelium-neutrophils takes place, could be addressed. Platelet aggregation and firm adhesion is mediated by GPIIb/IIIa. In models of experimental stroke blockade of GPIIb/IIIa exacerbates the outcome following ischemia/reperfusion and significantly increased the risk for intracranial bleeding [37]. In hepatic ischemia reperfusion, however, blockade of the integrin did not influence the degree of liver damage after three hours of reperfusion, nor did it reduce the number of infiltrating neutrophils (Fig. 27).

Murine platelets bear two (hem)ITAM receptors, namely GPVI and CLEC-2. Activation of these receptors leads to platelet activation and subsequent degranulation [54]. GPVI is the main collagen receptor and exclusively expressed on MKs and platelets. Studies of the last years confirmed GPVI to be a potential anti-platelet target as GPVI deficiency, either genetically or antibody-mediated, shows profound protection in thrombosis models [37] as well as ischemia reperfusion injuries such as myocardial infarction [59] and stroke [56], displaying only mild effects on hemostasis. CLEC-2 is highly expressed on MKs and platelets and at low levels on some immune cells [293] and essential for embryonic development, especially blood/lymphatic vessel separation [294]. The only endogenous ligand identified so far is *podoplanin* (PDPN), a small glycoprotein that is highly expressed on lymphatic vessels but can also be found on other endothelial cells [295]. Since PDPN is known to be involved in wound healing after skin inflammation [296], studies investigating the role of CLEC-2 and PDPN in inflammation are emerging. In models of acetaminophen induced liver injury, CLEC-2 and PDPN inhibition are able to ameliorate cellular damage and decrease liver damage markers [297]. Therefore, we

should also investigate, whether GPVI, CLEC-2 and PDPN have a role in hepatic ischemia reperfusion injury.

So far, our interest was focused on the immediate effect of neutrophil infiltration into the post-ischemic liver. It is known, that neutrophil depletion reduces cellular damage and lowers inflammation [298, 299]. However, the exact mechanism of the interaction between platelets and neutrophils and how these interactions modulate inflammation remained largely unknown. Therefore, we will conduct studies that address surface receptors known to be of importance for neutrophil interactions with other cells using P-selectin-deficient animals, blockade of neutrophil Mac-1 or combinations thereof, including combinations with p0p/B-treatment or *vWF*$^{-/-}$ mice.

In models of viral, bacterial or fungal infection of the liver, neutrophils are known to infiltrate the tissue and provide a capture mechanism for pathogens through release of condensed chromatin [300, 301]. The formation of these *neutrophil extracellular traps* (NET) is thereby able to influence inflammation. DNase I treatment dissolved the NETs and increased damage or inflammation [302]. We also wanted to investigate, whether NET formation takes place following ischemia. However, we were not able to detect NETs in our histological sections. This, however, might be due to the fact that the suggested antibody for NET staining, citrullinated histone 3 (citH3), is rather unspecific. We got either no signal at all or the same amount of staining as for the IgG control (data not shown). Therefore, our data is inconclusive and needs to be optimized and repeated.

We should also consider investigation of the interplay between other (immune) cells and platelets. It is known that CD4^{+}, but not CD8^{+} T cells are involved in reperfusion progression [182, 303]) and that Kupffer cell activation increases cellular damage, although CD4^{+} T cell numbers remained unaltered following p0p/B administration in our hands. Kupffer cells produce large amounts of reactive oxygen species which serve as a chemoattractant for neutrophils [166]. However, their interaction with platelets is understudied. To address this issue, flow cytometric analyses could be performed to determine platelet-immune cell populations in liver and peripheral blood and monitor changes regarding size and cytokine expression levels. Interactions of interest could then be observed using confocal intravital microscopy and determine spatio-temporal resolution of the interaction(s).

4.3 Intravital microscopy needs critical analysis and data evaluation

To study the pathomechanisms underling hepatic ischemia reperfusion injury or other inflammation models a plethora of techniques have been used. Among these are histological sections, immunofluorescence stainings, serum analyses, *enzyme-linked immunosorbent assays* (ELISA) or flow cytometry. However, these methods only provide information about a current snapshot, and do not provide information about spatial distributions and interactions of involved cells. To overcome these limitations, endpoint analyses are more and more combined with intravital imaging [304, 305], allowing for investigation of transient interactions not visible in *ex vivo* techniques.

However, to conduct intravital microscopy an in adequate way and without artefact induction, key features of the read-out need to be considered in advance. A short example: If I wanted to study the appearance of platelets after an inflammatory insult, the field of view would be rather large and imaged at low resolution, as long as the signal for platelets or aggregating platelets is clearly visible. Furthermore, time frames of the investigated period can be adjusted to own interests (e.g. every minute for a period of 10 minutes or every 30 minutes for several hours of observation). If I wanted to investigate the role of single platelets, however, the resolution would need to be increased in a way that a single platelet is not only visualized as one single pixel. Although a recent publication in a prestigious journal has used this approach [306], this is no proper way to obtain and evaluate data. In addition, signals of the size of just one or two pixels are usually removed, as they are considered to be background.

To study interactions between different cell types, the temporal resolution needs to be considered in addition to the general resolution. We wanted to investigate how temporal resolution affects the output of the obtained data. Therefore, we imaged the same area with a defined resolution but with different time intervals during acquisition (*dt*). The platelet channel was analyzed to compare the speed and track duration to check for the influence of the measurement interval *dt* on the result. With decreasing time resolution the speed of the platelets decreases (Fig. 44). Since all parameters but *dt* were identical, a comparable speed of platelets would be expected. However, this was not the case and therefore the real speed of the platelets could not be determined as the sampling speed was either lower than the velocity of the platelets or the area imaged was too large. If a comparison between two settings is wanted, e.g. platelet speed before ischemia and following ischemia, the same *dt* should be used to put them into perspective and determine relative changes. In addition, this would limit the comparability between different animals, as they might have minor differences in blood pressure, *per se*. In the setting of ischemia reperfusion injury, slower platelets in the reperfusion phase might indicate lower blood pressure and result in decreased reperfusion rates. These results demonstrate, that careful set up and evaluation of intravital microscopy is

critical. Therefore, we are still optimizing our settings to evaluate platelet-neutrophil interactions in the post-ischemic liver.

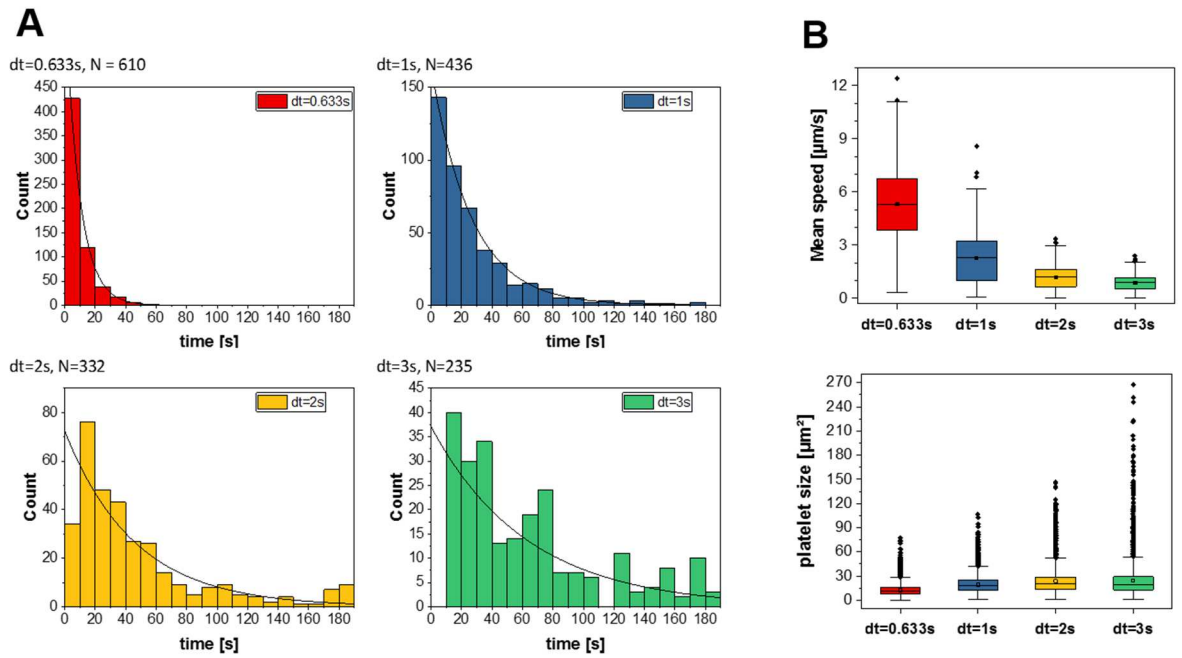

Figure 44: influence of temporal resolution on number and duration of tracks. (A) Total number of tracs and trac duration. Only tracks, where the platelet could be followed for at least 4 data points were considered, i.e. for 3 s the tracks had a minimal length of 12 s **(B**-upper**)** Mean speed of platelets. **(B**-lower**)** Platelet size. Microscopy data was evaluated by Dr. Katherina Hemmen (Bio-Imaging Center, Würzburg).

4.4 LTA_4H seems to be dispensable for normal platelet function but required for neutrophil recruitment in sterile injury of the liver

Platelet function is essential to maintain hemostasis. Overshooting platelet activation and aggregation can lead to vessel occlusions resulting in life threatening diseases or tissue damage. Bleeding disorders, however, are characterized by reduced platelet activation and aggregation [307]. In addition to these two classical roles, platelets have been shown to be involved in inflammation and wound healing [287, 308]. In addition to substances to regulate or exacerbate platelet activation, granules also consist of chemotactic molecules such as *platelet activating factor* (PAF) and LTB_4 [309]. LTB_4 is a very potent chemotactic agent and involved in neutrophil infiltration into inflamed tissue [99]. It is generated from arachidonic acid via the 5-LO pathway. The last step is catalyzed by LTA_4H, a bifunctional enzyme [310, 311]. To study the role of (platelet-derived) LTB_4, (conditional and) constitutive knockout mice for LTA_4H have been generated and characterized in different *in vitro* and *in vivo* models.

The presence of LTA_4H in platelets has been controversially discussed. Older studies reported that platelets and basophils lack this enzyme, while a recent publication reports otherwise. Peng *et al.* [312] were able to show that LTB_4 levels increase in CRP/thrombin activated

platelets. We were able to confirm the presence of LTA_4H in mouse platelets and liver samples via RNA (data not shown) and Western blot analysis. WT mice showed protein expression of LTA_4H in both liver and platelet lysates (Fig. 31). These bands were absent in constitutive knockout animal, confirming our knockout model.

Basal blood parameters of LTA_4H deficient animals were undistinguishable from WT animals (Fig. 31). Organ structure was also unaffected in these mice (data not shown). These findings are in line with the literature, where animal models lacking enzymes of the leukotriene biosynthesis pathway showed no obvious physiological alterations and appeared overall healthy [313]. However, these animals were more susceptible towards bacterial and fungal infections [250, 314].

Platelet numbers, size as well as platelet glycoprotein expression, platelet activation and degranulation were comparable between WT and *Lta4h*$^{-/-}$ mice (Fig. 32). In static *in vitro* assays platelets behaved completely normal and showed unaltered platelet spreading on collagen and aggregation towards all tested agonists (Fig. 33). Their ability to adhere to collagen under flow conditions was also unaltered (Fig. 34), indicating that LTA_4H and LTB_4 are neglectable for the aforementioned functions and thrombus formation. This is in contrast to a recent publication from Scheller *et al.* [315]. The mouse under investigation was deficient for Cotl1, a F-actin binding protein, which is also able to bind to and stabilize the enzyme 5-LO. This mouse showed a significant reduction in thrombus formation, especially under high shear (1000- 3000 s^{-1}) conditions. Lipidomic analysis revealed decreased amounts of LTB_4 in platelets and platelet supernatant of Cotl1 deficient animals. Scheller *et al*. investigated the role of LTB_4 on thrombus formation and found that preincubation of Cotl1-deficient platelets with LTB_4 completely restored thrombus formation to wildtype levels. Therefore, we would have expected that *Lta4h*$^{-/-}$ mice show reduced thrombus formation as well. To understand the reason for this discrepancy, we will conduct lipidomic analyses with LTA_4H-deficient platelets. We expect the LTA_4H deficiency to show no detectable LTB_4 levels. In addition, we want to see, whether LTA_4H-deficiency leads to changes in the synthesis of pro- or anti-inflammatory molecules.

A neutrophil transmigration assay was used to determine the chemotactic properties of LTB_4 and platelet supernatant (Fig. 36). In line with previous publications [220], a dose dependent effect of LTB_4 on neutrophil transmigration could be observed. Platelet supernatant showed a slight increase in neutrophil transmigration. Therefore, platelet supernatant from other knockout animals could be used to determine their chemotactic properties.

To study the role of LTA_4H *in vivo*, the mice were subjected the liver ischemia and the hot needle injury model. 30 minutes of ischemia were followed by three hours of reperfusion. The tested markers for liver damage showed no differences between WT and *Lta4h*$^{-/-}$ mice,

indicating that the absence of LTA_4H does not protect from liver injury. However, absence of LTA_4H leads to significantly decreased neutrophil infiltration into the post-ischemic liver. This is, at least partially, in accordance with a publication from Santos *et al.* [316]. They investigated fungal infection in 5-LO deficient animals and reported lung *myeloperoxidase* (MPO) and fungal load to be increased after 24- and 72-hours post infection in *Lta4h*$^{-/-}$ mice. This, however, correlated with decreased neutrophil and macrophage numbers as well as elevated mononuclear cell numbers in *bronchoalveolar fluid* (BALF). In addition, they found increased levels of pro-inflammatory cytokines and a reduced capacity of macrophages to phagocytose the fungus. Although the mechanisms between fungal infection and sterile ischemia reperfusion injury differ, it would be worthwhile to check other immune cell populations and their distribution as well as the expression levels of pro- and anti-inflammatory cytokines.

4.5 Rapid-spin isolation of murine BM as an alternative to classical flush isolation

The BM is the main compartment for hematopoiesis and critical for many research fields such as cancer metastasis, hematology or transplantation studies. In the process of hematopoiesis, HSCs develop into myeloid or lymphoid progenitors, which finally differentiate into all types of peripheral blood cells. This hierarchical process enables a high degree of flexible adaptation of blood cell types in response to specific demands such as massive blood loss to restore the hematopoietic equilibrium and ensures blood cell homeostasis under steady state conditions [8]. Therefore, composition, localization or differentiation of cell subsets can give information about health and disease.

To study the function of primary or cultured BM cells, mice are commonly used as model organisms. Isolation of the BM is achieved by repeated flushing of long bones with a liquid filled syringe, referred to as flush method [255]. In a recent publication an alternative method has been proposed, where BM is isolated via centrifugation [254]. We adapted this method to our experimental needs for primary and cultured BM MKs by decreasing centrifugation speed and centrifuging the cells into a small volume of liquid.

In this study (Heib and Gross *et al.*, accepted), we compared both isolation methods with each other and found a substantial time-saving effect when using the rapid-spin isolation as well as significantly increased cell yields. Visual inspection of the bones after BM extraction confirmed complete removal of the BM after centrifugation. Both methods showed comparable cell viability of about 90%: This data demonstrates, that the forces applied by both methods, although different, do not affect cellular viability. Using flow cytometry, hematopoietic stem and

immune cell (sub)populations were analyzed. Despite the increased cell number following rapid spin-isolation we found no noteworthy changes in all observed populations. Therefore, rapid-spin isolation can be used to obtain BM cells, where large quantities are needed. This is in particular true for BM transplantation. Using the rapid-spin isolation, one mouse is enough to recover enough cells for 2 transplants, whereas at least two mice were needed when using the flush method, reducing the number of animals needed for any kind of experiment. In addition, several experiments can now be performed with cells from the same animal, allowing direct comparison and better connectivity and ultimately leading to more conclusive interpretations.

We also applied functional studies on primary and cultured MKs after isolation with both methods (Fig. 45). Neither ploidy of primary MKs nor *in vitro* proplatelet formation of cultured MKs showed differences between both methods. We therefore conclude that centrifugation-based BM isolation does not increase fragmentation of MKs or other big cells.

We propose spin isolation as a preferable method for any kind of experiments requiring isolated BM cells, ranging from qPCR to FACS analysis or cell culture. Especially for experiments with demand of high cell numbers, such as stem cell transplantation, cell sorting and RNAseq, the spin isolation method helps to reduce experimental time, costs and animals needed. In addition, several comparative analyses can be performed with cells derived from the same animal.

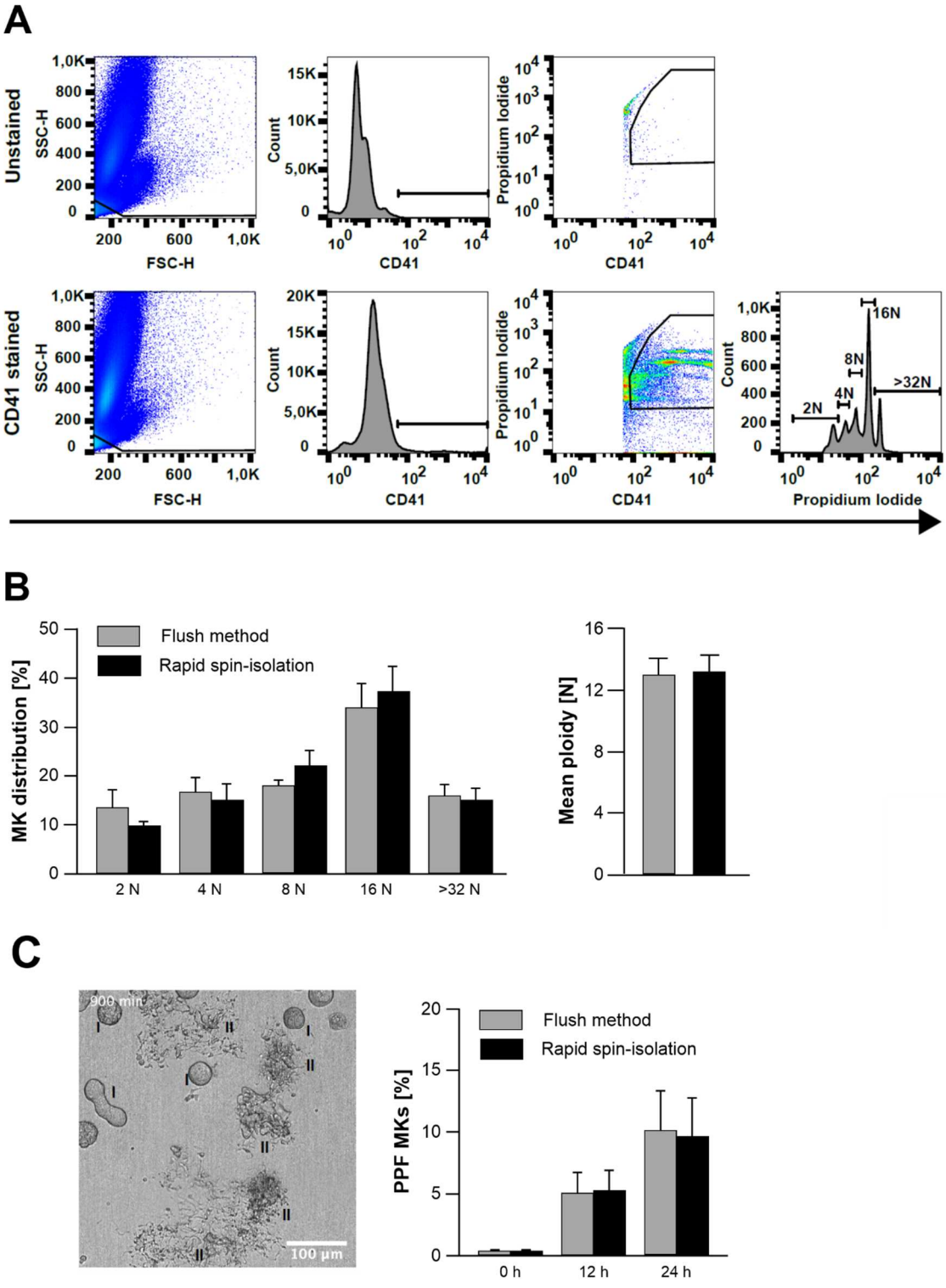

Figure 45: Functional analyses of primary and cultured BM MKs. (A) Gating strategy for primary BM MKs. Cells were determined by FSC and SSC properties and considered MKS, when strong expression of CD41 was detectable. Cells were plotted against propidium iodide (PI). The resulting histogram shows the ploidy distribution. **(B)** Distribution of ploidy stages (%) and mean MK ploidy (N) of primary MKs. **(C)** Representative image of proplatelet formation (PPF). MKs were recorded using a Leica SP8 confocal microscope. MKs were divided in Class I = Non-proplatelet-forming MKs (roundish or elongated) and Class II = Proplatelet-forming MKs (multiple branched protrusions with characteristic swellings ("beads-on-a-string") and nascent proplatelet-tips. Bar graph shows the quantification of proplatelet forming MKs at indicated time points. (Heib, Gross *et al.*, accepted) Experiments were performed by Tobias Heib.

4.6 Concluding remarks and further perspectives

The work presented here, can be divided into three major parts. The first covers the role of platelets in hepatic ischemia reperfusion injury, the second deals with characterization of the constitutive LTA_4H knockout mouse and the third with the comparison of two BM isolation techniques.

In the last decade platelets have been shown to be involved in more than just classical thrombosis and hemostasis. Several studies were able to show, that platelets alter the progression and severity of inflammation. To address the role of platelets in hepatic ischemia, a model of 70% warm ischemia and confocal intravital microscopy needed to be established. Functional analyses such as ELISA measurements, classical histology and intravital microscopy provided new insights into the role of platelets in hepatic ischemia reperfusion injury:

- Platelets are involved in the inflammatory response following ischemia and their depletion leads to decreased liver damage and neutrophil recruitment.
- In contrast to severe inflammatory settings, platelet function is unaltered after three hours of reperfusion (size, count, integrin activation and degranulation).
- Targeting of the GPIb-vWF axis with blocking Fab-fragments (p0p/B) or using transgenic mouse models (GPIb-IL4R, *vWF*$^{-/-}$) leads to reduced liver damage and decreased neutrophil numbers in the tissue.
- Blockade of GPIbα negatively affects the kinetics of neutrophil recruitment.
- Blockade of GPIIb/IIIa-mediated platelet aggregation (using JON/A) does not influence neutrophil recruitment or liver damage.

We will continue to investigate hepatic ischemia reperfusion injury using serum parameters, histology, flow cytometry and intravital microscopy. To observe a larger effect of ischemia we should prolong the ischemic phase from 30 to 60 minutes. Paraffin sections will give clearer histological results and cryosections can be analyzed regarding immune cell infiltration. Intravital microscopy will be used to analyze and determine platelet-immune cell interactions.

Candidates for next experiments are GPVI, CLEC-2 or CD84 deficient mice. Furthermore, P-selectin- PSGL-1 and GPIb-Mac-1 interactions will be investigated.

The complex regulatory network of pro- and anti-inflammatory mediators is under intensive investigation. Leukotrienes are arachidonic acid derived lipid mediators synthesized by the action of 5-lipoxygenase (5-LO) in the presence of 5-LO activating protein (FLAP). LTB_4 is a known chemotactic agent involved in neutrophil recruitment and activation, whereas cysteinyl leukotrienes (cys-LTs) are known to be involved in allergic reactions, especially asthma. Here, the effects of LTA_4H on platelet function and inflammation were investigated:

- LTA_4H is dispensable for normal platelet function and does not affect basal blood parameters.
- Neither thrombosis nor hemostasis is affected by loss of LTA_4H.
- Liver damage following hepatic ischemia is unaltered in *Lta4h*-deficient animals, although intravital microscopy of the liver revealed significantly decreased neutrophil numbers after three hours of reperfusion.
- Reduced neutrophil infiltration was also observed in the hot needle model.

The experiments planned for this project include repetitions for *in vivo* models to validate the initial observations. Furthermore, neutrophil transmigration assays with LTA_4H deficient platelet supernatant will be performed in order to recapitulate the *in vivo* phenotype. If this works out in our favor, this method can be used to test chemotactic properties of platelet supernatant from other knockout mice and test potential involvement in inflammation with low animal numbers. In addition, lipidome analysis of LTA_4H deficient platelets will give insights into the regulation of pro- and anti-inflammatory lipid mediator synthesis.

Investigation of the BM, as the main compartment of hematopoiesis, is critical in several research fields. To investigate primary or cultured bone marrow cells, isolation of murine long bones is a frequently used technique. Here, we compared the classical flush method with the rapid spin-isolation method. The rapid-spin isolation:

- Reduced BM isolation time by three-fold (10 min vs 35 min) and enhanced reproducibility through defined forces applied.
- Significantly increased cell yield without affecting cell viability.
- Showed comparable HSC and immune cell populations.
- Showed unaffected MK ploidy in primary MKs and unaltered proplatelet formation of cultured MKs.

5. References

1. Seita, J. and I.L. Weissman, *Hematopoietic stem cell: self-renewal versus differentiation.* Wiley Interdiscip Rev Syst Biol Med, 2010. **2**(6): p. 640-53.
2. He, S., D. Nakada, and S.J. Morrison, *Mechanisms of stem cell self-renewal.* Annu Rev Cell Dev Biol, 2009. **25**: p. 377-406.
3. Okada, S., et al., *In Vivo and In Vitro Stem Cell Function of c-kit- and Sca-1-Positive Murine Hematopoietic Cells.* Blood, 1992. **80**(12): p. 3044–3050.
4. Kiel, M.J., et al., *SLAM family receptors distinguish hematopoietic stem and progenitor cells and reveal endothelial niches for stem cells.* Cell, 2005. **121**(7): p. 1109-21.
5. Mayle, A., et al., *Flow cytometry analysis of murine hematopoietic stem cells.* Cytometry A, 2013. **83**(1): p. 27-37.
6. Challen, G.A., et al., *Mouse hematopoietic stem cell identification and analysis.* Cytometry A, 2009. **75**(1): p. 14-24.
7. Akashi, K., et al., *A clonogenic commonmyeloid progenitor that gives rise to all myeloid lineages.* Nature, 2000. **404**: p. 193-197.
8. Kondo, M., I.L. .Weissman, and K. Akashi, *Identification of Clonogenic Common Lymphoid Progenitors in Mouse Bone Marrow.* Cell, 1997. **91**: p. 661–672.
9. Ault, K.A. and C. Knowles, *In vivo biotinylation demonstrates that reticulated platelets are the youngest platelets in circulation.* Experimental hematology, 1995. **23**(9): p. 996-1001.
10. Folman, et al., *The role of thrombopoietin in post-operative thrombocytosis.* British Journal of Haematology, 2001. **114**(1): p. 126-33.
11. Ishiguro, A., et al., *Elevation of serum thrombopoietin precedes thrombocytosis in acute infections.* Br J Haematol, 2001. **116**: p. 612–618.
12. Schafer, A.I., *Thrombocytosis.* N Engl J Med, 2004. **350**: p. 1211-1219.
13. Long, M.W., N. Williams, and S. Ebbe, *Immature megakaryocytes in the mouse: physical characteristics, cell cycle status, and in vitro responsiveness to thrombopoietic stimulatory factor.* Blood, 1982. **59**(3): p. 569-75.
14. Bartley, T.D., et al., *Identification of cloning of a magekaryocyte growth and development factor that is the ligand for thecytokine receotpr Mpl.* Cell, 1994. **77**: p. 1117-l 124,.
15. Kaushansky, K., et al., *Promotion of megakaryocyte progenitor expansion and differentiation by hte c-Mpl ligand thrombopoietin.* Nature, 1994. **369**: p. 568–571.
16. Kuter, D.J., *The purification of megapoietin: A physiological regulator of megakaryocyte growth and platelet production.* Proc. Natl. Acad. Sci. USA, 1994. **91**: p. 11104-11108.
17. Lok, S., *Cloning and expression of murine thrombopoietin cDNA and stimulation of platelet production in vivo.* Nature, 1994. **369**: p. 565-568.
18. de Sauvage F. J., Hass P. E., and e.a. Spencer S. D., *Stimulation of megakaryocytopoiesis and thrombooiesis by the c-Mpl ligand.* Nature, 1994. **369**(6481): p. 533-538.
19. Miyakawa, Y., et al., *Thrombopoietin induces phosphoinositol 3-kinase activation through SHP2, Gab, and insulin receptor substrate proteins in BAF3 cells and primary murine megakaryocytes.* J Biol Chem, 2001. **276**(4): p. 2494-502.
20. Wendling, F., et al., *cMpl Ligand Is a Humoral Regulator of Megakaryocytopoiesis* Nature, 1994. **369**(6481): p. 571-574.

21. de Graaf, C.A. and D. Metcalf, *Thrombopoietin and hematopoietic stem cells.* Cell Cycle, 2011. **10**(10): p. 1582-9.
22. Geddis, A.E. and K. Kaushansky, *Endomitotic Megakaryocytes Form a Midzone in Anaphase but have a Deficiency in Cleavage Furrow Formation.* Cell Cycle, 2006. **5**(5): p. 538-545.
23. Machlus, K.R. and J.E. Italiano, Jr., *The incredible journey: From megakaryocyte development to platelet formation.* J Cell Biol, 2013. **201**(6): p. 785-96.
24. Thon, J.N. and J.E. Italiano, *Platelet formation.* Semin Hematol, 2010. **47**(3): p. 220-6.
25. Morgenstern, E., *The formation of compound granules from different types of secretory organelles in human platelets (dense granules and alpha-granules). A cryofixation/-substitution study using serial sections.* Eur J Cell Biol, 1995. **68**(2): p. 183-90.
26. Hartwig, J.H. and J.E. Italiano, *The birth of the platelet.* Journal of Thrombosis and Haemostasis, 2003. **1**: p. 1580–1586.
27. Grozovsky, R., K.M. Hoffmeister, and H. Falet, *Novel clearance mechanisms of platelets.* Curr Opin Hematol, 2010. **17**(6): p. 585-9.
28. Li, R., K.M. Hoffmeister, and H. Falet, *Glycans and the platelet life cycle.* Platelets, 2016. **27**(6): p. 505-11.
29. Nieswandt, B., I. Pleines, and M. Bender, *Platelet adhesion and activation mechanisms in arterial thrombosis and ischaemic stroke.* J Thromb Haemost, 2011. **9 Suppl 1**: p. 92-104.
30. Nieswandt, B., et al., *Platelets in atherothrombosis: lessons from mouse models.* J Thromb Haemost, 2005. **3**(8): p. 1725-36.
31. Weyrich, A.S. and G.A. Zimmerman, *Platelets: signaling cells in the immune continuum.* Trends Immunol, 2004. **25**(9): p. 489-95.
32. Jenne, C.N. and P. Kubes, *Platelets in inflammation and infection.* Platelets, 2015. **26**(4): p. 286-92.
33. Stegner, D., S. Dütting, and B. Nieswandt, *Mechanistic explanation for platelet contribution to cancer metastasis.* Thrombosis Research, 2014. **133**: p. S149-S157.
34. Nieswandt, B. and S.P. Watson, *Platelet-collagen interaction: is GPVI the central receptor?* Blood, 2003. **102**(2): p. 449-61.
35. Shattil, S.J. and P.J. Newman, *Integrins: dynamic scaffolds for adhesion and signaling in platelets.* Blood, 2004. **104**(6): p. 1606-15.
36. Boulaftali, Y., et al., *Platelet immunoreceptor tyrosine-based activation motif (ITAM) signaling and vascular integrity.* Circ Res, 2014. **114**(7): p. 1174-84.
37. Kleinschnitz, C., et al., *Targeting platelets in acute experimental stroke: impact of glycoprotein Ib, VI, and IIb/IIIa blockade on infarct size, functional outcome, and intracranial bleeding.* Circulation, 2007. **115**(17): p. 2323-30.
38. Varga-Szabo, D., I. Pleines, and B. Nieswandt, *Cell adhesion mechanisms in platelets.* Arterioscler Thromb Vasc Biol, 2008. **28**(3): p. 403-12.
39. Lof, A., J.P. Muller, and M.A. Brehm, *A biophysical view on von Willebrand factor activation.* J Cell Physiol, 2018. **233**(2): p. 799-810.
40. Bryckaert, M., et al., *Of von Willebrand factor and platelets.* Cell Mol Life Sci, 2015. **72**(2): p. 307-26.
41. Finney, B.A., et al., *CLEC-2 and Syk in the megakaryocytic/platelet lineage are essential for development.* Blood, 2012. **119**(7): p. 1747-56.
42. Contursi, A., et al., *Platelets as crucial partners for tumor metastasis: from mechanistic aspects to pharmacological targeting.* Cell Mol Life Sci, 2017. **74**(19): p. 3491-3507.

43. Cloutier, N., et al., *Platelets release pathogenic serotonin and return to circulation after immune complex-mediated sequestration.* Proc Natl Acad Sci U S A, 2018. **115**(7): p. E1550-E1559.
44. Herter, J.M., J. Rossaint, and A. Zarbock, *Platelets in inflammation and immunity.* J Thromb Haemost, 2014. **12**(11): p. 1764-75.
45. Ho-Tin-Noe, B., Y. Boulaftali, and E. Camerer, *Platelets and vascular integrity: how platelets prevent bleeding in inflammation.* Blood, 2018. **131**(3): p. 277-288.
46. Katz, J.N., K.P. Kolappa, and R.C. Becker, *Beyond thrombosis: the versatile platelet in critical illness.* Chest, 2011. **139**(3): p. 658-668.
47. Chen, C., et al., *Platelet glycoprotein receptor Ib blockade ameliorates experimental cerebral ischemia-reperfusion injury by strengthening the blood-brain barrier function and anti-thrombo-inflammatory property.* Brain Behav Immun, 2018. **69**: p. 255-263.
48. Kral, J.B., et al., *Platelet Interaction with Innate Immune Cells.* Transfus Med Hemother, 2016. **43**(2): p. 78-88.
49. Zuchtriegel, G., et al., *Platelets Guide Leukocytes to Their Sites of Extravasation.* PLoS Biol, 2016. **14**(5): p. e1002459.
50. Muller, W.A., *Getting leukocytes to the site of inflammation.* Vet Pathol, 2013. **50**(1): p. 7-22.
51. Massberg, S., et al., *A crucial role of glycoprotein VI for platelet recruitment to the injured arterial wall in vivo.* J Exp Med, 2003. **197**(1): p. 41-9.
52. Bergmeier, W., A.K. Chauhan, and D.D. Wagner, *Glycoprotein Ibalpha and von Willebrand factor in primary platelet adhesion and thrombus formation: lessons from mutant mice.* Thromb Haemost, 2008. **99**(2): p. 264-70.
53. Schuhmann, M.K., et al., *Blocking of platelet glycoprotein receptor Ib reduces "thrombo-inflammation" in mice with acute ischemic stroke.* J Neuroinflammation, 2017. **14**(1): p. 18.
54. Dutting, S., M. Bender, and B. Nieswandt, *Platelet GPVI: a target for antithrombotic therapy?!* Trends Pharmacol Sci, 2012. **33**(11): p. 583-90.
55. Andrews, R.K., J.F. Arthur, and E.E. Gardiner, *Targeting GPVI as a novel antithrombotic strategy.* J Blood Med, 2014. **5**: p. 59-68.
56. Bigalke, B., et al., *Expression of platelet glycoprotein VI is associated with transient ischemic attack and stroke.* Eur J Neurol, 2010. **17**(1): p. 111-7.
57. Siljander, P.R.M., *Platelet-derived microparticles – an updated perspective.* Thrombosis Research, 2011. **127**: p. S30-S33.
58. Boilard, E., et al., *Platelets amplify inflammation in arthritis via collagen-dependent microparticle production.* Science, 2010. **327**(5965): p. 580-3.
59. Pachel, C., et al., *Inhibition of Platelet GPVI Protects Against Myocardial Ischemia-Reperfusion Injury.* Arterioscler Thromb Vasc Biol, 2016. **36**(4): p. 629-35.
60. Andrews, R.K., et al., *Glycoprotein Ib–IX–V.* The International Journal of Biochemistry & Cell Biology, 2003. **35**(8): p. 1170-1174.
61. Phillips, D.R., I.F. Charo, and R.M. Scarborough, *GPIIb-IIIa: The Responsive Integrin.* Cell, 1991. **65**(3): p. 359-62.
62. Schneider, D.J., *Anti-platelet therapy: glycoprotein IIb-IIIa antagonists.* Br J Clin Pharmacol, 2011. **72**(4): p. 672-82.
63. B.S., C., *Platelet GPIIb/IIIa Antagonists: The First Anti-Integrin Receptor Therapeutics.* J. Clin. Invest., 1997. **99**(7): p. 1467–1471.
64. Schrör, K. and A.-A. Weber, *Comparative Pharmacology of GP IIb/IIIa Antagonists.* Journal of Thrombosis and Thrombolysis 2003. **15**: p. 71–80.

65. Kloner, R.A. and W. Dai, *Glycoprotein IIb/IIIa inhibitors and no-reflow.* J Am Coll Cardiol, 2004. **43**(2): p. 284-6.

66. Stoll, G. and B. Nieswandt, *Thrombo-inflammation in acute ischaemic stroke - implications for treatment.* Nat Rev Neurol, 2019. **15**(8): p. 473-481.

67. Adderley, S.R. and D.J. Fitzgerald, *Glycoprotein IIb/IIIa Antagonists Induce Apoptosis in Rat Cardiomyocytes by Caspase-3 Activation.* THE JOURNAL OF BIOLOGICAL CHEMISTRY, 2000. **275**(February 25): p. 5760–5766,.

68. Giordano, A., et al., *Effects of Glycoprotein IIb/IIIa Antagonists: Anti Platelet Aggregation and Beyond.* Current Drug Metabolism,, 2016. **17**.

69. Junghans, U., et al., *Bleeding Risk of Tirofiban, a Nonpeptide GPIIb/IIIa Platelet Receptor Antagonist in Progressive Stroke: An Open Pilot Study.* Cerebrovasc Dis 2001. **12**: p. 308–312.

70. Elgueta, R., et al., *Molecular mechanism and function of CD40/CD40L engagement in the immune system.* Immunol Rev, 2009. **229**(1): p. 152-72.

71. Grewal, I.S. and R.A. Flavell, *CD40 and CD154 in Cell-Mediated Immunity* Annu Rev Immunol, 1998. **16**: p. 111-35.

72. Zhang, B., et al., *The CD40/CD40L system: a new therapeutic target for disease.* Immunol Lett, 2013. **153**(1-2): p. 58-61.

73. van Kooten, C. and J. Banchereau, *CD40-CD40 ligand.* J Leukoc Biol, 2000. **67**(1): p. 2-17.

74. Antoniades, C., et al., *The CD40/CD40 ligand system: linking inflammation with atherothrombosis.* J Am Coll Cardiol, 2009. **54**(8): p. 669-77.

75. Prasad, K.S.S., et al., *The platelet CD40L/GPIIb-IIIa axis in atherothrombotic disease.* Curr Opin Hematol, 2003. **10**(5): p. 356-361.

76. Pamukcu, B., et al., *The CD40-CD40L system in cardiovascular disease.* Ann Med, 2011. **43**(5): p. 331-40.

77. Chakrabarti, S., et al., *CD40 ligand influences platelet release of reactive oxygen intermediates.* Arterioscler Thromb Vasc Biol, 2005. **25**(11): p. 2428-34.

78. Metharom, P., M. Falasca, and M.C. Berndt, *The History of Armand Trousseau and Cancer-Associated Thrombosis.* Cancers (Basel), 2019. **11**(2).

79. Egan, K., et al., *Platelet adhesion and degranulation induce pro-survival and pro-angiogenic signalling in ovarian cancer cells.* PLoS One, 2011. **6**(10): p. e26125.

80. Chiang, H.S., M.W. Swaim, and T.-F. Huang, *Characterization of platelet aggregation induced by human breast carcinoma and its inhibition by snake venom peptides, trigramin and rhodostomin.* Breast Cancer Research and Treatmen, 1995. **33**: p. 225-235.

81. Steinert, B.W., et al., *Studies on the Role of Platelet Eicosanoid Metabolism and Integrin Alpha IIb Beta 3 in Tumor-Cell-Induced Platelet Aggregation.* Int J Cancer, 1993. **54**(1): p. 92-101.

82. Takagi, S., et al., *Expression of Aggrus/podoplanin in bladder cancer and its role in pulmonary metastasis.* Int J Cancer, 2014. **134**(11): p. 2605-14.

83. Wicki, A. and G. Christofori, *The potential role of podoplanin in tumour invasion.* Br J Cancer, 2007. **96**(1): p. 1-5.

84. Mitrugno, A., et al., *A novel and essential role for FcgammaRIIa in cancer cell-induced platelet activation.* Blood, 2014. **123**(2): p. 249-60.

85. Demers, M., et al., *Increased efficacy of breast cancer chemotherapy in thrombocytopenic mice.* Cancer Res, 2011. **71**(5): p. 1540-9.

86. Gasic, G.J., T.B. Gasic, and C.C. Stewart, *Antimetastatic effects associated with platelet reduction.* Proc Natl Acad Sci U S A, 1968. **61**(1): p. 46–52.

87. Nierodzik, M.L., et al., *Thrombin Stimulates Tumor-Platelet Adhesion In Vitro and Metastasis In Vivo.* J Clin Invest., 1991. **87**(1): p. 229–236.

88. Ho-Tin-Noe, B., et al., *Platelet granule secretion continuously prevents intratumor hemorrhage.* Cancer Res, 2008. **68**(16): p. 6851-8.

89. Volz, J., et al., *Inhibition of platelet GPVI induces intratumor hemorrhage and increases efficacy of chemotherapy in mice.* Blood, 2019. **133**(25): p. 2696-2706.

90. Kim, K., et al., *NOX2 is critical for heterotypic neutrophil-platelet interactions during vascular inflammation.* Blood, 2015. **126**(16): p. 1952-64.

91. Lam, F.W., et al., *Platelets enhance neutrophil transendothelial migration via P-selectin glycoprotein ligand-1.* Am J Physiol Heart Circ Physiol, 2011. **300**(2): p. H468-75.

92. Weissmuller, T., et al., *PMNs facilitate translocation of platelets across human and mouse epithelium and together alter fluid homeostasis via epithelial cell-expressed ecto-NTPDases.* J Clin Invest, 2008. **118**(11): p. 3682-92.

93. Vowinkel, T., et al., *Mechanisms of platelet and leukocyte recruitment in experimental colitis.* Am J Physiol Gastrointest Liver Physiol, 2007. **293**(5): p. G1054-60.

94. Springer, T.A., *Traffic Signals for Lymphocyte Recirculation and Leukocyte Emigration: The Multistep Paradigm.* Cell, 1994. **76**(2): p. 301-314.

95. Ley, K., et al., *Getting to the site of inflammation: the leukocyte adhesion cascade updated.* Nat Rev Immunol, 2007. **7**(9): p. 678-89.

96. Rao, R.M., et al., *Endothelial-dependent mechanisms of leukocyte recruitment to the vascular wall.* Circ Res, 2007. **101**(3): p. 234-47.

97. Bengtsson, T., et al., *Platelets enhance neutrophil locomotion: evidence for a role of P-selectin.* Scand J Clin Lab Invest 1999. **59**: p. 439 ± 450.

98. Mayadas, T.N., et al., *Leukocyte rolling and extravasation are severely compromised in P selectin-deficient mice.* Cell, 1993. **74**(3): p. 541-554.

99. Pitchford, S., D. Pan, and H.C. Welch, *Platelets in neutrophil recruitment to sites of inflammation.* Curr Opin Hematol, 2017. **24**(1): p. 23-31.

100. Sreeramkumar, V., et al., *Neutrophils scan for activated platelets to initiate inflammation.* Science, 2014. **346**(6214): p. 1234-1238.

101. Moore, K.L., et al., *P-Selectin Glycoprotein Ligand-1 Mediates Rolling of Human Neutrophils on P-Selectin.* J Cell Biol, 1995. **128**(4): p. 661–671.

102. Patel, K.D., et al., *Neutrophils Use Both Shared and Distinct Mechanisms to Adhere to Selectins under Static and Flow Conditions.* J Clin Invest, 1995. **96**(4): p. 1887-96.

103. Wang, Y., et al., *Leukocyte integrin Mac-1 regulates thrombosis via interaction with platelet GPIbalpha.* Nat Commun, 2017. **8**: p. 15559.

104. Zarbock, A., et al., *PSGL-1-dependent myeloid leukocyte activation.* J Leukoc Biol, 2009. **86**(5): p. 1119-24.

105. Evangelista, V., et al., *Role of P-selectin, b2-integrins, and Src tyrosine kinases in mouse neutrophil–platelet adhesion.* Journal of Thrombosis and Haemostasis,, 2003. **1**: p. 1048–1054.

106. Yonekawa, K. and J.M. Harlan, *Targeting leukocyte integrins in human diseases.* J Leukoc Biol, 2005. **77**(2): p. 129-40.

107. Chavakis, T., et al., *The pattern recognition receptor (RAGE) is a counterreceptor for leukocyte integrins: a novel pathway for inflammatory cell recruitment.* J Exp Med, 2003. **198**(10): p. 1507-15.

108. Vestweber, D., *Adhesion and signaling molecules controlling the transmigration of leukocytes through endothelium.* Immunol Rev, 2007. **218**: p. 178-196.

109. Plow, E.F., et al., *Ligand binding to integrins.* J Biol Chem, 2000. **275**(29): p. 21785-8.

110. Wang, S., et al., *Venular basement membranes contain specific matrix protein low expression regions that act as exit points for emigrating neutrophils.* J Exp Med, 2006. **203**(6): p. 1519-32.

111. Shaw, S.K., et al., *Coordinated redistribution of leukocyte LFA-1 and endothelial cell ICAM-1 accompany neutrophil transmigration.* J Exp Med, 2004. **200**(12): p. 1571-80.

112. Barreiro, O., et al., *Dynamic interaction of VCAM-1 and ICAM-1 with moesin and ezrin in a novel endothelial docking structure for adherent leukocytes.* J Cell Biol, 2002. **157**(7): p. 1233-45.

113. Rose, D.M., R. Alon, and M.H. Ginsberg, *Integrin modulation and signaling in leukocyte adhesion and migration.* Immunol Rev, 2007. **218**: p. 126-134.

114. Kucharzik, T., et al., *Neutrophil Transmigration in Inflammatory Bowel Disease Is Associated with Differential Expression of Epithelial Intercellular Junction Proteins.* The American Journal of Pathology, 2001. **159**(6): p. 2001-2009.

115. Lechner, F., et al., *Antibodies to the Junctional Adhesion Molecule Cause Disruption of Endothelial Cells and Do Not Prevent Leukocyte Influx into the Meninges after Viral or Bacterial Infection.* The Journal of Infectious Diseases, 2000. **182**(3): p. 978-982.

116. Khandoga, A., et al., *Junctional adhesion molecule-A deficiency increases hepatic ischemia-reperfusion injury despite reduction of neutrophil transendothelial migration.* Blood, 2005. **106**(2): p. 725-33.

117. Zarbock, A., R.K. Polanowska-Grabowska, and K. Ley, *Platelet-neutrophil-interactions: linking hemostasis and inflammation.* Blood Rev, 2007. **21**(2): p. 99-111.

118. Barreiro, O., et al., *Endothelial adhesion receptors are recruited to adherent leukocytes by inclusion in preformed tetraspanin nanoplatforms.* J Cell Biol, 2008. **183**(3): p. 527-42.

119. Carman, C.V., et al., *Transcellular Diapedesis Is Initiated by Invasive Podosomes.* Immunity, 2007. **26**(6): p. 784–797.

120. Carman, C.V., *Mechanisms for transcellular diapedesis: probing and pathfinding by 'invadosome-like protrusions'.* J Cell Sci, 2009. **122**(Pt 17): p. 3025-35.

121. Carman, C.V. and T.A. Springer, *A transmigratory cup in leukocyte diapedesis both through individual vascular endothelial cells and between them.* J Cell Biol, 2004. **167**(2): p. 377-88.

122. Vasina, E., et al., *Platelets and Platelet-Derived Microparticles in Vascular Inflammatory Disease.* Inflamm Allergy Drug Targets, 2010. **9**(5): p. 346-354.

123. Pitchford, S.C., et al., *Platelets are necessary for airway wall remodeling in a murine model of chronic allergic inflammation.* Blood, 2004. **103**(2): p. 639-47.

124. Pitchford, S.C., et al., *Allergen induces the migration of platelets to lung tissue in allergic asthma.* Am J Respir Crit Care Med, 2008. **177**(6): p. 604-12.

125. Lowenhaupt, R.W., *Human Platelet Chemotaxis: Requirement for Plasma Factor(s) and the Role of Collagen* Am J Physiol, 1978. **235**(1): p. H23-8.

126. Lowenhaupt, R.W., et al., *A Quantitative Method to Measure Human Platelet Chemotaxis Using indium-111-oxine-labeled Gel-Filtered Platelets.* Blood, 1982. **60**(6): p. 1345-52.

127. Park, S.A. and Y.M. Hyun, *Neutrophil Extravasation Cascade: What Can We Learn from Two-photon Intravital Imaging?* Immune Netw, 2016. **16**(6): p. 317-321.

128. Gebhard, R., *Metabolic zonation of the liver: Regulation and implications for liver function.* Pharmac. Ther, 1992. **53**(3): p. 275-354.

129. Gandhi, C.R., *Cellular Anatomy of the Liver (Hepatocyte, Biliary Epithelial Cells, Endothelial Cells, Kupffer Cells and Hepatic Stellate Cells)*, in *Pathobiology of Human Disease*. 2014. p. 1759-1769.

130. Rogers, A.B. and R.Z. Dintzis, *Hepatobiliary System*, in *Comparative Anatomy and Histology*. 2018. p. 229-239.

131. Hollander, C.F., C.F.A. van Bezooijen, and H.A. Solleveld, *Anatomy, Function and Aging in the Mouse Liver.* Arch Toxicol Suppl, 1987. **10**: p. 244-50.

132. Hoehme, S., et al., *Prediction and validation of cell alignment along microvessels as order principle to restore tissue architecture in liver regeneration.* Proc Natl Acad Sci U S A, 2010. **107**(23): p. 10371-6.

133. Lowe, J.S. and P.G. Anderson, *Liver*, in *Stevens Lowes Human Histology*. 2015. p. 225-238.

134. Jensen, K.J., G. Alpini, and S. Glaser, *Hepatic nervous system and neurobiology of the liver.* Compr Physiol, 2013. **3**(2): p. 655-65.

135. Trefts, E., M. Gannon, and D.H. Wasserman, *The liver.* Curr Biol, 2017. **27**(21): p. R1147-R1151.

136. Shetty, S., P.F. Lalor, and D.H. Adams, *Liver sinusoidal endothelial cells - gatekeepers of hepatic immunity.* Nat Rev Gastroenterol Hepatol, 2018. **15**(9): p. 555-567.

137. Protzer, U., M.K. Maini, and P.A. Knolle, *Living in the liver: hepatic infections.* Nat Rev Immunol, 2012. **12**(3): p. 201-13.

138. Ben-Moshe, S. and S. Itzkovitz, *Spatial heterogeneity in the mammalian liver.* Nature Reviews Gastroenterology & Hepatology, 2019. **16**(7): p. 395-410.

139. Eltzschig, H.K. and T. Eckle, *Ischemia and reperfusion--from mechanism to translation.* Nat Med, 2011. **17**(11): p. 1391-401.

140. Nastos, C., et al., *Global consequences of liver ischemia/reperfusion injury.* Oxid Med Cell Longev, 2014. **2014**: p. 906-965.

141. Park, S.W., et al., *Paneth cell-derived interleukin-17A causes multiorgan dysfunction after hepatic ischemia and reperfusion injury.* Hepatology, 2011. **53**(5): p. 1662-75.

142. Karatzas, T., et al., *Rodent models of hepatic ischemia-reperfusion injury: time and percentage-related pathophysiological mechanisms.* J Surg Res, 2014. **191**(2): p. 399-412.

143. Delmas-Beauvieux, M.C., et al., *Phosphorus-31 nuclear magnetic resonance of isolated rat liver during hypothermic ischemia and subsequent normothermic perfusion.* Journal of Hepotology, 1992. **15**: p. 192-201.

144. Myagkaya, G., H. van Veen, and J. James, *Ultrastructural changes in rat liver sinusoids during prolonged normothermic and hypothermic ischemia in vitro.* Virchows Arch B Cell Pathol Incl Mol Pathol, 1984. **47**(4): p. 361-73.

145. Tchilikidi, K.Y., *Liver graft preservation methods during cold ischemia phase and normothermic machine perfusion.* World J Gastrointest Surg, 2019. **11**(3): p. 126–142.

146. Izuishi, K., et al., *Ischemic preconditioning of the murine liver protects through the Akt kinase pathway.* Hepatology, 2006. **44**(3): p. 573-80.

147. Yang, J., et al., *Human adrenomedullin and its binding protein attenuate organ injury and reduce mortality after hepatic ischemia-reperfusion.* Ann Surg, 2009. **249**(2): p. 310-7.

148. Jaeschke, H., *Mechanisms of reperfusion injury after warm ischemia of the liver.* J Hepatobiliary Pancreat Surg, 1998. **5**(4): p. 402-8.

149. Jaeschke, H., A. Farhood, and C.W. Smith, *Neutrophils contribute to ischemia/reperfusion injury in rat liver in vivo.* The FASEB Journal, 1990. **4**: p. 3355-3359.

150. Mukhopadhyay, P., et al., *Cannabidiol protects against hepatic ischemia/reperfusion injury by attenuating inflammatory signaling and response, oxidative/nitrative stress, and cell death.* Free Radic Biol Med, 2011. **50**(10): p. 1368-81.

151. Kim, M.S., et al., *CD44 disruption attenuates murine hepatic ischemia/reperfusion injury.* J Korean Med Sci, 2011. **26**(7): p. 919-26.

152. Wei, Y., et al., *Carbon monoxide-releasing molecule-2 (CORM-2) attenuates acute hepatic ischemia reperfusion injury in rats.* BMC Gastroenterol, 2010. **10**: p. 42.

153. Chattopadhyay, P., G. Shukla, and A.K. Wahi, *Protective effect of L-arginine against necrosis and apoptosis induced by experimental ischemic and reperfusion in rat liver.* Saudi J Gastroenterol, 2009. **15**(3): p. 156-62.

154. Tsung, A., et al., *The nuclear factor HMGB1 mediates hepatic injury after murine liver ischemia-reperfusion.* J Exp Med, 2005. **201**(7): p. 1135-43.

155. Batkai, S., et al., *Cannabinoid-2 receptor mediates protection against hepatic ischemia/reperfusion injury.* FASEB J, 2007. **21**(8): p. 1788–1800.

156. Kuboki, S., et al., *Distinct contributions of CD4+ T cell subsets in hepatic ischemia/reperfusion injury.* Am J Physiol Gastrointest Liver Physiol, 2009. **296**(5): p. G1054-9.

157. Liu, A., et al., *HMGB1 in ischemic and non-ischemic liver after selective warm ischemia/reperfusion in rat.* Histochem Cell Biol, 2011. **135**(5): p. 443-52.

158. Takamatsu, Y., et al., *Inhibition of inducible nitric oxide synthase prevents hepatic, but not pulmonary, injury following ischemia-reperfusion of rat liver.* Dig Dis Sci, 2006. **51**(3): p. 571-9.

159. Bourque, S.L., S.T. Davidge, and M.A. Adams, *The interaction between endothelin-1 and nitric oxide in the vasculature: new perspectives.* Am J Physiol Regul Integr Comp Physiol, 2011. **300**(6): p. R1288-95.

160. Black, S.M. and J.R. Fineman, *Oxidative and nitrosative stress in pediatric pulmonary hypertension: roles of endothelin-1 and nitric oxide.* Vascul Pharmacol, 2006. **45**(5): p. 308-16.

161. Pollock, J.S. and D.M. Pollock, *Endothelin and NOS1/nitric oxide signaling and regulation of sodium homeostasis.* Curr Opin Nephrol Hypertens, 2008. **17**(1): p. 70-75.

162. Rees, D.D., et al., *Characterization of three inhibitors of endothelial nitric oxide synthase in vitro and in vivo.* Br J Pharmacol, 1990. **101**(3): p. 746–752.

163. Lentsch, A.B., et al., *Inflammatory mechanisms and therapeutic strategies for warm hepatic ischemia/reperfusion injury.* Hepatology, 2000. **32**(2): p. 169-73.

164. Jaeschke, H., *Molecular mechanisms of hepatic ischemia-reperfusion injury and preconditioning.* Am J Physiol Gastrointest Liver Physiol, 2002. **284**: p. G15–G26.

165. Peralta, C., M.B. Jimenez-Castro, and J. Gracia-Sancho, *Hepatic ischemia and reperfusion injury: effects on the liver sinusoidal milieu.* J Hepatol, 2013. **59**(5): p. 1094-106.

166. Jaeschke, H., et al., *Superoxide Generation by Neutrophils and Kupffer Cells During in Vivo Reperfusion After Hepatic Ischemia in Rats* J Leukoc Biol, 1992. **54**(2): p. 377-82.

167. Serhan, C.N. and B.D. Levy, *Resolvins in inflammation: emergence of the pro-resolving superfamily of mediators.* J Clin Invest, 2018. **128**(7): p. 2657-2669.

168. Zhai, Y., et al., *Ischaemia-reperfusion injury in liver transplantation--from bench to bedside.* Nat Rev Gastroenterol Hepatol, 2013. **10**(2): p. 79-89.

169. Zhang, X.J., et al., *An ALOX12-12-HETE-GPR31 signaling axis is a key mediator of hepatic ischemia-reperfusion injury.* Nat Med, 2018. **24**(1): p. 73-83.

170. Drefs, M., et al., *Modulation of Glutathione Hemostasis by Inhibition of 12/15-Lipoxygenase Prevents ROS-Mediated Cell Death after Hepatic Ischemia and Reperfusion.* Oxid Med Cell Longev, 2017. **2017**: p. 8325754.

171. Radojkovic, M., et al., *Ischemic preconditioning vs adenosine vs prostaglandin E1 for protection against liver ischemia/reperfusion injury.* Braz J Med Biol Res, 2017. **50**(8): p. e6185.

172. Zhang, Y., et al., *Hepatic Ischemic Preconditioning Alleviates Ischemia-Reperfusion Injury by Decreasing TIM4 Expression.* Int J Biol Sci, 2018. **14**(10): p. 1186-1195.

173. Robertson, F.P., B.J. Fuller, and B.R. Davidson, *An Evaluation of Ischaemic Preconditioning as a Method of Reducing Ischaemia Reperfusion Injury in Liver Surgery and Transplantation.* J Clin Med, 2017. **6**(7).

174. Mendes-Braz, M., et al., *The current state of knowledge of hepatic ischemia-reperfusion injury based on its study in experimental models.* J Biomed Biotechnol, 2012. **2012**: p. 298657.

175. Urisono, Y., et al., *Von Willebrand Factor Aggravates Hepatic Ischemia-Reperfusion Injury by Promoting Neutrophil Recruitment in Mice.* Thromb Haemost, 2018. **118**(4): p. 700-708.

176. Finsterbusch, M., et al., *Measuring and interpreting platelet-leukocyte aggregates.* Platelets, 2018. **29**(7): p. 677-685.

177. Coller, B.S., et al., *A murine monoclonal antibody that completely blocks the binding of fibrinogen to platelets produces a thrombasthenic-like state in normal platelets and binds to glycoproteins IIb and/or IIIa.* The Journal of clinical investigation, 1983. **72**(1): p. 325-338.

178. Khandoga, A., et al., *Platelet adhesion mediated by fibrinogen-intercelllular adhesion molecule-1 binding induces tissue injury in the postischemic liver in vivo.* Transplantation, 2002. **74**(5): p. 681-8.

179. Khandoga, A., et al., *Platelet–endothelial cell interactions during hepatic ischemia–reperfusion in vivo: a systematic analysis.* Microvascular Research, 2003. **65**: p. 71–77.

180. van Golen, R.F., et al., *Platelet aggregation but not activation and degranulation during the acute post-ischemic reperfusion phase in livers with no underlying disease.* J Clin Transl Res, 2015. **1**(2): p. 107-115.

181. Nocito, A., et al., *Platelets and platelet-derived serotonin promote tissue repair after normothermic hepatic ischemia in mice.* Hepatology, 2007. **45**(2): p. 369-76.

182. Khandoga, A., et al., *CD4+ T cells contribute to postischemic liver injury in mice by interacting with sinusoidal endothelium and platelets.* Hepatology, 2006. **43**(2): p. 306-15.

183. Peralta, C., et al., *Preconditioning protects against systemic disorders associated with hepatic ischemia-reperfusion through blockade of tumor necrosis factor–induced P-selectin up-regulation in the rat.* Hepatology, 2001. **33**(1): p. 100-113.

184. Amersi, F., et al., *P-Selectin Glycoprotein Ligand-1 (rPSGL-Ig)-Mediated Blockade of CD62 Selectin Molecules Protects Rat Steatotic Liver Grafts from Ischemia/Reperfusion Injury.* American Journal of Transplantation, 2002. **2**(7): p. 600-608.

185. Pak, S., et al., *Platelet adhesion in the sinusoid caused hepatic injury by neutrophils after hepatic ischemia reperfusion.* Platelets, 2010. **21**(4): p. 282-8.

186. Montalvo-Jave, E.E., et al., *Factors in the Pathophysiology of the Liver Ischemia-Reperfusion Injury.* Journal of Surgical Research, 2008. **147**(1): p. 153-159.

187. Tamura, T., et al., *Interaction between Kupffer cells and platelets in the early period of hepatic ischemia-reperfusion injury--an in vivo study.* J Surg Res, 2012. **178**(1): p. 443-51.

188. Ogawa, K., et al., *Interaction of kupffer cells and platelets determines the severity of ischemia-reperfusion injury in steatosis.* Tohoku J Exp Med, 2014. **232**(2): p. 105-13.

189. Sindram, D., et al., *Platelets induce sinusoidal endothelial cell apoptosis upon reperfusion of the cold ischemic rat liver.* Gastroenterology, 2000. **118**: p. 183-191.

190. Rahier, J., J. Wallon, and J.C. Henquin, *Cell Populations in the Endocrine Pancreas of Human Neonates and Infants.* Diabetologia, 1981. **20**(5): p. 540-546.

191. Maclean, N. and R.F. Ogilvie, *Quantitative Estimation of the Pancreatic Islet Tissue in Diabetic Subjects.* Diabetes, 1955. **4**(5): p. 367-76.

192. Bunnag, S.C., S. Bunnag, and N.E. Warner, *Microcirculation in the Islets of Langerhans of the Mouse.* Anat. Rec., 1963. **146**: p. 117-123.

193. Watanabe, S., et al., *Changes in the Mouse Exocrine Pancreas after Pancreatic Duct Ligation: A Qualitative and Quantitative Histological Study.* Arch Histol Cytol, 1995. **58**(3): p. 365-374.

194. Böck, P., M. Abdel-Moneim, and M.E. Gerbacher, *Development of Pancreas.* Microsc. Res. Tech, 1997. **37**: p. 374–383.

195. Villasenor, A., et al., *Epithelial dynamics of pancreatic branching morphogenesis.* Development, 2010. **137**(24): p. 4295-305.

196. Hornblad, A., A. Cheddad, and U. Ahlgren, *An improved protocol for optical projection tomography imaging reveals lobular heterogeneities in pancreatic islet and beta-cell mass distribution.* Islets, 2011. **3**(4): p. 204-8.

197. Dolensek, J., M.S. Rupnik, and A. Stozer, *Structural similarities and differences between the human and the mouse pancreas.* Islets, 2015. **7**(1): p. e1024405.

198. Saito, K., N. Iwama, and T. Takahashi, *Morphometrical Analysis on Topographical Difference in Size Distribution, Number and Volume of Islets in the Human Pancreas.* Tohoku J Exp Med, 1978. **124**(2): p. 177-186.

199. Yaginuma, N., et al., *The Microvasculature of the Human Pancreas and Its Relation to Langerhans Islets and Lobules.* Pathology - Research and Practice, 1986. **181**(1): p. 77-84.

200. In't Veld, P. and M. Marichal, *Microscopic anatomy of the human islet of Langerhans.* Adv Exp Med Biol, 2010. **654**: p. 1-19.

201. Murakami, T., *Pancreatic insulo-acinar portal systems in humans, rats, and some other mammals: Scanning electron microscopy of vascular casts.* Microsc. Res. Tech., 1997. **37**(5-6): p. 478-488.

202. Watanabe, S., et al., *The Lobular Architecture of the Normal Human Pancreas: A Computer-Assisted Three-Dimensional Reconstruction Study.* Pancreas, 1997. **15**(1): p. 48-52.

203. Tadokoro, H., M. Takase, and B. Nobukawa, *Development and congenital anomalies of the pancreas.* Anat Res Int, 2011. **2011**: p. 351217.

204. Reichert, M. and A.K. Rustgi, *Pancreatic ductal cells in development, regeneration, and neoplasia.* J Clin Invest, 2011. **121**(12): p. 4572-8.

205. Wallig, M.A. and J.M. Sullivan, *Exocrine Pancreas*, in *Haschek and Rousseaux's Handbook of Toxicologic Pathology*. 2013. p. 2361-2390.

206. Hellman, B., *Actual Distribution of the Number and Volume of the Islets of Langerhans in Different Size Classes in Non-diabetic Humans of varying Ages.* Nature, 1959. **184**.

207. Kim, A., et al., *Islet architecture: A comparative study.* Islets, 2009. **1**(2): p. 129-36.

208. Kilimnik, G., et al., *Quantification of islet size and architecture.* Islets, 2012. **4**(2): p. 167-72.

209. Jo, J., M.Y. Choi, and D.S. Koh, *Size distribution of mouse Langerhans islets.* Biophys J, 2007. **93**(8): p. 2655-66.

210. Steiner, D.J., et al., *Pancreatic islet plasticity: interspecies comparison of islet architecture and composition.* Islets, 2010. **2**(3): p. 135-45.

211. Brissova, M., et al., *Assessment of human pancreatic islet architecture and composition by laser scanning confocal microscopy.* J Histochem Cytochem, 2005. **53**(9): p. 1087-97.

212. Cabrera, O., et al., *The unique cytoarchitecture of human pancreatic islets has implications for islet cell function.* Proc Natl Acad Sci U S A, 2006. **103**(7): p. 2334-9.

213. Andralojc, K.M., et al., *Ghrelin-producing epsilon cells in the developing and adult human pancreas.* Diabetologia, 2009. **52**(3): p. 486-93.

214. Samuelsson, B., *Leukotrienes: Mediators of Immediate Hypersensitivity Reactions and Inflammation.* Crit Rev Immunol, 1983. **4**(4): p. 307-334.

215. Evans, J.F., *Cysteinyl leukotriene receptors.* Prostaglandins & other Lipid Mediators, 2002. **68–69**: p. 587-597.

216. White, M., *Mediators of inflammation and the inflammatory process.* J Allergy Clin Immunol, 1999. **103**: p. 378-381.

217. Basavarajappa, D., et al., *Roles of coactosin-like protein (CLP) and 5-lipoxygenase-activating protein (FLAP) in cellular leukotriene biosynthesis.* Proc Natl Acad Sci U S A, 2014. **111**(31): p. 11371-6.

218. Hamberg, M. and B. Samuelsson, *On the specificity of the oxygenation of unsaturated fatty acids catalyzed by soybean lipoxidase.* J Biol Chem, 1967. **242**(22): p. 5329-35.

219. Murphy, R.C., S. Hammarström, and B. Samuelsson, *Leukotriene C: a slow-reacting substance from murine mastocytoma cells.* Proceedings of the National Academy of Sciences, 1979. **76**(9): p. 4275-4279.

220. Afonso, P.V., et al., *LTB4 is a signal-relay molecule during neutrophil chemotaxis.* Dev Cell, 2012. **22**(5): p. 1079-91.

221. Monteiro, A.P., et al., *Leukotriene B4 mediates neutrophil migration induced by heme.* J Immunol, 2011. **186**(11): p. 6562-7.

222. Surmiak, M., et al., *LTB 4 and 5-oxo-ETE From Extracellular Vesicles Stimulate Neutrophils in Granulomatosis With Polyangiitis* J Lipid Res, 2019. **61**(1): p. 1-9.

223. Dahlen, S.E., et al., *Leukotrienes are potent constrictors of human bronchi.* Nature, 1980. **288**: p. 484-486.

224. Hallstrand, T.S. and W.R. Henderson, Jr., *An update on the role of leukotrienes in asthma.* Curr Opin Allergy Clin Immunol, 2010. **10**(1): p. 60-6.

225. Zinn, S., et al., *The leukotriene B4 receptors BLT1 and BLT2 form an antagonistic sensitizing system in peripheral sensory neurons.* J Biol Chem, 2017. **292**(15): p. 6123-6134.

226. Nakamura, M. and T. Shimizu, *Leukotriene receptors.* Chem Rev, 2011. **111**(10): p. 6231-98.

227. Saeki, K. and T. Yokomizo, *Identification, signaling, and functions of LTB4 receptors.* Semin Immunol, 2017. **33**: p. 30-36.

228. Yokomizo, T., et al., *A Second Leukotriene B 4 Receptor, BLT2: A New Therapeutic Target in Inflammation and Immunological Disorders.* J Exp Med, 2000. **192**(3): p. 421–432.

229. Toda, A., T. Yokomizo, and T. Shimizu, *Leukotriene B4 receptors.* Prostaglandins Other Lipid Mediat, 2002. **68-69**: p. 575-585.

230. Kanaoka, Y. and J.A. Boyce, *Cysteinyl leukotrienes and their receptors; emerging concepts.* Allergy Asthma Immunol Res, 2014. **6**(4): p. 288-95.

231. Wan, M., et al., *Biosynthesis of leukotriene B(4).* Semin Immunol, 2017. **33**: p. 3-15.

232. Haeggström, J.Z., *Leukotrien A4 hydrolase and the committed step in leukotriene B4 biosynthesis.* Clinical Reviews in Allergy & Immunology, 1999. **17**(1): p. 111-131.

233. Sun, F.F. and J.C. McGuire, *Metabolism of arachidonic acid by human neutrophils: Characterization of the enzymatic reactions that lead to the synthesis of leukotriene B4.* Biochimica et Biophysica Acta (BBA) - Lipids and Lipid Metabolism, 1984. **794**(1): p. 56-64.

234. Profita, M., et al., *15(S)-HETE modulates LTB4 production and neutrophil chemotaxis in chronic bronchitis.* American Journal of Physiology-Cell Physiology, 2000. **279**(4): p. C1249-C1258.

235. De Caterina, R., et al., *Leukotriene B4 production in human atherosclerotic plaques.* Biomed Biochim Acta, 1988. **47**(10-11): p. S182-5.

236. Spanbroek, R., et al., *Expanding expression of the 5-lipoxygenase pathway within the arterial wall during human atherogenesis.* Proceedings of the National Academy of Sciences, 2003. **100**(3): p. 1238.

237. Larré, S., et al., *PGE2 and LTB4 tissue levels in benign and cancerous prostates.* Prostaglandins & Other Lipid Mediators, 2008. **87**(1): p. 14-19.

238. Ney, P. and K. Schrör, *E-type prostaglandins but not iloprost inhibit platelet activating factor-induced generation of leukotriene B4 by human polymorphonuclear leukocytes.* Br J Pharmacol, 1989. **96**(1): p. 186-92.

239. Becker, K., et al., *Influence of some prostaglandins and prostaglandin analogues on PAF-induced shock in mice.* Prostaglandins, Leukotrienes and Essential Fatty Acids, 1990. **40**(2): p. 157-160.

240. Snelgrove, R.J., et al., *A Critical Role for LTA4Hin Limiting Chronic Pulmonary Neutrophilic Inflammation.* Science, 2010. **330**(6000): p. 90-4.

241. Akthar, S., et al., *Matrikines are key regulators in modulating the amplitude of lung inflammation in acute pulmonary infection.* Nat Commun, 2015. **6**: p. 8423.

242. Gaggar, A., et al., *A novel proteolytic cascade generates an extracellular matrix-derived chemoattractant in chronic neutrophilic inflammation.* J Immunol, 2008. **180**(8): p. 5662-9.

243. Patel, D.F. and R.J. Snelgrove, *The multifaceted roles of the matrikine Pro-Gly-Pro in pulmonary health and disease.* Eur Respir Rev, 2018. **27**(148).

244. Dennis, E.A. and P.C. Norris, *Eicosanoid storm in infection and inflammation.* Nat Rev Immunol, 2015. **15**(8): p. 511-23.

245. Levy, B.D., et al., *Lipid mediator class switching during acute inflammation: signals in resolution.* Nat Immunol, 2001. **2**(7): p. 612-9.

246. Funk, C.D., *5-Lipoxygenase and Leukotrienes.* 2000.

247. Peters-Golden, M., et al., *Protection from Pulmonary Fibrosis in Leukotriene-Deficient Mice.* Am J Respir Crit Care Med, 2001. **165**(2): p. 229-35.

248. Bailie, M.B., et al., *Leukotriene-deficient mice manifest enhanced lethality from Klebsiella pneumonia in association with decreased alveolar macrophage phagocytic and bactericidal activities.* The Journal of Immunology, 1996. **157**(12): p. 5221.

249. Mancuso, P., P. Nana-Sinkam, and M. Peters-Golden, *Leukotriene B4 augments neutrophil phagocytosis of Klebsiella pneumoniae.* Infect Immun, 2001. **69**(4): p. 2011-6.

250. Secatto, A., et al., *5-Lipoxygenase deficiency impairs innate and adaptive immune responses during fungal infection.* PLoS One, 2012. **7**(3): p. e31701.

251. Haribabu, B., et al., *Targeted Disruption of the Leukotriene B4Receptor in Mice Reveals Its Role in Inflammation and Platelet-Activating Factor–Induced Anaphylaxis.* Journal of Experimental Medicine, 2000. **192**(3): p. 433-438.

252. Byrum, R.S., et al., *Determination of the Contribution of Cysteinyl Leukotrienes and Leukotriene B4 in Acute Inflammatory Responses Using 5-Lipoxygenase- and Leukotriene A4 Hydrolase-Deficient Mice.* J Immunol 2020. **163**(12): p. 6810-6819.

253. Abe, Y., et al., *Mouse model of liver ischemia and reperfusion injury: method for studying reactive oxygen and nitrogen metabolites in vivo.* Free Radic Biol Med, 2009. **46**(1): p. 1-7.

254. Amend, S.R., K.C. Valkenburg, and K.J. Pienta, *Murine Hind Limb Long Bone Dissection and Bone Marrow Isolation.* J Vis Exp, 2016(110).

255. Aguilar, A., et al., *Three-Dimensional Culture in a Methylcellulose-Based Hydrogel to Study the Impact of Stiffness on Megakaryocyte Differentiation.* Methods Mol Biol, 2018. **1812**: p. 139-153.

256. Nieswandt, B., et al., *Identification ofcritical antigen-specific mechanisms in the development of immune thrombocytopenic purpura in mice.* **Blood**, 2000. **96**(7): p. 2520-2527.

257. Nieswandt, **B.**, et al., *Long-term Antithrombotic Protection by In Vivo Depletion of Platelet Glycoprotein VI in Mice.* J. Exp. Med, 2001. **193**(4): p. 459–469.

258. May, F., et al., *CLEC-2 is an essential platelet-activating receptor in hemostasis and thrombosis.* Blood, 2009. **114**(16): p. 3464-72.

259. Hofmann, S., et al., *The SLAM family member CD84 is regulated by ADAM10 and calpain in platelets.* J Thromb Haemost, 2012. **10**(12): p. 2581-92.

260. Stritt, S., et al., *Rap1-GTP-interacting adaptor molecule (RIAM) is dispensable for platelet integrin activation and function in mice.* Blood, 2015. **125**(2): p. 219-22.

261. Nieswandt, B., et al., *Acute Systemic Reaction and Lung Alterations Induced by an Antiplatelet Integrin gpIIb/IIIa Antibody in Mice.* Blood, 1999. **94**(2): p. 684-693.

262. Bergmeier, W., et al., *Flow cytometric detection of activated mouse integrin αIIbβ3 with a novel monoclonal antibody.* Cytometry, 2002. **48**(2): p. 80-86.

263. Unkeless, J.C., *Characterization of a monoclonal antibody directed against mouse macrophage and lymphocyte Fc receptors.* J Exp Med, 1979. **150**(3): p. 580–596.

264. Slaba, I., et al., *Imaging the dynamic platelet-neutrophil response in sterile liver injury and repair in mice.* Hepatology, 2015. **62**(5): p. 1593-605.

265. Li, W., et al., *Intravital 2-photon imaging of leukocyte trafficking in beating heart.* J Clin Invest, 2012. **122**(7): p. 2499-508.

266. Sharif-Paghaleh, E., et al., *In Vivo SPECT Reporter Gene Imaging of Regulatory T Cells.* PLOS ONE, 2011. **6**(10): p. e25857.

267. Zehentmeier, S., et al., *Static and dynamic components synergize to form a stable survival niche for bone marrow plasma cells.* European Journal of Immunology, 2014. **44**(8): p. 2306-2317.

268. Tiedt, R., et al., *Pf4-Cre transgenic mice allow the generation of lineage-restricted gene knockouts for studying megakaryocyte and platelet function in vivo.* Blood, 2007. **109**(4): p. 1503-6.

269. Gee, J.M., et al., *Imaging activity in neurons and glia with a Polr2a-based and cre-dependent GCaMP5G-IRES-tdTomato reporter mouse.* Neuron, 2014. **83**(5): p. 1058-72.

270. Faust, N., et al., *Insertion of enhanced green fluorescent protein into the lysozyme gene creates mice with green fluorescent granulocytes and macrophages* Blood, 2000. **96**(2): p. 719–726.

271. Laemmli, *Cleavage of strucutral proteins during the assembly of the head of Bacteriophage T4.* Nature, 1970. **227**: p. 680-685.

272. Shivdasani, R.A. and H. Schulze, *Culture, Expansion, and Differentiation of Murine Megakaryocytes.* Current Protocols in Immunology, 2005. **67**(1): p. 22F.6.1-22F.6.13.

273. Marques, P.E., et al., *Imaging liver biology in vivo using conventional confocal microscopy.* Nature Protocols, 2015. **10**(2): p. 258-268.

274. Vergnon, J.M., R.M. Huber, and K. Moghissi, *Place of cryotherapy, brachytherapy and photodynamic therapy in therapeutic bronchoscopy of lung cancers.* Eur Respir J, 2006. **28**(1): p. 200-18.

275. Nurden, A.T., *Glanzmann thrombasthenia.* Orphanet J Rare Dis, 2006. **1**: p. 10.

276. El-Chemaly, S. and L.R. Young, *Hermansky-Pudlak Syndrome.* Clin Chest Med, 2016. **37**(3): p. 505-11.

277. Nieswandt, B., D. Varga-Szabo, and M. Elvers, *Integrins in platelet activation.* J Thromb Haemost, 2009. **7** Suppl 1: p. 206-9.

278. Lopez, J.A., et al., *Bernard-Soulier Syndrome.* Blood, 1998. **91**(12): p. 4397-4418.

279. Bergmeier, W., et al., *The role of platelet adhesion receptor GPIba far exceeds that of its main ligand, von Willebrand factor, in arterial thrombosis.* PNAS 2006. **103**(45): p. 16900–16905.

280. Kawahara, R., *Hematopoiesis*, in *xPharm: The Comprehensive Pharmacology Reference*, S.J. Enna and D.B. Bylund, Editors. 2007, Elsevier: New York. p. 1-5.

281. Rogers, I., et al., *Identification and analysis of in vitro cultured CD45-positive cells capable of multi-lineage differentiation.* Exp Cell Res, 2007. **313**(9): p. 1839-52.

282. McNeill, L., et al., *CD45 isoforms in T cell signalling and development.* Immunol Lett, 2004. **92**(1-2): p. 125-34.

283. Murray, C.J.L. and A.D. Lopez, *Mortality by cause for eight regions of the world: Global Burden of Disease Study.* The Lancet, 1997. **349**(9061): p. 1269-1276.

284. Golebiewska, E.M. and A.W. Poole, *Platelet secretion: From haemostasis to wound healing and beyond.* Blood Rev, 2015. **29**(3): p. 153-62.

285. Shen, S.Q., Y. Zhang, and C.L. Xiong, *The protective effects of 17beta-estradiol on hepatic ischemia-reperfusion injury in rat model, associated with regulation of heat-shock protein expression.* J Surg Res, 2007. **140**(1): p. 67-76.

286. Chauhan, A., et al., *Platelets: No longer bystanders in liver disease.* Hepatology, 2016. **64**(5): p. 1774-1784.

287. Margraf, A. and A. Zarbock, *Platelets in Inflammation and Resolution.* J Immunol, 2019. **203**(9): p. 2357-2367.

288. Deppermann, C., *Platelets and vascular integrity.* Platelets, 2018. **29**(6): p. 549-555.

289. Kaplan, Z.S. and S.P. Jackson, *The role of platelets in atherothrombosis.* Hematology Am Soc Hematol Educ Program, 2011. **2011**: p. 51-61.

290. Funken, D., et al., *In situ targeting of dendritic cells sets tolerogenic environment and ameliorates CD4(+) T-cell response in the postischemic liver.* FASEB J, 2017. **31**(11): p. 4796-4808.

291. Khan, H.A., et al., *Crosstalk of liver immune cells and cell death mechanisms in different murine models of liver injury and its clinical relevance.* Hepatobiliary & Pancreatic Diseases International, 2017. **16**(3): p. 245-256.

292. Serhan, C.N., *Novel lipid mediators and resolution mechanisms in acute inflammation: to resolve or not?* Am J Pathol, 2010. **177**(4): p. 1576-91.

293. Suzuki-Inoue, K., et al., *Involvement of the snake toxin receptor CLEC-2, in podoplanin-mediated platelet activation, by cancer cells.* J Biol Chem, 2007. **282**(36): p. 25993-6001.

294. Bertozzi, C.C., et al., *Platelets regulate lymphatic vascular development through CLEC-2-SLP-76 signaling.* Blood, 2010. **116**(4): p. 661-70.

295. Pan, Y., W.D. Wang, and T. Yago, *Transcriptional regulation of podoplanin expression by Prox1 in lymphatic endothelial cells.* Microvasc Res, 2014. **94**: p. 96-102.

296. Honma, M., et al., *Podoplanin expression in wound and hyperproliferative psoriatic epidermis: regulation by TGF-beta and STAT-3 activating cytokines, IFN-gamma, IL-6, and IL-22.* J Dermatol Sci, 2012. **65**(2): p. 134-40.

297. Chauhan, A., et al., *The platelet receptor CLEC-2 blocks neutrophil mediated hepatic recovery in acetaminophen induced acute liver failure.* Nat Commun, 2020. **11**(1): p. 1939.

298. Huang, H., et al., *Damage-associated molecular pattern-activated neutrophil extracellular trap exacerbates sterile inflammatory liver injury.* Hepatology, 2015. **62**(2): p. 600-14.

299. Moxon-Emre, I. and L.C. Schlichter, *Neutrophil Depletion Reduces Blood-Brain Barrier Breakdown, Axon Injury, and Inflammation After Intracerebral Hemorrhage.* J Neuropathol Exp Neurol, 2011. **70**(3): p. 218-235.

300. McDonald, B., et al., *Intravascular neutrophil extracellular traps capture bacteria from the bloodstream during sepsis.* Cell Host Microbe, 2012. **12**(3): p. 324-33.

301. Fuchs, T.A., et al., *Novel cell death program leads to neutrophil extracellular traps.* J Cell Biol, 2007. **176**(2): p. 231-41.

302. Yipp, B.G., et al., *Infection-induced NETosis is a dynamic process involving neutrophil multitasking in vivo.* Nat Med, 2012. **18**(9): p. 1386-93.

303. Kolachala, V.L., et al., *Loss of L-selectin-guided CD8(+) , but not CD4(+) , cells protects against ischemia reperfusion injury in a steatotic liver.* Hepatology, 2017. **66**(4): p. 1258-1274.

304. Pittet, M.J. and R. Weissleder, *Intravital imaging.* Cell, 2011. **147**(5): p. 983-91.

305. Chojnacki, A., et al., *Intravital imaging allows real-time characterization of tissue resident eosinophils.* Commun Biol, 2019. **2**: p. 181.

306. Lefrancais, E., et al., *The lung is a site of platelet biogenesis and a reservoir for haematopoietic progenitors.* Nature, 2017. **544**(7648): p. 105-109.

307. Cattaneo, M., *Inherited platelet-based bleeding disorders.* J Thromb Haemost 2003. **1**: p. 1628–36.

308. van der Meijden, P.E.J. and J.W.M. Heemskerk, *Platelet biology and functions: new concepts and clinical perspectives.* Nat Rev Cardiol, 2019. **16**(3): p. 166-179.

309. Whiteheart, S.W., *Platelet granules: surprise packages.* Blood, 2011. **118**(5): p. 1190-1191.

310. Mueller, M.J., et al., *Leukotriene A4 hydrolase: Mapping of a henicosapeptide involved in mechanism-based inactivation.* Proc Natl Acad Sci U S A, 1995. **92**(18): p. 8383–8387.

311. Thunnissen, M.M., P. Nordlund, and J.Z. Haeggström, *Crystal structure of human leukotriene A4 hydrolase, a bifunctional enzyme in inflammation.* Nat Struct Biol, 2001. **8**(2): p. 131-135.

312. Peng, B., et al., *Identification of Key Lipids Critical for Platelet Activation by Comprehensive Analysis of the Platelet Lipidome* Blood, 2018. **132**(5): p. e1-e12.

313. Turek, G. and R. Pawliczak, *Leukotrienes deficiency.* Alergologia Polska - Polish Journal of Allergology, 2014. **1**(1): p. 19-26.

314. Goulet, J.L., et al., *Altered inflammatory responses in leukotriene-deficient mice.* Proc. Natl. Acad. Sci. USA, 1994. **91**: p. 12852-12856.

315. Scheller, I., et al., *Coactosin-like 1 integrates signaling critical for shear-dependent thrombus formation in mouse platelets.* Haematologica, 2019.

316. Santos, P.C., et al., *The pivotal role of 5-lipoxygenase-derived LTB4 in controlling pulmonary paracoccidioidomycosis.* PLoS Negl Trop Dis, 2013. **7**(8): p. e2390.

6. Appendix

6.1 Abbreviations

12-HETE	12-Hydroxyeicosatetraenoic acid
5-HpETE	5-hydroperoxyeicosatetraenoic acid
5-LO	5-lipoxygenase
ADP	adenosine diphosphate
AKT	serine/threonine kinase 1
ALOX12	arachidonate 12-lipoxygenase
ALT	alanine transaminase
AMI	acute myocardial infarction
AST	aspartate transaminase
ATP	adenosine triphosphate
BALF	bronchoalveolar lavage fluid
BLT1	leukotirene B_4 receptor 1
BM	bone marrow
BSA	bovine serum albumin
CD40L	CD40 ligand
CLEC2	c-type lectin 2
CLP	common lymphoid progenitor
CMP	common myeloid progenitor
Cotl1	coactosin-like protein 1
CXCR1/2	C-X-C chemokine receptor 1
DMS	demarcation membrane system
EAPs	endothelial adhesive platforms
ECM	extracellular matrix
ERK	extracellular signal-regulated kinase
FcRγ	FC receptor γ-chain
FCS	fetal calf serum
FITC	fluorescein isothiocyanate
GM-CSF	granulocyte-macrophage colony stimulating factor
GMP	granulocyte/macrophage progenitor

GP	glycoprotein
GPCR	G-protein coupled receptor
h I/RI	hepatic I/RI
HSC	hematopoietic stem cell
HepSC	hepatic stellate cell
I/RI	ischemia reperfusion injury
ICAM-1	intracellular adhesion molecule 1
IL-1	interleukin-1
ILP	invadosome-like protrusion
INF-g	interferon gamma
ITAM	immunoreceptor tyrosine-based activation
IVM	intravital microscopy
JAK2	janus kinase 2
JAM-A	junctional adhesion molecule A
KC	Kupffer cell
LDH	lactate dehydrogenase
LFA-1	leukocyte function antigen 1
LSEC	liver sinusoidal endothelial cell
LT	leukotriene
LTA4H	Leukotriene A4 hydrolase
LT-HSC	long-term HSC
Mac-1	macrophage antigen 1
MAPK, MEK	mitogen-activated protein kinase
MEP	megakaryocyte/erythrocyte progenitor
MFI	mean fluorescence intensity
MK	megakaryocyte
Mpl	myeloproliferative leukemia protein
MPO	myeloperoxidase
MPP	multipotent progenitor cell
mTOR	mechanistic target of rapamycin
NAP-2	neutrophil activating peptide-2
NET	neutrophil extracellular trap

NO	nitric oxide
PAF	platelet activating factor
PCR	polymerase chain reaction
PDPN	podoplanin
PE	phycoerythrin
PECAM1	platelet endothelial cell adhesion molecule 1
PF4	platelet factor 4
PGP	Pro-Gly-Pro
PI	propidium iodide
PI3K	phosphoinositide-3-kinase
PKC	protein kinase C
PS	phosphatidylserine
PSGL-1	P-selectin glycoprotein ligand-1
PVDF	polyvinylidene difluoride
RAGE	receptor for advanced glycation endproducts
ROS	reactive oxygen species
RT	room temperature
Sca-1	stem cell antigen 1
SN	supernatant
STAT	signal transducers and activators of transcription
ST-HSC	short-term HSC
TF	tissue factor
TNF-a	tumor necrosis factor alpha
TPO	thrombopoietin
TRITC	tetramethylrhodamindextran
TxA2	thromboxane A2
U46	U46619
UV	ultra violet
VCAM-1	vascular cell adhesion molecule 1
vWF	von Willebrand factor

6.2 Acknowledgements

The work presented here was accomplished at the Institute of Experimental Biomedicine I, University Hospital and Rudolf Virchow Center for Experimental Biomedicine, University of Würzburg, Germany, in the group of Dr. David Stegner between April 2016 and July 2020.

Several persons supported me throughout my PhD studies, whom I would like to thank for their help:

- My supervisor, Dr. David Stegner, for the opportunity to work in his junior research group “vascular imaging” and complete my PhD within a quite microscopy-based topic. I am grateful for his constant support, his ideas and the chance to become an expert in intravital imaging. Furthermore, he introduced me into the scientific community, allowing the presentation of my work at international conferences.
- The members of my thesis committee for helpful discussions throughout my PhD period and reviewing my thesis.
- My collaborators in Tübingen for teaching me the model of hepatic ischemia.
- Our technicians, secretaries and animal caretakers without whom our life would be much harder, if not even impossible.
- The team of the Graduate School of Life Sciences for providing a fellowship that allowed me to visit an international conference in Australia, the great scientific course program, from which I would have liked to attend some additional courses. Furthermore, I would like to thank them for their constant support, especially during my time as part of the DRC and the Eureka organizing committee.
- The “platelets in disease” seminar for fruitful discussions and critical data evaluation and troubleshooting.
- All colleagues, former and present members of the Institute, who carried me through this sometimes very hard PhD time, supported me in many different ways and were always there for me. I am very grateful to have such valuable people around me. Also special thanks to those who have proofread this thesis.
- My family and close friends for constant support, encouragement and unfailing trust in my competences and work. Without them, I wouldn’t be where I am right now. To all of them: Thank you so much- I love you.

6.3 Curriculum Vitae

6.4 Publications

6.4.1. Original articles

- Tobias Heib*, Carina Gross*, Martha-Lena Müller, David Stegner, Irina Pleines. *Isolation of murine bone marrow by centrifugation or flushing for the analysis of hematopoietic cells – a comparative study.* **Platelets** 2020.
  *shared-first

- Isabelle C. Becker*, Inga Scheller*, …, Carina Gross, … and Bernhard Nieswandt. *Actin/microtubule crosstalk during platelet biogenesis in mice is critically regulated by Twinfilin1 and Cofilin1.* **Blood advances** 2020. 4(10), 2124–2134

6.4.2 Oral presentations

- ISTH Congress 2019, Melbourne (Australia)
  GPIb-vWF Interactions Promote Neutrophil Recruitment Resulting in Aggravated Liver Damage in the Acute Phase of Hepatic Ischemia-reperfusion Injury

6.4.3 Poster presentations

- Eureka! 2017, Würzburg (Germany):
  GPIb-α blockades reduces hepatic ischemia reperfusion injury

- Joint symposium of the CRC688 and the Comprehensive Heart Failure Center Würzburg (Germany):
  GPIb-α blockades reduces hepatic ischemia reperfusion injury

- Eureka! 2018, Würzburg (Germany):
  GPIb-vWF interactions contribute to acute hepatic damage following ischemia reperfusion injury

6.5 Affidavit

I hereby confirm that my thesis entitled “The role of platelets in hepatic ischemia reperfusion injury in mice” is the result of my own work. I did not receive any help or support from commercial consultants. All sources and/or materials applied are listed and specified in the thesis.

Furthermore, I confirm that this thesis has not yet been submitted as part of another examination process neither in identical nor in similar form.

Würzburg, July 2020 _____

6.6 Eidesstattliche Erklärung

Hiermit erkläre ich an Eides statt, die Dissertation „Die Rolle von Thrombozyten im hepatischen ischämischen Reperfusionsschaden in Mäusen“ eigenständig, d.h. insbesondere selbständig und ohne Hilfe eines kommerziellen Promotionsberaters, angefertigt und keine anderen als die von mir angegebenen Quellen und Hilfsmittel verwendet zu haben.

Ich erkläre außerdem, dass die Dissertation weder in gleicher noch in ähnlicher Form bereits in einem anderen Prüfungsverfahren vorgelegen hat.

Würzburg, Juli 2020 _____